

WORKSHOP ON
THERMAL EMISSION SPECTROSCOPY AND
ANALYSIS OF DUST, DISKS, AND REGOLITHS

1999 APR 28-30
1999

LN-70

1999

April 28-30, 1999
Lunar and Planetary Institute, Houston, Texas

LPI Contribution No. 969



Compiled in 1999 by
LUNAR AND PLANETARY INSTITUTE

The Institute is operated by the Universities Space Research Association under Contract No. NASW-4574 with the National Aeronautics and Space Administration.

Material in this volume may be copied without restraint for library, abstract service, education, or personal research purposes; however, republication of any paper or portion thereof requires the written permission of the authors as well as the appropriate acknowledgment of this publication.

This volume may be cited as

Sprague A. L., Lynch D. K., and Sitko M., eds. (1999) *Workshop on Thermal Emission Spectroscopy and Analysis of Dust, Disks, and Regoliths*. LPI Contribution No. 969, Lunar and Planetary Institute, Houston. 34 pp.

This volume is distributed by

ORDER DEPARTMENT
Lunar and Planetary Institute
3600 Bay Area Boulevard
Houston TX 77058-1113, USA
Phone: 281-486-2172
Fax: 281-486-2186
E-mail: order@lpi.jsc.nasa.gov

Mail order requestors will be invoiced for the cost of shipping and handling.

Preface

This volume contains abstracts that have been accepted for presentation at the Workshop on Thermal Emission Spectroscopy and Analysis of Dust, Disks, and Regoliths, April 28–30, 1999, in Houston, Texas. The workshop conveners are Ann L. Sprague (*University of Arizona*), David K. Lynch (*The Aerospace Corporation*), and Michael Sitko (*University of Cincinnati*).

Logistics, administrative, and publications support for the workshop were provided by the staff of the Publications and Program Services Department of the Lunar and Planetary Institute.

Contents

A Disk Model for the 10-Micrometer Spectra of Young Stellar Objects with Dust-dominated Continua <i>J. E. Bowey and A. J. Adamson</i>	1-1
The Mineralogical Evolution of Silicate Dust in Interstellar Environments <i>J. E. Bowey, A. J. Adamson, and A. K. Speck</i>	2-2
Comparison of Collected Interplanetary Dust Particles with Dust in Space <i>J. P. Bradley and L. P. Keller</i>	4-3
Interpretation of Extragalactic Extinction Measurements Using the Maximum Entropy Method <i>G. C. Clayton, M. J. Wolff, K. D. Gordon, and K. A. Misselt</i>	5-4
Building a Network of Self-Consistent Mid-Infrared Calibration Stars <i>M. Cohen, R. G. Walker, and F. C. Witteborn</i>	5-5
First Detection of Polarization in the CO Bandhead Emission in Young Stellar Objects: A Signature of the Inner Regions of Disks in SSV 13 and DG Tau <i>C. Colomé</i>	6-6
The Thermal Infrared Spectra of Comets Hale-Bopp and 103P/Hartley 2 Observed with the Infrared Space Observatory <i>J. Crovisier, K. Leech, D. Bockelée-Morvan, E. Lellouch, T. Y. Brooke, M. S. Hanner, B. Altieri, H. U. Keller, T. Lim, T. Encrenaz, A. Salama, M. Griffin, T. de Graauw, E. van Dishoeck, and R. F. Knacke</i>	7-7
AIRES: An Airborne Infrared Echelle Spectrometer for SOFIA <i>J. Dotson, E. Erickson, M. Haas, S. Colgan, J. Simpson, C. Telesco, J. Wolf, and E. Young</i>	8-8
Axisymmetric Modeling of Silicate Circumstellar Disks <i>S. K. Dunkin and M. J. Barlow</i>	8-9
Laboratory Measurements of Spectral Emissivity of Materials Analogs to the Martian Soil and Dust <i>S. Fonti, A. Blanco, M. I. Blecka, F. De Carlo, V. Orofino, and S. Solazzo</i>	9-10
Theoretical Modeling of Radiative Transfer in Planetary Regoliths <i>B. W. Hapke</i>	11-11
Optical Properties of Cosmic Dust Analogs <i>Th. Henning</i>	11-12

Problems in Infrared Laboratory Spectroscopy of Silicon Carbide Resulting from High Extinction Coefficients: Inferences from Nanocrystals and Quantitative Methods <i>A. M. Hofmeister, A. K. Speck, and L. Rosen</i>	11-13
Transient Dust Features in Carbon-rich Circumstellar Envelopes of Evolved Stars <i>S. Hony, R. J. Sylvester, L. B. F. M. Waters, and M. J. Barlow</i>	12-16
Silicates as Probes of the Mass Loss History of Oxygen-rich Evolved Stars <i>C. Kemper, R. J. Sylvester, L. B. F. M. Waters, T. de Jong, M. J. Barlow, F. J. Molster, and X. G. G. M. Tielens</i>	13-15
Utilizing Night Spectra of Mars for Mineralogy <i>L. E. Kirkland and K. C. Herr</i>	14-16
Modeling the Infrared Emission of Dust in Born-Again Planetary Nebulae <i>J. Koller and S. Kimeswenger</i>	15-17
ISOPHOT Polarization Measurements of the Asteroids 6 Hebe and 9 Metis at 25 Micrometers <i>J. S. V. Lagerros, T. G. Müller, U. Klaas, and A. Erikson</i>	16-18
The Dust Emission Features in the Infrared Space Observatory Spectrum of NGC 6302 <i>T. L. Lim, F. J. Molster, R. J. Sylvester, M. J. Barlow, and L. B. F. M. Waters</i>	16-19
Adventures in Modeling Thermal Emission Spectra of Comets <i>D. K. Lynch and S. Mazuk</i>	17-20
Infrared Space Observatory Spectroscopy of Circumstellar Dust Disks Surrounding “ISO”lated Herbig Ae/Be Stars, Their Evolution, and the Relationship with Our Own Solar System <i>K. Malfait and C. Waelkens</i>	17-21
A Comparative Study of Infrared Spectral Features in Herbig Ae/Be Stars <i>G. Meeus and C. Waelkens</i>	18-22
Crystalline Silicates: From Nothing to Main Thing <i>F. J. Molster and L. B. F. M. Waters</i>	19-23
Martian Mineralogy with the Infrared Space Observatory Short Wavelength Spectrometer <i>P. W. Morris, T. de Graauw, E. Lellouch, B. Henderson, T. Encrenaz, S. Erard, H. Feuchtgruber, M. Burgdorf, G. Davis, and M. Griffin</i>	19-24
Asteroid 4 Vesta as Seen with the Infrared Space Observatory Short Wavelength Spectrometer <i>P. W. Morris, A. M. Heras, B. Vandenbussche, and R. Dijkstra</i>	19-25

Effects of Grain Morphology and Impurities on the Infrared Spectra of Silicon Carbide Particles <i>H. Mutschke, D. Clement, and Th. Henning</i>	20	26
DUSTY: A Publicly Available Code for Continuum Radiative Transfer in Astrophysical Environments <i>M. Nenkova, Z. Ivezić, and M. Elitzur</i>	20	27
Nucleation, Growth, Annealing, and Coagulation of Refractory Oxides and Metals: Recent Experimental Progress and Applications to Astrophysical Systems <i>J. A. Nuth, F. J. M. Rietmeijer, S. L. Hallenbeck, and P. A. Withey</i>	22	28
Thermal Emission Spectra of Mercury <i>A. E. Potter, B. L. Cooper, R. M. Killen, and T. H. Morgan</i>	23	29
EXES: An Echelon-Cross-Echelle Spectrograph for SOFIA <i>M. J. Richter, J. H. Lacy, D. T. Jaffe, and M. K. Hemenway</i>	24	30
Investigating the Martian Environment with the Mars Global Surveyor Thermal Emission Spectrometer <i>T. L. Roush</i>	25	31
Development of Thermal Infrared Emission Spectroscopy for Geological Investigations of Earth and Mars <i>S. W. Ruff</i>	27	32
Extrazodiacal Light Detection Prospects with the Keck Interferometer <i>E. Serabyn</i>	28	33
Silicon Carbide: The Problem with Laboratory Spectra <i>A. K. Speck, A. M. Hofmeister, and M. J. Barlow</i>	28	34
Thermal Emission Spectroscopy of Solar System Regoliths <i>A. L. Sprague</i>	29	35
Shadow-Hiding Effect in Regolithlike Media <i>D. G. Stankevich and Yu. G. Shkuratov</i>	30	36
Thermal Emission Spectroscopy with the Space Infrared Telescope Facility <i>J. Van Cleve</i>	30	37
Dust Emission from Herbig Ae/Be Stars: Evidence for Disks and Envelopes <i>D. Vinkovic, A. Miroshnichenko, Z. Ivezić, and M. Elitzur</i>	30	38
Thermal Emission Spectroscopy of Laboratory Regoliths <i>C. Wagner</i>	32	39

Solid-State Spectroscopy of Circumstellar Dust: Infrared Space Observatory Results <i>R. Waters</i>	33 ^{-2/10}
Thermal Emission Spectroscopy of 1 Ceres: Evidence for Olivine <i>F. C. Witteborn, T. L. Roush, and M. Cohen</i>	33 ^{4/1}
Abundant Cool Magnesium-rich Pyroxene Crystals in Comet Hale-Bopp <i>D. H. Wooden</i>	34 ^{.42}

Abstracts

A DISK MODEL FOR THE 10-MICROMETER SPECTRA OF YOUNG STELLAR OBJECTS WITH DUST-DOMINATED CONTINUA.

J. E. Bowey^{1,2} and A. J. Adamson^{1,3}, ¹University of Central Lancashire, Preston, UK, ²Queen Mary and Westfield College, London, UK (j.e.bowey@qmw.ac.uk), ³UK Infrared Telescope (UKIRT), Joint Astronomy Centre, Hilo HI, USA (a.adamson@jach.hawaii.edu).

Introduction: Young stellar object (YSO) spectra vary widely [e.g., 1,2] and are characterized primarily by nonphotospheric dust emission and frequently with silicate emission or absorption features. The 10- μm disk model was initially developed to estimate the quantity of optically-thick and optically-thin emission in the spectra of Taurus-Elias 7 (Har06-10) and HL Tau but unlike previous representations, which reproduce the observed spectrum by modeling the flux emitted by dust as power laws, this model reveals information about the YSO disks themselves. The derived absorption profiles may be used to study the silicates and to diagnose the presence of ices.

Sources: HL Tau and Elias 7 (Har06-10) are two bright pre-main-sequence T Tauri stars in the Taurus Molecular Cloud (TMC) whose 10- μm spectra exhibit negligible photospheric emission, no PAH emission, and deep silicate absorption features (Fig. 1). The HL Tau system has been well studied at a variety of wavelengths [4]; its photosphere is obscured by dust associated with expanding cavities perpendicular to a stable 150-AU disk inclined at 67°. Elias 7 is a binary system with optical and infrared components [e.g., 5,6] that may be surrounded by a disklike circumbinary envelope [5].

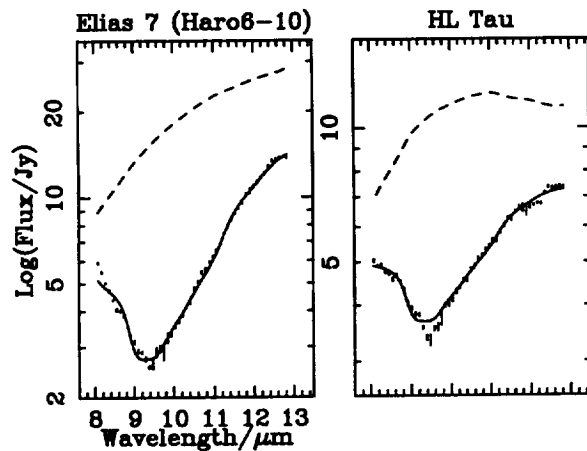


Fig. 1. 10- μm flux spectra of Elias 7 and HL Tau with modeled fluxes (solid) and derived continua (dashed). The derived continua of HL Tau are partially optically thin, with silicate emission features; those of Elias 7 are optically thick. (Since the southern component of Elias 7 is not significantly extinguished by silicates, the flux from this component was subtracted from the observed spectrum before fitting the silicate feature.) 8–13- μm spectroscopy was carried out using CGS3 at UKIRT.

Model: After Adams et al. [7] and Mannings et al. [8], the dusty disk is assumed to have radial temperature and density distributions

$$T(r) = T_*(R_*/r)^q \quad (1)$$

$$\Sigma(r) = \Sigma_*(R_*/r)^p \quad (2)$$

where T_* is the temperature of dust at the stellar radius, R_* , and the surface density of material, $\Sigma(r)$ is equal to Σ at the stellar radius, q is the index of the temperature distribution, and the mass density index, $p = 7/4$, is adopted from protostellar theory [e.g., 7].

To avoid making assumptions about R_D and unlike [7] and [8] we integrate over temperature instead of radius. The flux emitted by silicates in the disk becomes

$$F_{\text{disk}} = a \int_{r_{\text{sil}}}^{R_0} B_\nu(T) [1 - \exp(-c\epsilon_\nu r(T)^{-p})] r(T)^{q+2} dT \quad (3)$$

where $r(T)$ is obtained from equation (1).

Assuming that optically thin emission in the 10- μm band is dominated by silicates, the emission optical depth, $\tau_\nu(r, \theta)$, is given by

$$\tau_\nu = k\epsilon_\nu \frac{\Sigma_0}{\cos\theta} \left(\frac{R_0}{r} \right)^p = c\epsilon_\nu r(T)^{-p} \quad (4)$$

where θ is the angle of inclination of the disk to the sky plane and

$$c = \frac{k\Sigma_0 R_0^p}{\cos\theta} \quad (5)$$

k is a constant that scales the silicate emissivity, ϵ_ν . Σ and R_0 are defined as the mass density and radius where $T(r) = T_0 = 1000\text{K}$ at the inner edge of the silicate disk. R_0 is estimated from equation (1), with $R_* = 2R_\odot$, the radius of a typical T Tauri star [8].

The intrinsic flux of the disk is extinguished by material in the cooler outer regions of the disk and foreground molecular cloud the flux observed, F_ν , becomes

$$F_\nu = F_{\text{disk}} \exp\{-\tau_{\text{cont}}(\lambda)\} \exp\{-c_{\text{sil}}\epsilon_\nu\} \quad (6)$$

where ϵ_ν (normalized to unity at its peak) is assumed to be the same within the protostellar disk and TMC. The continuum optical depth, $\tau_{\text{cont}}(\lambda)$ is derived from A_ν using a power-law extinction curve based on that observed in the ρ Oph Molecular Cloud [see 3].

Parameters a , q , c , and c_{sil} are fitted by χ^2 -minimization. The silicate emissivities used during fitting were those that best represent the silicate absorption feature of dust in quiescent regions of the TMC toward the field star Taurus-Elias 16 [3]. The quality of fit is insensitive to changes in T_* and A_ν . However, changes in T_* and A_ν affect the derived disk radius.

Fits and Derived Absorption Profiles: The flux spectra of Elias 7 and HL Tau, like those of the TMC sources Elias 16 and 18 [3], are best fitted with the Trapezium emissivity [9] ($\chi^2_\nu = 24$

and 9.1 respectively); the flux spectra, fits and derived continua are given in Fig. 1. Structure in the modeled continuum of HL Tau indicates that the disk emission is optically thin in regions of the disk that emit significantly at 10 μm ; Elias 7 is optically thick.

The derived absorption profiles of HL Tau, Elias 7 and Elias 16 (a field star obscured only by cold molecular cloud material [3]) are shown in Fig. 2; the similarity of these profiles [10] suggests that the 10- μm disk model has successfully separated the 10- μm emission and absorption components.

Radial Temperature Distribution: The fitted temperature indices, $q = 0.33$ and 0.43 , for Elias 7 and HL Tau, respectively, are lower than the 0.5 – 0.61 range obtained by [8] using the ALS disk

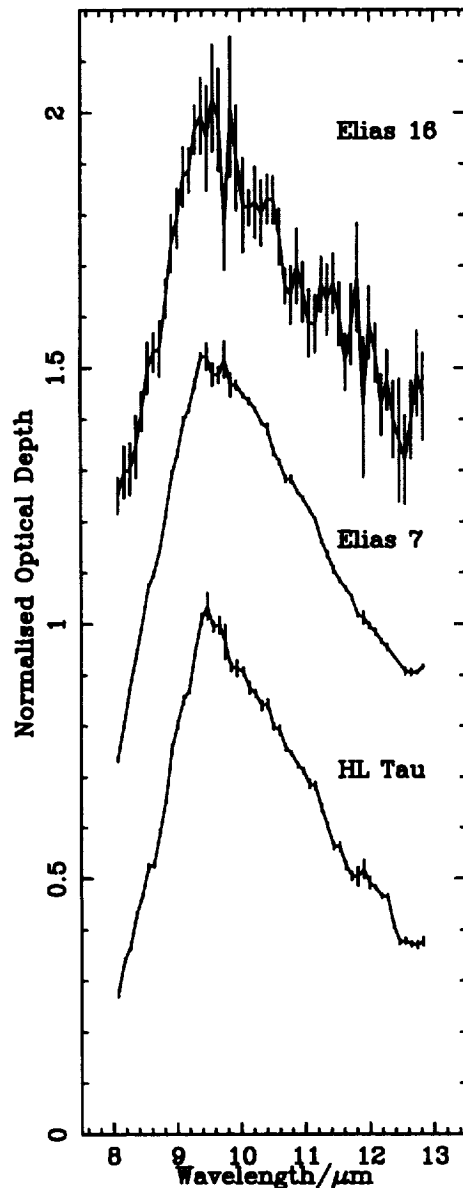


Fig. 2. Normalized 10- μm optical depth profiles of TMC dust: Elias 16 [3], quiescent molecular cloud; Elias 7 and HL Tau, YSO and foreground molecular cloud. Each spectrum is offset by 0.5 from the one below it.

model [7]. However, our results are consistent with the MIR temperature distribution produced by Boss' [11] radiative and hydrodynamical protoplanetary disk models for T Tau [12]. In these models the radial power-law temperature distribution is modified in the disk mid-plane ($1 \text{ AU} \leq r \leq 10 \text{ AU}$), by the effects of grain condensation and evaporation on opacity, causing $T(r)$ to plateau at radii of ~ 2 – 4 AU , which corresponds to the 200 – 300 K temperature range.

Inferred 10- μm Disk Radius, R_{sil} : We may infer the radius of a 10- μm image using equation (1). We define the radius of the disk when $\lambda = 10 \mu\text{m}$, R_{sil} , to be that where the interpolated annular flux, $F_{\text{annulus}} = F_{\text{pk}}/e$. F_{pk} is the largest annular flux component at $10.0 \mu\text{m}$. The $\sim 400 \text{ AU}$ 10- μm disk of Elias 7 ($T_* = 4000 \text{ K}$; $A_v = 6$ – 10^m) is consistent with the extent of the flattened circumbinary envelope proposed by [5]. In the L band the radius of our disk would be about 20 AU , or $\sim 0.14''$, which roughly coincides with the 75% contour of their L-band residual emission. However, our estimate of 730 – 1400 AU ($T_* = 4400 \text{ K}$; $A_v = 12$ – 22^m) at 34 K for HL Tau is not consistent with the value of 100 AU obtained by [13] using the ALS model. Given the non-uniformity of the mass-density and temperature distributions with radius, reliable estimates of the radius and mass of the entire infrared-submillimeter disk cannot be obtained from fits with the 10- μm disk model.

References: [1] Hanner M. S. et al. (1995) *Astrophys. J.*, 438, 250–258. [2] Hanner M. S. et al. (1998) *Astrophys. J.*, 502, 871. [3] Bowey J. E. et al. (1998) *MNRAS*, 298, 131. [4] Close L. M. et al. (1997) *Astrophys. J.*, 478, 766–777. [5] Menard F. et al. (1993) *Astrophys. J. Lett.*, 414, L117–L120. [6] Van Cleve J. E. et al. (1994) *Astrophys. Space Sci.*, 212, 231–238. [7] Adams F. C. et al. (1998) *Astrophys. J.*, 326, 865–883. [8] Mannings V. and Emerson J. P. (1994) *MNRAS*, 267, 361–378. [9] Forrest W. J. et al. (1975) *Astrophys. J.*, 195, 423–440. [10] Bowey J. E. (1998) *Interpreting the 10- μm Astronomical Silicate Feature*, Univ. of Central Lancashire, Preston, UK. [11] Boss A. P. (1996) *Astrophys. J.*, 469, 906–920. [12] Boss A. P. and Yorke H. W. (1996) *Astrophys. J.*, 469, 366–372. [13] Adams F. C. et al. (1990) *Astrophys. J.*, 357, 606–620.

57-30

THE MINERALOGICAL EVOLUTION OF SILICATE DUST IN INTERSTELLAR ENVIRONMENTS.

J. E. Bowey^{1,2}, A. J. Adamson^{1,3}, and A. K. Speck^{1,4}, ¹University of Central Lancashire, Preston, UK, ²Queen Mary and Westfield College, London, UK (j.e.bowey@qmw.ac.uk), ³UK Infrared Telescope (UKIRT), Joint Astronomy Centre, Hilo HI, USA (a.adamson@jach.hawaii.edu), ⁴University College London, London, UK (aks@star.ucl.ac.uk).

Introduction: Attempts to fit the 10- μm astronomical silicate feature in a wide variety of environments (circumstellar, diffuse medium, YSO and comets) using the spectra of single specimens of amorphous laboratory silicate have been largely unsuccessful [e.g., 1–3]. In contrast to previous assumptions, 20–45- μm ISO spectra indicate the presence of crystalline silicates in circumstellar dust and the Red Rectangle [4,5] and grains from meteoritic sources (GEMS, crystalline IDPs, and chondrules) exhibit significant chemical and mineralogical variation. Similarly we find that the average 10- μm spectrum obtained from a number of finely

determined 250 K-emission profiles of O-rich circumstellar dust (where the UV flux is insufficient to excite PAH or ionized PAH bands if a carbonaceous dust component were found) and in the absorption profiles of dust in the diffuse medium and quiescent and YSO environments of the Taurus molecular cloud (where the abundances of HMT and methanol ice are consistent with zero optical depth [2]) are associated with those of crystalline minerals. Absence of a distinct 11.2- μm feature in interstellar spectra suggests that the fraction of crystalline olivine in these environments must not be large, while the blending of bands due to mixed crystalline pyroxenes makes their identification in 10- μm spectra difficult. However, narrow structures at 9.4 μm (TMC YSOs) and 9.7–9.8 μm (circumstellar dust) indicate the presence of layer silicates similar to talc and clay minerals, and together with a common serpentine (10.0–10.6 μm) band suggest that hydroxylated minerals with spectral properties similar to terrestrial layer silicates are a ubiquitous component of cosmic silicate dust.

Evolution: The silicate profile peaks at a wavelength that decreases between circumstellar, diffuse medium, and molecular-cloud environments, indicating [after 7] that the amorphous pyroxene content of initially olivine-rich interstellar dust increases between these environments, and hence with the age of the grains. In geology, direct olivine-plus-SiO₂ to pyroxene reactions occur only at high pressure within the terrestrial mantle and Fe-rich silicates are extremely resistant to chemical alteration while Mg-rich olivines are among the most reactive of silicate minerals. Therefore the most plausible mechanism for the increase in pyroxene is the hydroxylation of Mg-rich olivine to form a serpentine-like silicate that is subsequently annealed to become a mixture of amorphous pyroxene and olivine. This mechanism is particularly appealing, since terrestrial and laboratory olivine samples are readily converted to serpentine in the presence of water and, after extended annealing of the hydrated silicate, the first crystalline band to appear is the 11.2- μm olivine feature frequently observed in cometary spectra.

References: [1] Mutschke H. et al. (1998) *Astron. Astrophys.*, 333, 188. [2] Bowey J. E. et al. (1998) *MNRAS*, 298, 131–138. [3] Jaeger C. et al. (1994) *Astron. Astrophys.*, 292, 641–655. [4] Waters L. B. F. M. et al. (1996) *Astron. Astrophys.*, 315, L361–L364. [5] Waters L. B. F. M. et al. (1998) *Nature*, 39, 868–871. [6] Hanner M. S. et al. (1994) *Astrophys. J.*, 425, 274–285. [7] Guertler J. and Henning T. (1986) *Astrophys. Space Sci.*, 128, 163. [8] Ferraro J. R. (1982) *The Sadtler Infrared Spectra Handbook of Minerals and Clays*, Sadtler Research Laboratories. [9] Bowey J. E. and Adamson A. J. (1999) *JGR*, submitted. [10] Bowey J. E. (1998) Ph.D. thesis, *Interpreting the 10- μm Astronomical Silicate Feature*. Univ. of Central Lancashire, Preston, UK. [11] Blanco A. et al. (1993) *ASP Conf. Series*, 41, 267. [12] Speck A. K. et al. (1999) in preparation.

COMPARISON OF COLLECTED INTERPLANETARY DUST PARTICLES WITH DUST IN SPACE. J. P. Bradley and L. P. Keller, MVA Inc., Norcross GA 30093, USA (jbradley@mva-inc.com).

Infrared (IR) spectroscopy enables direct comparison of dust in space with interplanetary dust particles (IDPs) in the laboratory [1,2]. The Infrared Space Observatory (ISO) has provided new data about circumstellar, interstellar, and cometary dust. One of the

most important findings of ISO is the detection of crystalline Mg-rich silicates (together with glassy silicates) around both young and old stars and Comet Hale-Bopp [3–5]. (Comet Halley's dust also contains Mg-rich silicates [6].) The ISO findings are significant because Mg-rich silicates are rare in primitive meteorites (and polar micrometeorites) but abundant in IDPs, specifically the fluffy chondritic porous (CP) subset of IDPs, some of which are almost certainly from comets [7]. Together with glassy silicate grains (i.e., GEMS), submicrometer enstatite (MgSiO₃) and forsterite (Mg₂SiO₄) are the major crystalline silicates in CP IDPs. Some of these crystals exhibit morphological, crystallographic, and/or compositional evidence of vapor phase growth [7]. It has been proposed that GEMS are surviving presolar interstellar "amorphous silicates" [6]. If true, the IR silicate features should be similar to those observed in astronomical spectra.

Previous studies have demonstrated that it is possible to measure the IR spectral properties of individual IDPs and thin sections of IDPs [1,2]. Obtaining IR data from "pure" GEMS is exceedingly difficult because (1) they are small with subnanogram masses, (2) they are usually intimately mixed with other silicates (e.g., enstatite and forsterite), and (3) they absorb weakly in the IR (relative to crystalline silicates). However, the IR beamline at the National Synchrotron Light Source (NSLS) at Brookhaven National Laboratory is uniquely suited for IR spectroscopy of GEMS because it provides a spot >100 \times brighter than conventional laboratory IR benches [9], plus a detector covering the 2.5–25- μm (400–4000 cm⁻¹) wavelength range.

We have collected IR spectra at NSLS from GEMS-rich regions of thin sections of IDPs sectioned in a sulfur and supported on carbon-film TEM grids, GEMS-rich fragments of IDPs mounted on carbon-film TEM grids, and whole (CP) IDPs pressed into potassium bromide (KBr) substrates. IDPs mounted and sectioned in sulfur (rather than epoxy) are most suitable for the IR measurements because the sulfur can be removed (sublimed) after sectioning, thereby minimizing spectral background in low signal-to-noise GEMS spectra.

Transmission IR spectra are usually collected over the wavelength range of 4000–400 cm⁻¹ (2.5–25 μm) with an aperture (up to 20 \times 20 μm) positioned around each specimen. An open area (no sample) serves as a reference. Background spectra are acquired from the carbon thin-film substrate alongside the thin section. Final baseline corrected (and smoothed) spectra are obtained by subtracting the background from the sample spectrum. Between 256 and 1000 scans (interferograms) were collected from each specimen with spectral resolution of 4 cm⁻¹.

Most "GEMS-rich" thin sections also contain significant amounts of submicrometer enstatite and/or forsterite crystals. Their 10- μm (Si-O stretch) features are broad (2–3.5 μm FWHM) with absorption maxima between 9.3 and 10 μm and often show a broad excess absorption on the long-wavelength wing of the profiles. If a thin section contains significant amounts of enstatite, the absorption maximum trends toward ~9.3 μm . If there is significant forsterite, the absorption maximum shifts toward 10 μm with a pronounced shoulder at ~11.2 μm . Preliminary spectra have also been collected from regions of essentially "pure" GEMS regions of several thin sections. In all cases, the 10- μm silicate features exhibit absorption maxima at ~9.8 μm .

We have also measured the 10- (Si-O stretch) and 18- μm (Si-O bending) features of two chondritic porous IDPs pressed into KBr. Both IDPs exhibit glassy "GEMS-like" silicate features with

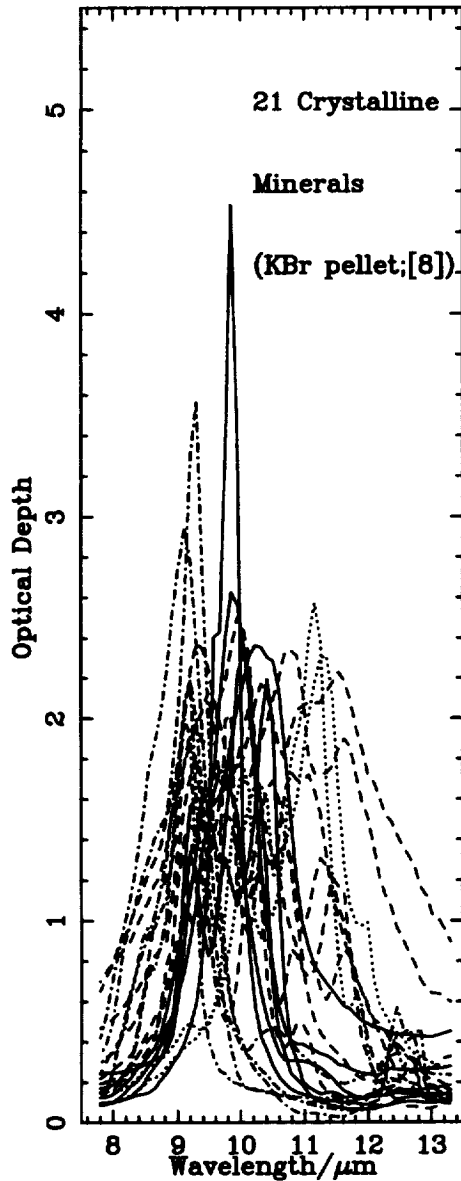


Fig. 1. Unnormalized spectra of Mg-rich, Fe-rich, and SiO_2 minerals — layer silicates (clays, talc, and serpentines; solid); pyroxenes or chain silicates (dashed); olivines (dotted); and silicas or SiO_2 minerals (dot-dash). The strongest band is that due to talc. Olivine, pyroxene, and serpentine spectra are due to individual members of each solid solution series in which the ratios of one metal to another vary.

structured crystalline minerals of cosmic elemental composition is an almost smooth, broad band (Fig. 1). Fine structure in interstellar profiles is closely matched by an average spectrum obtained from a subset of crystalline MgFe and MgFe-rich meteoritic minerals with or without a fraction of amorphous silicate.

Observations: Molecular cloud absorption profiles are broader than those of circumstellar and diffuse medium silicates, due mainly to a $\sim 2\text{-}\mu\text{m}$ -wide excess centered at $\sim 11.5\ \mu\text{m}$ (Fig. 2).

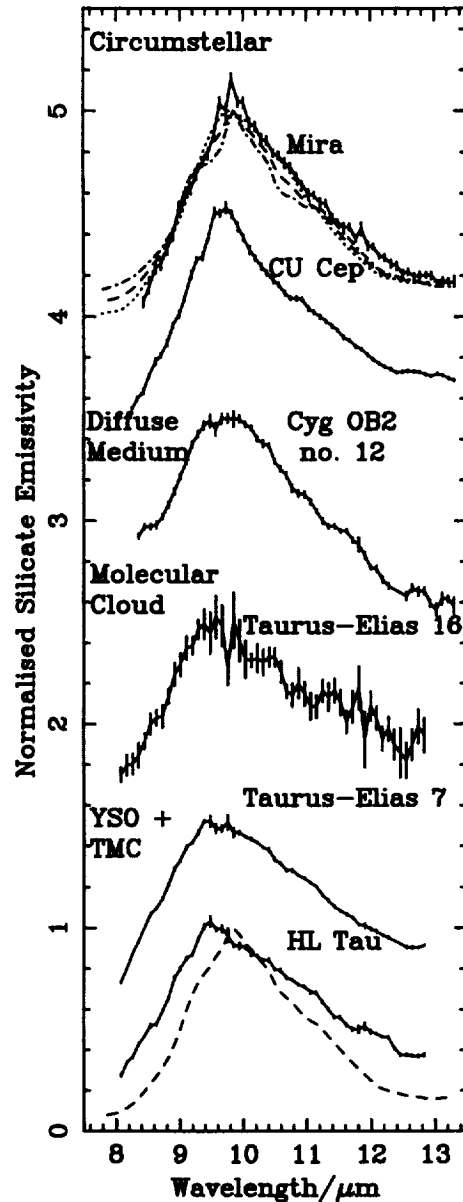


Fig. 2. The $10\text{-}\mu\text{m}$ silicate feature in astronomical environments (solid with error bars); average of plotted crystalline minerals excluding silicas (dashed); 1:1 average of crystalline and amorphous silicate (dot-dash); average of five amorphous (KRS-5 substrate) spectra from [11] (dotted). Spectra are normalized to unity and offset in the y-axis by multiples of 0.5. References: circumstellar spectra [12]; Elias 16 and Cyg OB2 no. 12 [2]; TMC (Taurus molecular cloud) + YSO [9,10].

This shoulder has previously been interpreted as the shifted peak characteristic of large grain sizes ($< 1\ \mu\text{m}$) [e.g., 2,6]; however, it could indicate the presence of a large fraction of chemically-varied crystalline pyroxenes or the existence of more Al-rich silicates in molecular clouds.

Fine Structure: Bearing in mind the uncertainties due to telluric ozone, wavelength shift with laboratory matrix, grain size, and the metal content of crystalline silicates, fine structure in well-

broad 10 μm profiles (2.1 and 2.9 FWHM respectively), absorption maxima at 9.2 μm and 9.8 μm , broad excess absorption on the long-wavelength wing of the profiles, and an 11.2 μm "bump" due to crystalline olivine. (Weak features at ~ 16.5 μm may also be due to olivine.) The ~ 18 - μm features are broad and featureless with absorption maxima at 18.9 μm and 19.4 μm respectively.

How do astronomical silicates compare with GEMS? First, 10- μm astronomical silicates exhibit significant variation. For example, there is a decrease in the wavelength of maximum absorption (or emission) between circumstellar, diffuse medium, and molecular cloud environments that has been attributed to the "amorphous pyroxene" content of initially olivine-rich dust with age [10,11]. Features from individual GEMS-rich specimens exhibit similar variation. The similarity is intriguing because attempts to fit the 10- μm astronomical silicate feature in a wide variety of environments (circumstellar, diffuse medium, young stellar objects, and comets) using the spectra of other amorphous and crystalline silicate minerals have been largely unsatisfactory [12–14]. The greatest discrepancy occurs in the FWHM of the features since silicate minerals range between 1.7 and 2.5 μm , while the astronomical features are typically >2.5 μm wide. Molecular cloud profiles (e.g., Trapezium) are broader than those of circumstellar and diffuse medium silicates, due mainly to a ~ 2 - μm -wide excess centered at ~ 11.5 μm . This feature has been interpreted as the shifted peak characteristic of large grain sizes (>1 μm) [13,15,16], or indicative of the presence of a large fraction of compositionally variable silicates [10]. The ~ 18 - μm astronomical feature is broad and featureless, peaks at ~ 18.5 μm , and is relatively constant. The two IDP ~ 18 - μm features so far measured peak at significantly longer wavelengths.

References: [1] Sandford S. A. and Walker R. M. (1985) *Astrophys. J.*, 291, 838. [2] Bradley J. P. et al. (1992) *Astrophys. J.*, 394, 643. [3] Waters L. B. F. M. et al. (1996) *Astron. Astrophys.*, 315, L361. [4] Mailfai K. et al. (1998) *Astron. Astrophys.*, 332, L25. [5] Crovisier J. et al. (1997) *Science*, 275, 1904. [6] Jessberger E. K. et al. (1988) *Nature*, 332, 691. [7] Bradley J. P. et al. (1999) in *Solid Interstellar Matter: The ISO Revolution*. Les Houches No 11 (L. d'Hendecourt et al., eds.), EDP Sciences, Les Ullis, 295 pp. [8] Bradley J. P. (1994) *Science*, 265, 925. [9] Reffner J. G. et al. (1994) *Synch. Rad. News*, 7, 30. [10] Bowey (1998) Ph.D. thesis, Univ. of Central Lancashire, Preston, UK. [11] J. Gürtler and Henning T. (1986) *Astrophys. J.*, 128, 163. [12] Mutschke H. (1998) *Astron. Astrophys.*, 333, 188. [13] Bowey (1998) Ph.D. thesis, Univ. of Central Lancashire, Preston, UK. [14] Jäger C. (1994) *Astron. Astrophys.*, 292, 641. [15] Hanner M. S. et al. (1994) *Astrophys. J.*, 425, 274. [16] Simpson J. P. (1991) *Astron. Astrophys.*, 368, 570.

INTERPRETATION OF EXTRAGALACTIC EXTINCTION MEASUREMENTS USING THE MAXIMUM ENTROPY METHOD. G. C. Clayton¹, M. J. Wolff², K. D. Gordon¹, K. A. Misselt¹, ¹Department of Physics and Astronomy, Louisiana State University, Baton Rouge LA 70803, USA (gclayton@fenway.phys.lsu.edu), ²Space Science Institute, Suite 294, 1234 Innovation Drive, Boulder CO 80303-7814, USA (wolff@colorado.edu).

Introduction: Understanding interstellar dust and its role in the universe are very important. Virtually all observations of astrophysical objects and their physical processes are affected by the

presence of dust either within the system being studied or along its line of sight. Properties of galactic dust have been amenable to study through observations of scattering and absorption along individual sightlines toward point sources, and through high spatial resolution observations of extended sources. The assumption of galactic dust properties in modeling the effects of extragalactic dust can and does lead to large errors. With the aid of NASA observatories such as Hubble Space Telescope (HST), interstellar dust in the Local Group galaxies can be subjected to the same kind of observations used to study galactic dust. Individual sightlines can be observed at high spatial resolution allowing simple geometries to be studied.

Results and Discussion: We present size distributions of interstellar dust grains derived from several sightlines in three Local Group galaxies: the Small and Large Magellanic Clouds, and M31. Employing the maximum entropy method (MEM) algorithm, as developed by Kim et al. [1–3], we fit interstellar extinction measurements which span the wavelength range 0.125–3 μm . In order to facilitate comparison, our sample includes several galactic sightlines whose extinction curves share some similarities with the extragalactic targets. Our work has greatly benefited from the recent reanalysis of IUE observations of the Magellanic Clouds [4,5]. The grain models employed for this presentation are the simplistic homogeneous sphere models (i.e., [6] (MRN)) with two (graphite, silicate) or three (graphite, silicate, and amorphous C) components. Though such usage is only a first step, the results do provide interesting insight into the use of grain size as a diagnostic of extragalactic environment.

The versatility of the MEM technique allows one to easily include a range of grain models in the analysis, from the simple MRN-like approach, to more realistic composite grains that can include the effects of porosity, solid inclusions (silicate, graphite, superparamagnetic, etc.), and alignment.

References: [1] Kim S.-H. and Martin P. G. (1994) *Astrophys. J.*, 431, 783. [2] Kim S.-H. et al. (1994) *Astrophys. J.*, 422, 164. [3] Kim S.-H. and Martin P. G. (1995) *Astrophys. J.*, 442, 172. [4] Gordon K. D. and Clayton G. C. (1998) *Astrophys. J.*, 500, 816. [5] Misselt K. A. et al. (1999) *Astrophys. J.*, in press. [6] Mathis J. S. et al. (1977) *Astrophys. J.*, 217, 425.

BUILDING A NETWORK OF SELF-CONSISTENT MID-INFRARED CALIBRATION STARS. M. Cohen¹, R. G. Walker¹, and F. C. Witteborn², ¹Vanguard Research Inc., 5321 Scotts Valley Drive, Suite 204, Scotts Valley, CA 95066, USA, ²Mail Stop 245-6, NASA Ames Research Center, Moffett Field CA 94035-1000, USA.

Introduction: Once spectrometers are operating under stable reproducible conditions (e.g., in space), the ultimate limitation to spectral accuracy and reliability becomes our knowledge of calibration stars. I discuss the methods we have used to establish an all-sky network of absolute calibrators spanning a 12- μm dynamic range of 160 [1]. We have taken great care to assure the self-consistency of this network: that is, whether using a faint or a bright standard, one obtains the same $\mu\text{V/s}$ detector output per W/cm^2 incident irradiance.

Network: The network consists fundamentally of an inverted pyramid. At the apex are two hot stars represented by Kurucz theoretical models (Sirius and Vega) [2]. The second rank consists

of 12 bright K0-M0III; and derived from these are 422 fainter cool giants within the same spectral range. There are direct ties to the absolute calibrations of COBE/DIRBE [3], both the near- and mid-infrared IRTS spectrometers; MSX; ISO, particularly the SWS; and WIRE. First space-based validations from the IRTS/NIRS demonstrate this self-consistency, while MSX absolute radiometry (analysis still in progress) assures a precision of better than 3% for the tier of bright giants and Sirius, our primary reference star.

Future Developments: All the observed spectra (as distinct from the Kurucz models) are low-resolution (resolving power ~ 50 –250), 1.2–35 μm complete (except for tiny gaps in the terrestrial CO_2 bands at 4.3 μm). I describe how one might extend these calibrators down in intensity and up in resolving power to meet the needs of future groundbased, airborne, and spaceborne spectrometers. Both these advances will be necessary to support the new generation of infrared instruments and astronomical questions.

Goals: One long-term goal is to use theoretical model atmospheres to predict the emergent spectra of cool giants at resolving powers of at least 2000 (like the highest non-Fabry-Perot modes of ISOSWS and comparable to several groundbased instruments). Another is to rely partially on normal A-dwarfs whose spectra can be well modeled. Yet another is to extend the current network down from a 12- μm flux density of 5 Jy to 5 mJy. I illustrate these new directions through use of ISO spectra, KAO spectra of asteroids, and the calibration needs of WIRE.

References: [1] Cohen M. et al. (1999) *Astrophys. J.*, in press. [2] Cohen M. et al. (1992) *Astrophys. J.*, 104, 1650. [3] Cohen M. (1998) *Astrophys. J.*, 115, 2092.

FIRST DETECTION OF POLARIZATION IN THE CO BANDHEAD EMISSION IN YOUNG STELLAR OBJECTS: A SIGNATURE OF THE INNER REGIONS OF DISKS IN SSV 13 AND DG TAU. C. Colomé, Instituto de Astronomía, Universidad Nacional Autónoma de México, México, and McDonald Observatory, University of Texas–Austin, Austin TX, USA.

We report the first detection of polarization in the CO bandhead emission at near-infrared wavelengths ($\lambda = 2.3$ mm). In this paper we describe the results for two young stellar objects: SSV 13 and DG Tau. The near-infrared polarization ($P \geq 13\%$) of the CO bandhead in both objects is considerably higher than the polarization in their continua. This suggests that, at least in those two objects, the CO emission originates in disks, rather than in stellar winds.

It has been 20 years since the first detection of the first overtone bands of CO in the Becklin-Neugebauer (BN) object [1]. Possible mechanisms for the excitation of the vibrational states of CO have been described by Scoville et al. [2] and Krotkov et al. [3]. The detection of the CO bandhead in the BN object and further NIR spectroscopy of the same region [4] showed that in order to reproduce the relative band strengths, high vibrational temperatures are required (~ 3500 K). It was also noticed since then [1,4] that the CO bandhead emission must be localized within a small radius (a few AU) of the BN object, since the features are seen with the same strength in spectra taken with quite different apertures.

TABLE 1. CO and continuum polarization.

Object	Filter	P($\pm 2\%$)	Q($\pm 3^\circ$)
SSV13	CO bandhead ($v = 2-0$)	16	66
	Kw' (1.9–2.4 mm)	5	73
DG Tau	CO bandhead ($v = 2-0$)	13	79
	Kw' (1.9–2.4 mm)	6	108

Dozens of young stellar objects (YSOs) have been detected via their CO bandhead, either in emission or absorption [5–11]. All the observations exhibit band strengths that are consistent with excitation temperatures of 2500–4000 K. It is still not known how this gas is excited and where it is located, nor it has been possible to study its kinematics. Two possible scenarios have been proposed for the origin of the CO emission: (1) an outflowing wind, or (2) a neutral circumstellar disk [7 and references therein]. Recent high-resolution infrared spectroscopy in the CO bandhead [10–12] of YSOs shows more evidence for a “disk” origin for the CO emission, rather than a wind origin. All these recent observations show that the bandhead often exhibits the characteristic shape of emission from a rotating disk [12 and references therein]. A contribution from a wind to the CO emission of a rotating disk can be ruled out by the absence of line asymmetries in the NIR spectra. Line asymmetries would be expected due to the occultation the receding flow by an optically thick disk. An additional line asymmetry would be expected if the wind (cooler than the star and disk) would absorb the stellar and disk continuum. These effects have not been observed to date.

The motivation for this work is the increasingly common detection of the CO bandhead emission in YSOs [7] since it was first discovered by Scoville et al. [1]. Most YSOs are surrounded by dust envelopes, which scatter not only the continua of young stars but also the radiation originating in the inner regions of their disks (if present). Scatter radiation can be detected as “polarized light.” Narrow-band polarimetry and centered at 2.3 mm, the first overtone ($v = 2-0$) of the CO emission, of YSOs could provide perhaps the best method to distinguish between the two possible origins: circumstellar disks or neutral stellar (or disks) winds.

As part of an ongoing observational project at McDonald Observatory SSV 13 DG Tau have been observed at near-infrared wavelengths using the polarimetric near-infrared camera ROKCAM [13] of the University of Texas. The CO bandhead emission from both SSV 13 and DG Tau is unresolved with our resolution. Their FWHM are approximately 1.2" (3 pixels). For both objects the polarization measured with the narrow band filter centered in the CO bandhead is much higher than the one obtained using a broader K-band filter. The results are summarized in Table 1. For these two objects the polarimetry provides evidence for a “disk” origin for the CO emitting region, rather than a wind origin. In the latter case we would expect the scattering dust to see a more “isotropic” radiation from the CO gas, locally produced, and in such case, the large values of the polarization ($P \geq 13\%$) are difficult to reproduce.

References: [1] Scoville N. Z. et al. (1979) *Astrophys. J.*, 232, L121. [2] Scoville N. Z. et al. (1980) *Astrophys. J.*, 240, 929. [3] Krotkov R. et al. (1980) *Astrophys. J.*, 240, 940. [4] Scoville N. Z. et al. (1983) *Astrophys. J.*, 275, 201. [5] Thompson R. I. (1985) *Astrophys. J.*, 299, L41. [6] Geballe T. R. and Persson

S. E. (1987) *Astrophys. J.*, 312, 297. [7] Carr J. S. (1989) *Astrophys. J.*, 345, 522. [8] Carr J. S. and Tokunaga A. T. (1992) *Astrophys. J.*, 393, L67. [9] Carr J. S. et al. (1993) *Astrophys. J.*, 411, L37. [10] Chandler C. J. et al. (1993) *Astrophys. J.*, 412, L71. [11] Chandler C. J. et al. (1995) *Astrophys. J.*, 446, 793. [12] Najita J. et al. (1996) *Astrophys. J.*, 462, 919. [13] Colomé C. and Harvey P. M. (1993) *RevMexAA*, 27, 29.

57-96

THE THERMAL INFRARED SPECTRA OF COMETS HALE-BOPP AND 103P/HARTLEY 2 OBSERVED WITH THE INFRARED SPACE OBSERVATORY. J. Crovisier¹, K. Leech², D. Bockelée-Morvan¹, E. Lellouch¹, T. Y. Brooke³, M. S. Hanner³, B. Altieri², H. U. Keller⁴, T. Lim^{2,5}, T. Encrenaz¹, A. Salama², M. Griffin⁵, T. de Graauw⁶, E. van Dishoeck⁷, and R. F. Knacke⁸, ¹Observatoire de Paris–Meudon, F-92195 Meudon, France (crovisie@obspm.fr), ²Infrared Space Observatory Data Centre, Astrophysics Division of ESA, Villafraanca, Spain, ³Jet Propulsion Laboratory, Pasadena CA, USA, ⁴Max-Planck-Institut für Aeronomie, Katlenburg-Lindau, Germany, ⁵Queen Mary and Westfield College, London, UK, ⁶SRON, Groningen, The Netherlands, ⁷Leiden Observatory, The Netherlands, ⁸Pennsylvania State University, Erie PN, USA.

Introduction: The Infrared Space Observatory (ISO) offered us the opportunity to observe celestial bodies over the full infrared range from 2.4 to 196 μm . This spectral domain is of peculiar interest for comets. Cometary parent molecules, likely to have sublimated from the nucleus ices, can be investigated through their fundamental bands of vibration in the 2.5–12- μm region. With temperatures ranging between 100 and 400 K or more, cometary grains show thermal emission peaking in the 5–200- μm region, where spectral features related to their chemical nature may be expected.

Observations: We report here on spectroscopic observations of comets that were conducted with ISO by an international team of investigators. Other programs by other teams were aimed at photometric and imaging observations, in order to study cometary dust in the coma, the tails and the trails, and to try to disentangle the emission of the comet nuclei from that of the dust.

Our observations were undertaken in the frame of two programs. The first one, a guaranteed time program, had to be planned on advance. It was thus aimed at short-period, predictable comets. The nominal target, 22P/Kopff, was weaker than expected and could not be observed at the moment it was the brightest. Fortunately, it was possible to observe a second comet, 103P/Hartley 2, during the extended lifetime of ISO, when the comet was at its brightest near perihelion [7]. The second program, an open-time target-of-opportunity program, was aimed at any bright comet that might appear during ISO's lifetime. We were lucky to benefit from the apparition of the exceptional Comet Hale-Bopp (1995 O1). Unfortunately, because of the visibility constraints of ISO, the comet could only be observed when it was at $r_h > 2.8$ AU from the Sun. Observations were secured preperihelion on April 1996 ($r_h = 4.6$ AU) and September–October 1996 ($r_h = 2.8$ AU) and postperihelion on December 1997 ($r_h = 3.9$ AU) and April 1998 ($r_h = 4.9$ AU) [1–6].

The observations of gas-phase species will not be discussed in detail here: H_2O , CO_2 , and CO were detected, and their produc-

tion rates, as well as physical parameters for cometary water, were determined as a function of heliocentric distance [1–4,6,7].

Results on Comet Hale-Bopp: For the four observing periods of Comet Hale-Bopp, low-resolution spectra were observed from 2.5 to 12 μm with the grating spectrometer of the ISO photometer. All spectra show a strong silicate band at 10 μm with a peak at 11.3 μm indicating the presence of crystalline olivine. This constituent is observed to be present whatever the heliocentric distance (4.9 to 2.8 AU), both pre- and postperihelion.

In September–October 1996, high signal-to-noise ratio spectra of the comet were obtained with the short- and long-wavelength spectrometers of ISO. Beyond 6 μm , the spectrum of Comet Hale-Bopp was dominated by dust thermal continuum emission, upon which broad emission features were superimposed, the strongest appearing at 10, 19.5, 23.5, and 33.5 μm . The wavelengths of all these peaks correspond to those of Mg-rich crystalline olivine (namely forsterite, Mg_2SiO_4) [2–4,6]. A careful study of the ISO spectrum, complemented by groundbased spectra of the 10- μm region obtained at smaller heliocentric distances, show that amorphous silicates as well as pyroxenes are also present [8,9]. It is remarkable that the spectrum of Comet Hale-Bopp in this spectral domain closely resembles that of the dust disks around some young stars (such as that of HD 100546, an intermediate star between Vega-like objects and Herbig Ae-Be stars) that were also observed by ISO [10]. Thus, the dust contained in such disks should be similar to cometary dust. This contrasts with interstellar silicates, which are amorphous.

In the September–October 1996 spectra, emission features at 44 and 65 μm and possible absorption at 2.9–3.2 μm were detected, characteristic of crystalline water ice. A temperature of 165 K was inferred for this water ice. This suggests that grains of water ice were still present at a distance of 2.9 AU from the Sun and that they could be a significant source of water release in the coma [5].

No sign of PAHs could be found in the spectrum of Comet Hale-Bopp (especially in the 6–9 μm region, where they are expected to have strong bands not blended with silicate features). However, one cannot exclude that cometary PAHs are revealed at shorter heliocentric distances than those of the ISO observations of Comet Hale-Bopp.

Results on Comet P/Hartley 2: Whereas Hale-Bopp was a long-period comet presumably coming from the Oort cloud, 103P/Hartley 2 is a Jupiter-family comet that supposedly originated from the Edgeworth-Kuiper belt. It was observed in December 1997–January 1998 at $r_h \approx 1$ AU. A 6–17- μm low-resolution spectrum obtained with the VF of ISOCAM showed a weak 10- μm silicate band with an intensity only 15% of the continuum [7]. The presence of a peak at 11.3 μm revealed the presence of crystalline silicates

Conclusion: ISO observations — complemented by ground-based spectroscopic observations in the infrared and radio domains — show that there is a great similarity in the composition of interstellar and cometary ices. This agrees with the hypothesis that comets could have formed from basically unprocessed interstellar matter. However, the presence of crystalline silicates in the dust of both a Oort-cloud comet and a Jupiter-family comet shows that these bodies have also incorporated processed material at some stage of their formation.

References: [1] Crovisier J. et al. (1996) *Astron. Astrophys.*, 315, L385–L388. [2] Crovisier J. et al. (1997) *Science*, 275,

1904–1907. [3] Crovisier J. et al. (1997) *ESA SP-419*, 137–140. [4] Leech K. et al. (1998) *Earth Moon Planets*, in press. [5] Lellouch E. et al. (1998) *Astron. Astrophys.*, 339, L9–L12. [6] Crovisier J. et al. (1999) *ESA SP-427*, in press. [7] Crovisier J. et al. (1999) *ESA SP-427*, in press. [8] Brucato J. R. et al. (1999) *Planet. Space Sci.*, in press. [9] Wooden D. H. et al. (1999) *Astron. Astrophys. J.*, in press. [10] Malfait K. et al. (1998) *Astron. Astrophys.*, 332, L25–L28.

88-89

AIRES: AN AIRBORNE INFRARED ECHELLE SPECTROMETER FOR SOFIA. J. Dotson¹, E. Erickson², M. Haas², S. Colgan², J. Simpson¹, C. Telesco³, J. Wolf⁴, and E. Young⁵, ¹SETI Institute, Mail Stop 245-6, NASA Ames Research Center, Moffett Field CA 94035, USA (dotson@cygnus.arc.nasa.gov), ²NASA Ames Research Center, Moffett Field CA 94035, USA, ³Department of Astronomy, Bryant Space Science Building, University of Florida, Gainesville FL 32611, USA, ⁴DLR, Germany, ⁵University of Arizona, Tucson AZ, USA.

SOFIA will enable astronomical observations with unprecedented angular resolution at infrared wavelengths obscured from the ground. To help open this new chapter in the exploration of the infrared universe, we are building AIRES, an Airborne Infra-Red Echelle Spectrometer. AIRES will be operated as a first generation, general purpose facility instrument by USRA, NASA's prime contractor for SOFIA. AIRES is a long-slit spectrograph operating from 17–210 μm . In high-resolution mode the spectral resolving power is $\sim 10^6 \mu\text{m}/\lambda$ or $\sim 10^4$ at 100 μm . In low-resolution mode the resolving power is about 100 \times lower. AIRES includes a slit-viewing camera that operates in broad bands at 18 and 25 μm .

AIRES will be ideal for spectral imaging of gas-phase phenomena in the interstellar medium (ISM). Far-infrared line observations probe the excitation, pressure, density, luminosity, chemical composition, heating and cooling rates, mass distribution, and kinematics in the various components of the ISM. The lines offer invaluable and often unique diagnostics of conditions in such diverse places as star-forming regions, circumstellar shells, the Galactic Center, starbursts in galaxies, and the nuclei of active galaxies. AIRES will provide astronomers with new insights into these and other environments in the ISM. It will also be useful for studies of solar system phenomena such as planetary atmospheres and comets, for example.

AIRES' low-resolution mode will enable comparison of infrared continuum emission with line emission from interstellar clouds. It will also permit measurement of long wavelength features of interstellar grains and solid surfaces of solar system bodies, as well as a variety of other problems.

89-90

AXISYMMETRIC MODELING OF SILICATE CIRCUMSTELLAR DISKS. S. K. Dunkin and M. J. Barlow, Department of Physics and Astronomy, University College London, Gower Street, London WC1E 6BT, UK (skd@star.ucl.ac.uk).

Introduction: The presence of dust grains around many stars is not disputed. However, the composition and size of these dust grains, as well as the geometry and inclination the dust takes as

a whole, is. There are three main classes of infrared (IR) excess star whose dust may be representative of either the beginning or remnants of planetary systems: the main-sequence Vega-like stars and pre-main sequence Herbig Ae/Be (HAeBe) and T Tauri stars.

There have been many attempts to model the spectral energy distributions (SEDs) of HAeBe stars and their lower mass counterparts to determine the characteristics of the dust [e.g., 1–4]. Attention has also been paid to the prototype Vega-like stars too, which exhibit only a mid- or far-IR excess, but relatively little work has been carried out on the class of Vega-like stars that have substantial near-IR excess as well. The excess emission from some of these stars cannot be modeled completely using optically thin codes [5,6], and this work concentrates on modeling one of them using an optically thick radiative transfer code.

Modeling: Several Vega-like stars from the list of [7] were studied and one, HD 144432, with both a near- and far-IR excess, was chosen for modeling. This star has a very strong silicate emission feature (Fig. 1 and [8]). Such a signature helps to place strong constraints on the compositional parameter of the model.

The code used here is a modified version of that used by [9]. Skinner et al. [10] explains the major refinements of the code, and Dunkin [11] describes in more detail the various parameters and usage of it. There are many free parameters in this code, but it is still possible to place constraints on certain values.

Spherical vs. nonspherical distributions. While asymmetric geometries have been positively identified for a few stars (e.g., β Pic [12], HD 163296, and AB Aur [13]), the dust geometries of most IR excess stars remains uncertain. Before attempting modeling, it is possible to provide evidence for or against the presence of spherical envelopes by comparing the extinction observed towards a star to that expected if such an envelope was present. By using this method (as outlined in [13]) we determined that only two of the 11 Vega-like stars we looked at could potentially have spherical distributions of dust, neither of which was our modeled star, HD 144432. Miroshnichenko et al. [4] have been able to produce fits to several HAeBe stars using spherical envelopes with

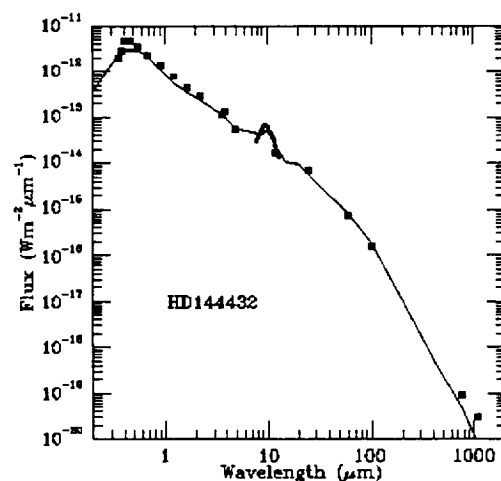


Fig. 1. Optically thick silicate model of HD 144432 plotted on observational data. Note the large silicate feature at 10 μm .

dust density profiles obeying an $r^{-1.5}$ power law. Their model is sufficiently similar to the one used here for comparisons to be made between the two. We created models for two of their stars using parameters as close as possible to theirs. We confirmed that spherical envelopes may produce reasonable fits to the data for these stars, and used these parameters as a base for the modeling of our chosen star. No spherical model could be made to fit the observed data for HD 144432, despite changing inclination, grain size distribution, optical depth, density distribution, and composition. We therefore conclude that HD 144432 has its dust distributed in a nonspherical geometry, most likely in a disk.

Composition of the disk. Sylvester et al. showed HD 144432 to have a very strong silicate feature [8]. Models were run using composite grains of amorphous C and silicate, but only a model using 100% silicate grains could reproduce the observed silicate peak. It is unlikely that the actual disk is pure silicate, but this model does show that silicate grains must dominate the total population.

Other parameters. A grain size distribution was used as opposed to a single grain size as this is probably a more realistic situation. Interestingly, millimeter-sized grains were found to be necessary to produce the flux seen at millimeter wavelengths. This implies that at least some of the dust has accreted to form large grains. We cannot put an upper limit on the grain growth in this system, but cannot rule out the possibility of even larger grains being present. An inner radius of the disk at 0.13 AU was required to produce the near-IR excess: If the inner regions of the disk were further out, not enough flux at these short wavelengths can be produced. Farther out, large grains and an outer radius of ~ 1300 AU is required to reproduce the millimeter-wave flux. The outer radius is more uncertain than the inner radius, and may well be larger. 1300 AU in our solar system places us somewhere in or just outside the Kuiper belt where a lot of "left-over" debris from the formation of our planets resides. However, HD 144432 is an A9/F0 star and is therefore hotter and more massive than our own Sun, so direct comparisons between systems is difficult to make. The disk is optically thick, with an optical depth, τ , of 3.0 required to produce the flux seen. The disk is therefore quite substantial, with a mass of 2.71×10^{-6} solar masses. Since the inclination of the system is unknown, an inclination of 45° was assumed (edge-on and face-on inclinations are ruled out by the $v \sin i$ of the star). Inclination is known to have little effect on the resultant models using this code, unless it is close to 0° or 90° [11]. The final model is shown in Fig. 1 below.

Summary: In summary, we have used an optically thick radiative transfer code to model a Vega-like star, HD 144432, with near-IR excess. The dust around this star is not distributed in a spherical geometry and can be fit well using a flattened disk distribution. The large silicate feature at $10 \mu\text{m}$ implies that the dust in this system is dominated by silicate grains, a fact reflected in the final model.

This code can best be used in situations where the dust is likely to be optically thick, as in the case of HD 144432. Further work is underway to model other stars, both main sequence and pre-main sequence, to compare with the results presented here.

Acknowledgments: SKD was funded by the Particle Physics and Astronomy Research Council (PPARC), UK, for the duration of this work. Extensive use was made of the Starlink computing facilities funded by the PPARC.

References: [1] Adams F. C. et al. (1988) *Astrophys. J.*, 326, 865 [2] Hartmann L. et al. (1993) *Astrophys. J.*, 407, 219. [3] Mannings V. G. (1994) *MNRAS*, 271, 587. [4] Miroshnichenko A. et al. (1997) *Astrophys. J., Lett.*, 475, L41. [5] Sylvester R. J. and Skinner C. J. (1996) *MNRAS*, 283, 457. [6] Sylvester R. J. et al. (1997) *MNRAS*. [7] Walker H. J. and Wolstencroft R. D. (1988) *PASP*, 100, 1509. [8] Sylvester R. J. et al. (1996) *MNRAS*, 279, 915. [9] Collison A. J. and Fix J. D. (1991) *Astrophys. J.*, 368, 545. [10] Skinner C. J. et al. (1997) *Astron. Astrophys.*, 328, 290. [11] Dunkin S. K. (1997) Chapter 6, Ph.D. thesis, Univ. of London. [12] Smith B. A. and Terrile R. J. (1984) *Science*, 226, 1421. [13] Mannings V. G. and Sargent A. I. (1997) *Astrophys. J.*, 490, 792.

92-91

LABORATORY MEASUREMENTS OF SPECTRAL EMISSIVITY OF MATERIALS ANALOGS TO THE MARTIAN SOIL AND DUST. S. Fonti¹, A. Blanco¹, M. I. Blecka², F. De Carlo¹, V. Orofino¹, and S. Solazzo¹, ¹Physics Department, University of Lecce, C.P. 193, 73100 Lecce, Italy (fonti@le.infn.it), ²Space Research Centre, Polish Academy of Sciences, ul. Bartycka 18a, 00-176 Warsaw, Poland.

Introduction: In recent years the debate about the climatic history of Mars has been quite alive. In particular the presence of liquid water in large basins for long periods is supported by several indications [1,2]. One of the main issues is to understand if such climatic conditions lasted long enough to allow the development of some form of life [3]. Although it seems premature to expect a definite answer on the subject, interesting suggestions could be given by a systematic spectroscopic survey of the martian surface. As an example, the detection of carbonates in selected regions of the planet [4], can be important to assess that the presence of large bodies of standing water has lasted long enough to allow an abundant precipitation of such compounds.

Unfortunately, up to now no definite identification has been made by any instrument orbiting around Mars. In fact, the Thermal Emission Spectrometer (TES), onboard Mars Global Surveyor, has set only an upper limit of about 10% to the amount of these materials [5], while the detection, yet to be confirmed, about the possible presence of carbonates comes from two observations made from the Earth [6,7]. In these cases, however, it is almost impossible to link the observation to a specific area of the planet.

In this scenario an important role can be played by laboratory measurements on materials, such as carbonates, which are supposed to be present on the martian surface, as well as in the atmospheric dust. The measurements should be carried out in different environmental conditions, on both bulk and dust samples, varying not only the composition, but also the average grain size and the compactness of the granulated specimen [8]. The output of the laboratory measurements can be fed into an appropriate radiation transfer model able to produce reliable synthetic spectra of the martian surface and atmosphere. Such spectra could be conveniently compared with the actual spectra of Mars, which will be available from current (Mars Global Surveyor) and future (Mars Express) martian missions for the identification of the spectroscopic signatures of materials. In this respect it is worthwhile to note that most of such materials (carbonates, sulfates, silicates, etc.) exhibit their characteristic bands in the mid-infrared region

of the spectrum (5–50 μm) and that in this range the martian spectra are dominated by the thermal emission of the surface.

The emissivity measurements presented in this work are part of a research program, carried out in the Astrophysics Laboratory of the Department of Physics of the University of Lecce, aimed to a systematic study of the possible analogs to the martian materials.

Experiment: The measurements of spectral emissivity have been performed using a Perkin-Elmer Fourier Spectrometer Model Spectrum 2000, equipped with an emission port. The spectral range was limited between 2000 and 500 cm^{-1} (5–20 μm), due to the presence of high noise level outside this interval. It would be useful to extend the range on the long wavelength side and we are presently working in this direction. An optomechanical accessory was especially designed and manufactured in our laboratory, in order to concentrate the energy emitted by the sample into the input port of the spectrometer. Such accessory allows, by means of a moveable mirror, to look alternatively to the sample, kept at a nominal temperature variable between ambient and 300°C, a reference black body at the same nominal temperature, and a second black body at constant ambient temperature.

The comparison between the spectrum obtained looking at the sample and that of the hot black body is the basic process for calculating the spectral emissivity, while the spectrum of the cold black body allows to account for the real zero of the spectrometer. However, the actual procedure is more complicated and requires several intermediate steps in order to assess some important preliminary parameters. As an example, we can consider the unavoidable difference between the nominal temperature at which the thermostatic devices are set and the real temperature of the emitting surfaces. To account for this, it is necessary to perform several measurements at different nominal temperature and compare the results. The effective temperature of the emitting surfaces is found by means of an iterative calculation, based on the comparison between the experimental results and the theoretical predictions.

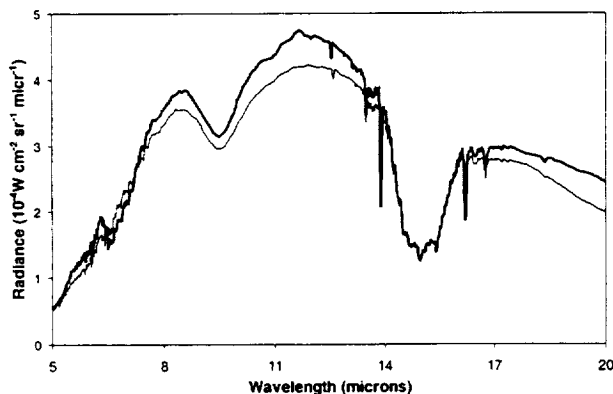


Fig. 1. Synthetic spectra of Mars, calculated in vertical geometry, obtained using the laboratory measured emissivity of palagonite and limestone. The two spectra refer to a surface of pure limestone (thick line) and of pure palagonite (thin line); in both cases the atmosphere is thought to be loaded with micrometer-sized grains of pure palagonite.

It is important to stress that, although the temperature can be varied in a wide range, the best results have been obtained for a nominal temperature higher than 150°C. Even if other authors [9–11] have done emissivity measurements using a considerably lower temperature, our choice has the great advantage to reduce drastically the influence of the reflected radiation on the result of the measurement. On the other hand, using a temperature much higher than the ambient temperature can produce temporal instability and spatial inhomogeneity. For the second point, the use of the effective temperature of the emitting surface, directly evaluated from the measurements, will conveniently average on possible small inhomogeneities. As far as the temporal instability is concerned, we think that the use of a fast instrument, such as a Fourier spectrometer, together with a continuous monitoring of the black body kept at ambient temperature, ensures that the level of a possible temporal instability will be within a few percent.

Results and Discussion: In order to perform a preliminary check of the visibility of the carbonate component in the spectra of Mars, we measured the spectral emissivity of a typical carbonate as limestone and of palagonite, which is assumed to be the best terrestrial analog to martian silicates. We then fed our measured emissivities in an advanced model of radiative transfer calculation [12], which takes into account the emission of the martian surface and the emission and the extinction by the atmospheric dust and gases. The resulting synthetic spectra, shown in Fig. 1, have been obtained using as main input parameters to the model the vertical optical thickness of the dust at 10 μm ($\tau_D = 1.1$), the pressure ($p_S = 6$ mbar), and the temperature ($T_S = 270$ K) at the surface of Mars. A more detailed discussion of the model can be found elsewhere [13].

As it can be seen, two main features characterize the spectrum obtained assuming a pure carbonate surface (thick line): the typical band at 6.7 μm and another minor, but still evident structure at 11.4 μm . Of course, these features are not seen in the calculation assuming pure palagonite surface (thin line). It is interesting to note that these features are detectable even when the atmosphere is loaded with palagonite dust. Obviously, in order to draw a specific conclusion, more tests have to be done, using composite surfaces with variable percentages of the main components. We can conclude, however, that the results of the present work indicate that the comparison of the synthetic spectra with the observational ones can be a very promising tool for the spectroscopic identification of carbonates and other materials on the surface of Mars.

Acknowledgments: This work has been partially supported by the Italian Space Agency and by the Polish State Committee for Scientific Research under grants 2P03C01010 and P03C00515.

References: [1] Goldspiel J. M. and Squyres S. W. (1991) *Icarus*, 89, 392–410. [2] Scott D. H. et al. (1995) *USGS Misc. Inv. Ser. Map I-2461*. [3] McKay D. S. et al. (1996) *Science*, 273, 924–930. [4] Orofino V. et al. (1999) *Proceedings of the 2nd Italian Meeting of Planetary Sciences, Bormio, 20–25 January 1998*, in press. [5] Christensen P. R. et al. (1998) *Science*, 279, 1692–1698. [6] Pollack J. B. et al. (1990) *JGR*, 95, 14595–14627. [7] Lellouch E. et al. (1999) *Proceedings of the International Symposium on Mars Exploration Program and Sample Return Mission, Paris, 2–5 February 1999*, 011/52 (40). [8] Arnold G. (1991) *Vibrational Spectroscopy*, 2, 245–249. [9] Nerry F. et al. (1990) *JGR*, 95, 7027–7044. [10] Christensen P. R. and Thliveris

Harrison S. (1993) *JGR*, 98, 19819–19834. [11] Salisbury J. W. et al. (1994) *JGR*, 99, 11897–11911. [12] Blecka M. I. et al. (1997) *Adv. Space Res.*, 19, 1281–1284. [13] Blecka M. I. (1999) *Adv. Space Res.*, in press.

THEORETICAL MODELING OF RADIATIVE TRANSFER IN PLANETARY REGOLITHS. B. W. Hapke, Department of Geology and Planetary Science, University of Pittsburgh, Pittsburgh PA 15260, USA.

The status of theories of thermal emission from particulate media, such as planetary regoliths, is discussed. When the particles are large compared with the wavelength, models based on the radiative transfer equation (RTE), which assumes that the particles scatter independently, appear adequate. Geometric optics can be used to calculate the optical properties of the particles because diffraction by the particles effectively disappears. The emissivities of individual particles can display spectral features of high contrast. However, multiple scattering in a regolith may greatly reduce the contrast, decreasing the usefulness of thermal IR spectral measurements for remote compositional identifications [1]. The maximum in the spectral emissivity does not occur exactly at the Christiansen frequency, as is commonly assumed (although it is close), but rather at the wavelength in a reststrahlen band where the light scattered from a particle changes over from scattering within the interior of the particle (volume scattering) to reflection from the surface [2].

In order to calculate the emissivity and subsurface temperature, the RTE must be simultaneously solved along with the heat transfer equation [3]. Such solutions intrinsically include radiative conductivity and the solid state greenhouse effect. Including radiative effects quantitatively alters the calculated subsurface temperature distribution.

The status of thermal emission models is much less satisfactory when the particle size is comparable to or smaller than the wavelength. The use of the RTE is questionable then because coherent effects do not allow the particles to scatter independently. Unfortunately, this case probably includes most planetary regoliths. Since coherent effects have a range of roughly a wavelength, this suggests an approach in which the regolith is averaged over wavelength-sized boxes to obtain effective particles whose optical properties may be inserted into the RTE.

References: [1] Hapke B. (1993) *Theory of Reflectance and Emittance Spectroscopy*, Cambridge Univ. [2] Hapke B. (1996) *JGR*, 101, 16833. [3] Hapke B. (1996) *JGR*, 101, 16817.

OPTICAL PROPERTIES OF COSMIC DUST ANALOGS. Th. Henning, Astrophysical Institute and University Observatory, Friedrich Schiller University, Schillergässchen 3, D-07745 Jena, Germany (henning@astro.uni-jena.de).

Small solid particles form an important component of our galaxy and others. Although they are only minor contributors to the mass of these systems, they determine the thermal, dynamical, and chemical state of the dense phases of the interstellar medium, thereby controlling the star formation process. The coagulation of

these particles in circumstellar disks is a first but decisive step toward the formation of planetesimals.

Cosmic dust grains are a very interesting system of small particles interacting with radiation, other grains, and gas particles under the extreme conditions of interstellar space. Laboratory investigations have to supply the basic data for these interactions in order to interpret the results of ultraviolet, optical, and infrared spectroscopy of dusty objects.

The talk will review laboratory measurements of the optical data of cosmic dust analogs. It will give an introduction how such materials are produced and characterized. The main techniques to measure optical constants with their pros and cons will be discussed.

Computational methods to calculate absorption and scattering efficiencies for fluffy and inhomogeneous particles from the optical constants will be presented.

References: [1] Dorschner J. and Henning Th. (1995) *Astron. Astrophys.*, 6, 271–333. [2] Henning Th. (1998) *Chem. Soc.*, 27, 315–321. [3] Henning Th. and Salama F. (1998) *Science*, 282, 2204–2210. [4] Henning Th. (1999) *Asymptotic Giant Branch Stars*, IAU Symp. 191, 221–232.

PROBLEMS IN INFRARED LABORATORY SPECTROSCOPY OF SILICON CARBIDE RESULTING FROM HIGH EXTINCTION COEFFICIENTS: INFERENCES FROM NANOCRYSTALS AND QUANTITATIVE METHODS.

A. M. Hofmeister,¹ A. K. Speck², and L. Rosen³, ¹Department of Earth and Planetary Science, Washington University, St. Louis MO, USA (hofmeist@levee.wustl.edu), ²Department of Physics and Astronomy, University College London, UK, ³Department of Mechanical Engineering, Washington University, St. Louis MO, USA.

Introduction: Infrared measurements of minerals in the laboratory are needed for identification of phases detected remotely in comets or in circumstellar dust. Silicon carbide is of particular interest due to its association with cool, C-rich stars. Unfortunately, problems with convolution of the baseline spectrum with that of the sample have gone unrecognized. As a result, spectral artifacts have been attributed to intrinsic features. Such problems are accentuated for SiC due to high reflectivity [1] and consequent high absorptivity [2].

It is generally assumed that micrometer or submicrometer particles transmit intense IR bands. As a consequence, the weight of the particles in the pellet have been used to determine the extinction coefficient, and the extinction coefficients inferred from single-crystal reflectance studies have been discounted because these were too large in comparison. However, recent study of single crystals of grossular and andradite garnets thinned by ion-milling and of powders compressed into a thin film in a diamond anvil cell showed that thicknesses below 0.1 μm are needed to transmit the most intense Si-O modes. Moreover, the results are consistent with absorptivity calculated from reflectance spectra [3,4]. These data indicate that intense peaks in a KBr pellet are due only to the finest grains, or arise from edges of grains. Because “opaque” grains exist in the sample, the baseline depends on the sample spectrum, and as a result, peak positions, widths, and

shape are falsified when the ratio of the raw data to a reference pellet is calculated.

Related problems exist in IR spectra from small particles obtained with an IR microscope. Because the image is typically masked, rather than the sample, light leakage (e.g., diffraction) around the edges of essentially opaque particles alters the zero percent transmission line [5,6]. The resulting spectra are problematic.

Experiments: To further our understanding of extinction coefficients and to delineate circumstances under which spectra are intrinsic, rather than circumstantial, we examined IR spectra from small single crystals of α -SiC, nanocrystals of structurally related AlN and TiN, and β -SiC, and commercial polycrystals. All nanosamples have grains with 2–10-nm sizes.

The nanocrystals of AlN and TiN were encapsulated in NaCl during crystallization. Standard pellets produced very broad bands, however, if the sample was diluted by compression, the spectra gradually changed into a moderately sharp peak, the position of which was replicated by a thin film of commercial, bulk sample. The production of same spectra of nano and bulk sample confirms the high extinction coefficients, the production of IR modes essentially by nearest neighbor interactions, the inconsequential contribution of surface modes, and the neutral role of the salt matrix.

Nanocrystals of β -SiC occur as clusters without a salt matrix. Grinding reduced the cluster size to micrometers as measured by TEM of one of our KBr pellets. Their thin film spectra are dominated by the TO mode at 12.2 μm , and dispersion spectra have TO and LO modes subequal in intensity. The dispersion spectrum most closely resembles thin film spectra of commercial β sample [2]. These results are consistent with the extreme hardness of SiC and initial crystal sizes. For the nanocrystals, grinding did not reduce the cluster size to sufficiently small sizes to obtain an intrinsic spectrum, but crushing did, whereas macroscopic crystals of β -SiC could not be sufficiently thinned even under pressure. Further experiments with smaller clusters are underway.

Hexagonal α -SiC platelets, 150 μm across by 5 μm thick, have maximum absorbance >2 units when sample is placed on a 100- μm aperture, but the same crystal yields a flat topped peak at 0.5 units if the image is masked to an equivalent aperture instead. For 200- μm -diameter crystals the disparity is less, but still exists. This suggests that diameters of the sample must be $>4\times$ that of the effective aperture for spectra to be representative of the sample.

Reflectivity measurements of SiC repeated for E perpendicular to c axis confirm the results of Spitzer et al. [1]. Their absorbance data does not agree with our above measurements, probably because their film was spotty. However, their calculate extinction coefficients are confirmed.

Discussion: All the above data, taken together, indicate that for SiC particles to transmit all wavelengths, the path length must be considerably below 0.1 μm . For larger path lengths, peak height and profiles are altered through instrumental errors, specifically by convolution of the baseline with the spectrum. For thickness above a micrometer, the spectra are essentially all artifacts. Hence, most published absorbance spectra of SiC have artifacts to varying degrees, and connection of trends in peak parameters with factors such as grain size, grain shape, and use of a matrix are unsupported.

Reasonable data can be obtained from dispersions if grain size distribution is restricted to small sizes and a narrow size range, as

well as to dilute samples, as in the finest particle distributions published to date [7]. Use of heavy dispersions and maximum peak heights above 0.5 to 1 absorbance units distort the peak profiles because the total path length is likely to be opaque at the peak center, while still transparent to the shoulders or sides of the peak.

It is recommended to use a thin film [2], as path length is controlled, and the same sample can be thinned until the spectrum no longer changes. Typically, the spectra no longer change once peak height is below 0.5 absorbance units. This effect occurs because the thin films are not perfectly uniform.

Conclusions: Comparing laboratory spectra to circumstellar spectra requires caution as the baseline subtraction procedures differ. However, if both the absorptions from the laboratory and in astronomical data are weak, the problems should be minimized.

References: [1] Spitzer W. G. et al. (1962) *Phys. Rev.*, 113, 127. [2] Speck A. K. et al. (1999) *Astrophys. J.*, in press. [3] McAloon B. P. and Hofmeister A. M. (1993) *Am. Mineral.*, 78, 957. [4] Hofmeister A. M. (1995) in *A Practical Guide to IR Microscopy* (H. J. Humicki, ed.), pp. 377–416. [5] Messerschmidt R. G. (1995) in *A Practical Guide to IR Microscopy* (H. J. Humicki, ed.), pp. 1–40; Reffner J. A. and Maroglio P. A. (1995) in *A Practical Guide to IR Microscopy* (H. J. Humicki, ed.), pp. 41–84. [6] Reffner J. A. et al. (1997) *Micros. Microanalysis*, 3, 867. [7] Borghesi A. et al. (1985) *Astron. Astrophys.*, 153, 1.

1998-99

TRANSIENT DUST FEATURES IN CARBON-RICH CIRCUMSTELLAR ENVELOPES OF EVOLVED STARS.

S. Hony¹, R. J. Sylvester², L. B. F. M. Waters^{1,3}, and M. J. Barlow²,
¹Astronomical Institute, University of Amsterdam, Kruislaan 403, 1098 SJ Amsterdam, The Netherlands (hony@astro.uva.nl),
²Department of Physics and Astronomy, University College London, London WC1E 6BT, UK. ³SRON Laboratory for Space Research Groningen, P.O. Box 800, 9700 AV Groningen, The Netherlands.

Introduction: The last stages in the life cycle of intermediate mass stars, with masses ranging between 1 and 10 \times the mass of our Sun is characterized by a very rapid evolution in structure, luminosity, and surface temperature. Changes in luminosity of the asymptotic giant branch stars (AGB stars) induce convection in the outer parts of the stars, causing nuclear burning products from the CNO cycle to be transported to the surface. This causes the abundances of the various elements in the atmosphere of these stars to change. When, by this process, the ratio of C- over O-atoms becomes larger than unity it changes the chemistry dramatically and the atmosphere becomes C-rich. This is caused by the stability of the CO molecule, which locks up most of the C- and O-atoms, and only the more abundant species is available to form other molecules.

At the same time these stars are affected by strong mass loss, sometimes reaching values of 10⁻⁴ \odot /yr. In the resulting high-density outflows dust will condensate into grains with a composition dependent on the abundances of the available species.

From AGB Stars to Planetary Nebula: When the outflow stops the gas and dust move away from the star, the star contracts and heats up from T \sim 10³ K to T \sim 10⁵ K with a timescale of \sim 10,000 yr. When the star becomes hot enough, T \sim 10⁴ K, to

ionize the expelled gas and dust, the system appears as a planetary nebula. During this rapid evolution several transient solid-state emission bands are observed in the infrared spectra from these objects. The main features observed are 6–9 and 10–15 μm attributed to large PAH or HAC [1]; 21 μm unidentified [4]; and 24–50 μm unidentified, possibly MgS [3].

Transient Features: In this poster we study the properties of the dust in the rapidly changing physical conditions of these circumstellar environments. We present new infrared observations, from AGB stars to planetary nebulae, secured with both the Short Wavelength Spectrometer (SWS) and the Long Wavelength Spectrometer (LWS) onboard ESA's Infrared Space Observatory (ISO). Here we focus on a broad solid-state emission feature ranging from 24 to 50 μm peaking around 30 μm . This 30- μm feature was first reported to be present in the spectra of C-rich stars by Forrest et al. [2]. Goebel and Moseley [3] suggested that solid MgS could be the carrier of this feature. However, because of the broadness of the feature and the difficulties of observing at these wavelengths, no positive identification has yet been possible.

The very large wavelength coverage of the two ISO instruments combined (2–200 μm) allows us to derive reliable band strengths and shapes for the 30- μm feature. We detect a change in shape and peak position of the feature with evolutionary status of the central star, leading us to conclude that at least two separate components are visible. The first feature is strongest in the AGB stars and peaks near 30 μm . The second component peaks near 35 μm and becomes more prominent in the planetary nebulae. We compare the observed spectra with model spectra of MgS and graphite grains and discuss the possibility of grain destruction by ultraviolet photons of the stellar radiation field and the effects of grain temperature on the emitted radiation. For identification purposes, we discuss the correlation of these components with the other main solid-state emission features at shorter wavelengths.

References: [1] Buss R. H. Jr. et al. (1990) *Astrophys. J. Lett.*, 365, L26. [2] Forrest W. J. et al. (1981) *Astrophys. J.*, 248, 195. [3] Goebel J. H. and Moseley S. H. (1985) *Astrophys. J. Lett.*, 290, L35. [4] Kwok S. et al. (1989) *Astrophys. J. Lett.*, 345, L51.

SILICATES AS PROBES OF THE MASS LOSS HISTORY OF OXYGEN-RICH EVOLVED STARS. C. Kemper¹, R. J. Sylvester², L. B. F. M. Waters^{1,3}, T. de Jong^{1,4}, M. J. Barlow², F. J. Molster¹, and X. G. G. M. Tielens³, ¹Astronomical Institute, University of Amsterdam, Kruislaan 403, 1098 SJ Amsterdam, The Netherlands (ciska@astro.uva.nl), ²Department of Physics and Astronomy, University College London, London WC1E 6BT, UK, ³SRON Laboratory for Space Research Groningen, P.O. Box 800, 9700 AV Groningen, The Netherlands, ⁴SRON Laboratory for Space Research Utrecht, Sorbonnelaan 2, 3584 CA Utrecht, The Netherlands.

Introduction: In the late stages of stellar evolution, intermediate mass stars undergo severe mass loss (up to $10^{-4} M_{\odot}/\text{yr}$) while ascending the asymptotic giant branch (AGB). The outer layers of the star are enriched with elements produced by the nuclear processes in the core of the evolved star. These elements include C, N, and O, where in most cases O is more abundant than C. When the circumstellar material cools due to expansion, gaseous SiO,

together with Fe and Mg, will condense, thus forming silicates. As observations have shown [1], we can identify amorphous and crystalline silicates, whereas the different types probably originate at different temperatures and densities.

One reason to study the infrared spectrum of AGB stars is that the emission and absorption features of crystalline and amorphous silicates will provide us with information on the physical and chemical conditions in the circumstellar dust shell. However, this is still future work. We intend to derive the temperature and density gradients, thus revealing the mass loss history of O-rich AGB stars, and finally we may be able to put constraints on the nature of the mass loss mechanism. Here we will present spectra of O-rich evolved stars obtained with the Infrared Space Observatory (ISO). We will analyze the relation between the spectral features of silicates and the energy distribution.

Energy Distribution: The dust shell surrounding the central star causes a redistribution of the emission. Radiation from the star in the visible wavelength region is (partly) absorbed by the dust and reemitted in the infrared region, thus causing an infrared excess. In case of a high mass loss rate and high column densities toward the central star, the dust shell will be optically thick at visible wavelengths and sometimes even in the near-infrared. The central star is then completely obscured. This is the case for OH/IR stars. Bedijn [2] models the energy distribution using the dust shell surrounding O-rich stars due to (accelerated) mass loss. In this study the optical properties of amorphous silicate are taken into account. This provides a measure of the optical depth, since the amorphous silicate features at 9.7 and 18 μm are in emission for low column densities. The features go into self-absorption and absorption for increasing column density. Moreover, for increasing optical depth, the $\tau = 1$ surface will migrate outward to lower temperatures, which causes a redward shift of the peak of the energy distribution for increasing mass loss.

From observations performed with ISO it becomes clear that the crystalline silicate features will become stronger for higher integrated mass loss. It is generally believed that annealing of the amorphous material into crystalline dust will happen only at high temperatures, i.e., above the glass temperature. In high mass loss objects, the density at the inner edge of the dust shell is higher. In that case, the dust condensation may start at a higher temperature and the dust stays at those high temperatures for a longer period. Thus we increase the duration of the annealing period, which leads to a higher abundance of crystalline silicates.

Observations: We present the combined Long Wavelength Spectrometer (LWS) and Short Wavelength Spectrometer (SWS) ISO data of Miras and OH/IR stars with different mass loss rates, e.g., OH26.5, WX Psc, OH104.9 and OH127.8. The infrared spectra span the wavelength range from 2.4 to 195 μm , which includes practically all the flux emitted by the sources.

Analysis: The objects are ordered with increasing optical depth, using the 10- μm silicate band, as well as the peak position of the energy distribution. We find that the crystalline silicate features become stronger for cooler shells. The pseudocontinuum, i.e., the thermal emission from the dust shell, is determined in order to ascertain the presence of absorption and emission features. In cases when the dust shell is optically thick at the near-infrared, we find that the peak of the pseudocontinuum is at $\sim 20 \mu\text{m}$, which corresponds to a dust temperature of $\sim 145 \text{ K}$. The spectral features of our sample are compared with pure emission spectra, like those

of NGC 6302 and AFGL 4106 [3], in order to determine the shape of the absorption features, and the optical depth at different wavelengths. The identification of the several crystalline features is done using laboratory spectra.

Results: We find that the amorphous silicates show extremely broad absorption bands; depending on what pseudocontinuum one defines, the 18- μm band is well in absorption until approximately 25–30 μm . Next to amorphous silicates, another material, like FeO, may contribute to this absorption feature. On the other hand, crystalline silicates occur already in emission at 25 μm and longward. Depending on which pseudocontinuum is selected, the crystalline silicate features may be in emission, superposed on the broad amorphous silicate absorption band. This implies that the crystalline and amorphous dust grains may not have the same spatial distribution, possibly due to a different radial distribution or due to deviations from spherical symmetry.

References: [1] Waters L. B. F. M. et al. (1996) *Astron. Astrophys. Lett.*, 315, L361. [2] Bedijn P. J. (1987) *Astron. Astrophys.*, 186, 136. [3] Molster F. J. et al. (1999) *Astron. Astrophys.*, in press.

91

UTILIZING NIGHT SPECTRA OF MARS FOR MINERALOGY. L. E. Kirkland¹ and K. C. Herr², ¹Lunar and Planetary Institute and Rice University, Houston TX, USA (kirkland@lpi.jsc.nasa.gov), ²The Aerospace Corporation, El Segundo CA, USA.

Summary: Thermal infrared spectra measured of the night side of Mars have advantages over day measurements for examining the aerosol dust mineralogy because they contain fewer atmospheric gas and surface features. Despite the advantages night spectra offer, they have rarely been utilized because the methodology to convert them to transmission was poorly understood. Here we present a method for converting night and day spectra to apparent transmission. We also discuss the advantage for mineralogical studies of apparent transmission vs. apparent emissivity.

Background: In 1969, IRS returned high-quality spectra of Mars covering the wavelength region 1.8–14.4 μm . These spectra have recently been recovered from the original data tapes and calibrated from 5–14.4 μm with heavy involvement from members of the original IRS team [1–3]. We use these spectra here because IRS has the high signal-to-noise ratio needed for night measurements.

Previous Aerosol Studies: Previous studies have used only day spectra from IRS or 1971 Mariner IRIS to examine the composition of the aerosol dust. These studies presented a wide variety of results, concluding that the the aerosol dust consists mainly of an oxidized tholeiitic basalt [4], rock of intermediate [5] or felsic composition [6], montmorillonite [7], a mixture of basalt and clay [8], or palagonite [9].

All those studies concluded that the aerosol consists of particles <10 μm in size. Widely separated particles this small behave in a manner similar to a gas [10–12], so their transmission (τ) and emission (ϵ) spectra have the same shape, although bands that appear as transmission troughs appear as emission peaks ($\tau = 1 - \epsilon$).

Night Spectra Advantages: Night measurements contain less contribution from atmospheric gases and the surface, which allows a more direct examination of the aerosol signature. Night spectra

have received less attention mainly because it was not clear how to convert them from radiance to transmission.

Since the atmosphere is so cold at night, night spectra contain very little contribution from atmospheric hot bands (which are from transitions from an excited state rather than the ground state). The population of higher energy states decreases exponentially with temperature (Boltzmann distribution), so the intensity of a hot band decreases rapidly with decreasing temperature.

Apparent Transmission: Mineralogical studies using thermal infrared spectra of Mars typically use spectra converted from radiance to apparent emissivity (ϵ_A) [10]. However, ϵ_A spectra have two undesirable artifacts: (1) The spectral contrast depends on the background temperature for both day and night spectra, even though a true measure of transmission does not have this dependence; and (2) restrahlen bands in night ϵ_A spectra have an emissivity >1, which is clearly incorrect.

Apparent emissivity is calculated by dividing the spectrum measured of Mars by the Planck radiance curve at the surface temperature, taken as the brightness temperature (T_B) at 7.75 μm . Figures 1 and 2 show typical day and night IRS spectra, with the surface 7.75- μm T_B curve shown as a solid line.

Day measurements are dominated by atmospheric transmission and surface emission features, which have restrahlen bands (e.g., the 9- μm band) that appear as troughs relative to the surface 7.75- μm T_B Planck curve (Fig. 1).

However, night spectra have restrahlen bands that appear as peaks relative to the surface 7.75- μm T_B Planck curve (Fig. 2). Thus night ϵ_A spectra appear “upside down” relative to day spectra, and have $\epsilon_A > 1$. This is because single-particle reemission features dominate night spectra, so restrahlen bands appear as peaks rather than troughs. An apparent emissivity calculation fails glaringly in this case because it does not account for the reemission of the dust. Since the process involved is highly nonlinear, the problem cannot be fixed simply by inverting the night ϵ_A spectra.

To address this problem, we use a method similar to [13] to convert the spectra from radiance to apparent transmission (τ_A)

$$\tau_A = \frac{\text{Mars} - \text{aerosol}_{\text{BB}}}{\text{background}_{\text{BB}} - \text{aerosol}_{\text{BB}}}$$

and

$$\tau_{A_0} = 1 - \{(1 - \tau) \times \log_{10} [10 \times \cos\Theta]\}$$

where $\tau_{A_0} = \tau_A$ normalized for atmospheric path length; Mars = radiance spectrum measured of Mars; aerosol_{BB} = Planck radiance curve at the temperature of the aerosol dust; source_{BB} = Planck radiance curve at the temperature of the surface; Θ = emission angle.

The log term in the τ_{A_0} equation accounts for absorptions adding logametrically rather than linearly (Beer’s Law). The surface temperature is taken as the brightness temperature at 7.75 μm . The aerosol temperature is derived iteratively, and incorporates the brightness temperature from spectra measured at the terminator, where the flat spectral shape indicates the aerosol and surface temperatures are equal.

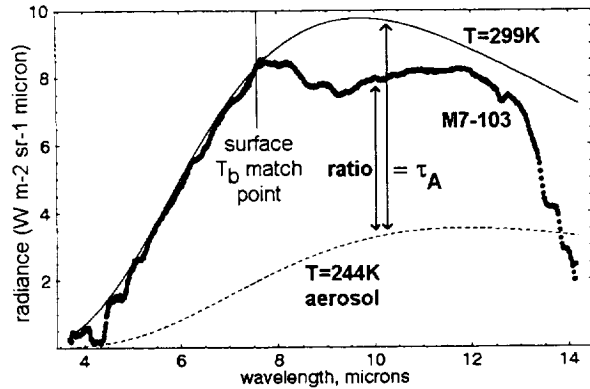


Fig. 1. Conversion of day spectrum to apparent transmission. This shows a typical IRS spectrum measured of Mars during the day. To convert to apparent transmission, the spectrum is referenced to both the Planck blackbody curve of the background (solid line) and the zero reference line (dashed line). The background is the surface, which is assumed to behave as a perfect blackbody with an emissivity of 1. The zero reference line is set at the assumed temperature of the aerosol, and is value that would be seen if the transmission of the aerosol is zero.

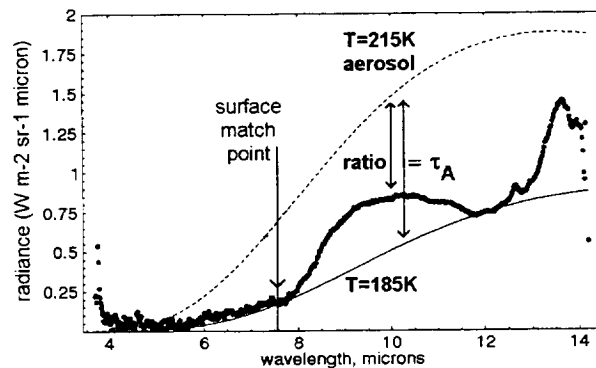


Fig. 2. Conversion of night spectrum to apparent transmission. This shows a typical IRS spectrum measured of Mars at night. The spectrum is converted to apparent transmission as described above. However, in night spectra, the background (surface, solid line) is colder than the zero reference line (dashed). The zero reference line gives the value that would be seen if the aerosol transmission is zero.

Discussion: The conversion to τ_A produces a more accurate spectral shape because it accounts for the reemission of the aerosol, thus allowing a more accurate comparison to laboratory spectra for mineralogical studies of the aerosol. It also provides a method to utilize night spectra for mineralogical work. However, it assumes the emissivity of the surface is 1, so it does not work well where there are strong surface emissivity features. Nonetheless, it works well for Mars, because transmission features dominate over the very subtle surface features. It is especially suited to night measurements, which have even less contribution from the surface.

References: [1] Forney P. B. and Kirkland L. E. (1997) *LPS XXVIII*, 373. [2] Kirkland et al. (1998) *LPS XXIX*, Abstract #1516. [3] Kirkland et al. (1999) *LPS XXX*, Abstract #1693. [4] Herr K. C. et al. (1971) *BASS*, 3, 466. [5] Hanel R. et al. (1972) *Icarus*, 17, 423. [6] Aronsen J. R. and Emslie A. G. (1975) *JGR*, 80, 4925. [7] Hunt G. et al. (1973) *Icarus*, 18, 459. [8] Toon O. B. et al. (1977) *Icarus*, 30, 663. [9] Clancy et al. (1995) *JGR*, 100, 5251. [10] Conel J. (1969) *JGR*, 74, 1614. [11] Hunt G. R. and Logan L. M. (1972) *Appl. Optics*, 11, 142. [12] Logan et al. (1973) *JGR*, 78, 4983. [13] Polak M. et al. (1995) *Appl. Optics*, 34, 5406.

MODELING THE INFRARED EMISSION OF DUST IN BORN-AGAIN PLANETARY NEBULAE. J. Koller¹ and S. Kimeswenger¹, ¹Institute of Astronomy, University of Innsbruck, Technikerstrasse 25/8, A-6020 Innsbruck, Austria (Josef.Koller@uibk.ac.at).

Introduction: We present a model of the IR emission of dust in born-again planetary nebulae (PNe) including the emission of small dust particles with temperature fluctuations. The IR emission in PNe was previously described using a single grain size and a temperature equilibrium state (see Pottasch et al. [1] and references therein). This was sufficient to explain the IRAS measurements. However, this simple equilibrium model cannot explain the emission at wavelengths below 10 μm . Born-again PNe (late He flash objects described in Iben et al. [2]) radiate at those wavelengths even stronger than "regular" PNe [3,4]. Thus the emission has to be described with small dust particles that undergo temperature fluctuations. We adopted the technique introduced by Guhathakurta and Draine [5] with a further detailed description by Siebenmorgen et al. [6]. Our results show how important such calculations are in the case of a low-density radiation field with high-energy photons. Central stars of planetary nebulae (CSPN) provide such a dilute field. The required data about the radiation field of a late-He flash star, which differs from that of a normal CSPN, has been made available by Rauch [7].

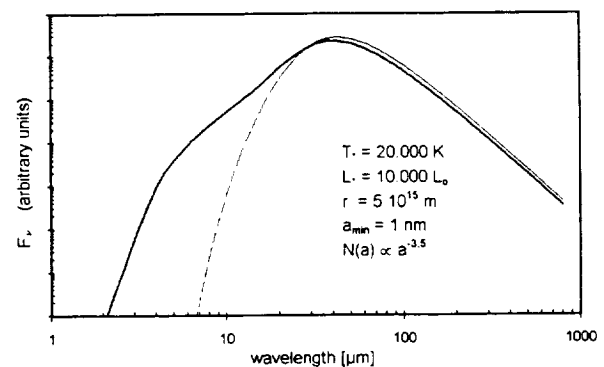


Fig. 3. The total emission of carbonaceous dust grains at a certain distance from the exciting source. While the two models (solid line = transiently heated dust, dashed curve = equilibrium temperature) are very similar at longer (IRAS) wavelengths, they differ strongly below 10 μm .

Method: The emission of large dust grains (diameter $a \geq 10 \text{ nm} \approx 500,000 \text{ C atoms}$) is calculated with assuming an equilibrium between the incident UV radiation and the cooling by IR emission. This can be applied if the cooling timescale τ_c is significantly larger than the timescale τ_l between the incident photons. Due to a weak dependency of the absorption cross section, the resulting temperature (and the corresponding emission) is only weakly dependent on the grain size. A model using a single grain size with a single temperature may be applied.

A small dust grain ($a \approx 0.7 \text{ nm} \approx 180 \text{ C atoms}$), which has a low heat capacity, is excited by a single high-energy photon to rather high temperatures. As the cooling rate is much higher than the rate of incident photons, such grains are not in equilibrium. The result of a high-energy photon collision is the instant raise of temperature, high above the theoretical equilibrium temperature. During the cooling process the energy is re-radiated at near infrared wavelengths. The density of the radiation field and its energy distribution effects a transition zone from equilibrium temperature to transiently heated grains.

Input Parameters and Results: The spectrum of emitted radiation depends on the grain material and the grain size. We use carbonaceous grains as in Harrington et al. [3] and the optical parameters calculated by Laor and Draine [8]. We show that the slope of the grain size distribution (a power law distribution like that of Mathis et al. [9]) does not affect the spectrum at wavelengths below $10 \mu\text{m}$, while the cutoff radius a_{min} strongly influences this emission. Furthermore, we show how the distance from the exciting source (thus the density of the radiation field) and the spectrum of the CSPN radiation field affects the MIR and FIR spectrum. In the end we apply this method to the PN Abell 58 (= Nova Aql 1919) to fit the unusual IR radiation of this source found by ISO [4]. As the different parameters give their "fingerprints" to different parts of the emission spectrum, we are able to "pin down" the physical properties independently.

Acknowledgments: This research has been supported by the Austrian *Fonds zur Förderung der wissenschaftlichen Forschung*, project number P11675-AST.

References: [1] Pottasch S. R. et al. (1984) *Astron. Astrophys.*, 138, 10–18. [2] Iben I. et al. (1983) *Astrophys. J.*, 264, 605–612. [3] Harrington J. P. et al. (1994) *Astrophys. J.*, 435, 722–733. [4] Kimeswenger S. et al. (1998) *MNRAS*, 296, 614–618. [5] Guhathakurta P. and Draine B. T. (1989) *Astrophys. J.*, 345, 230–244. [6] Siebenmorgen R. et al. (1992) *Astron. Astrophys.*, 266, 501–512. [7] Rauch T. (1999) private communication. [8] Laor A. and Draine B. T. (1993) *Astrophys. J.*, 402, 441–468. [9] Mathis J. S. et al. (1977) *Astrophys. J.*, 217, 425–433.

ISOPHOT POLARIZATION MEASUREMENTS OF THE ASTEROIDS 6 HEBE AND 9 METIS AT 25 MICROMETERS.

J. S. V. Lagerros¹, T. G. Müller², U. Klaas³, and A. Erikson⁴, ¹Five College Radio Astronomy Observatory, LGRC-619, University of Massachusetts, Amherst MA 01003, USA (Johan.Lagerros@fcrao.umass.edu), ²ISO Data Centre, Astrophysics Division, Space Science Department of ESA, Villafranca, Box 50727, E-28080 Madrid, Spain (tmueller@iso.vilspa.esa.es), ³Max-Planck-Institut für Astronomie, Königstuhl 17, D-69117 Heidelberg, Germany (klaas@mpia-hd.mpg.de), ⁴DLR, Institute of Planetary Exploration, Rudower Chaussee 5, D-12489 Berlin, Germany (Anders.Erikson@dlr.de).

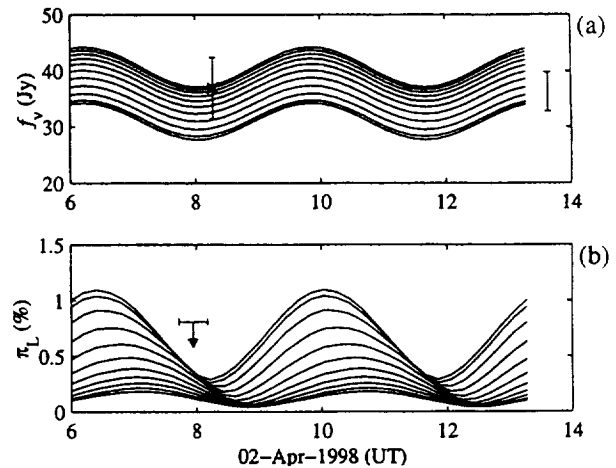


Fig. 1. Model thermal lightcurves for 6 Hebe at $25 \mu\text{m}$, assuming a refractive index of $n = 2$, and r.m.s. slopes $\rho = 0, 0.1, \dots, 1.0$. (a) Observed and predicted flux f_v . The model fluxes increase with the surface roughness ρ . To the right is the typical error bar for the model fluxes, due to the uncertainty in the occultation diameter only. (b) The time span and detection degree of linear polarization π_L . The predicted degree of linear polarization increases with lower surface roughness. The upper limit by the ISOPHOT observation is shown.

The subsurface thermal IR emission of asteroids becomes linearly polarized when scattered across the surface. The disk integrated mid-IR Stokes parameters are computed by extending the new thermophysical model by Lagerros [1,2]. The small hemispherical segment craters covering a smooth surface. Analytical solutions are used for the multiple scattered solar and thermally emitted radiation inside the craters. The surface roughness enhances the emission toward the solar direction, but randomizes the scattering planes which lowers the polarization. In general the predicted degree of linear polarization increases with higher refractive index of the surface material, and a more elongated shape of the asteroid.

The asteroids 6 Hebe and 9 Metis were observed at $\lambda = 25 \mu\text{m}$ with ISOPHOT onboard the Infrared Space Observatory (ISO). The model absolute fluxes are in good agreement with the photometric results. Although no linear polarization was detected, the upper limits together with the extended model enable us to put useful constraints on the regolith properties of the target asteroids. The derived detection limits are compared to model polarization, by spanning a range in surface roughness, refractive index, and thermal inertia parameter space. The Metis observations favor a low refractive index and high surface roughness, but the Hebe observations are inconclusive since they coincided with a minimum in the polarization curve.

References: [1] Lagerros J. S. V. (1996) *Astron. Astrophys.*, 315, 625–632. [2] Lagerros J. S. V. (1998) *Astron. Astrophys.*, 332, 1123–1132.

59-90
THE DUST EMISSION FEATURES IN THE INFRARED SPACE OBSERVATORY SPECTRUM OF NGC 6302. T. L. Lim¹, F. J. Molster², R. J. Sylvester³, M. J. Barlow³, and L. B. F. M. Waters², ¹Space Science Department, Rutherford Appleton

Laboratory, Chilton, Didcot, Oxon OX11 0QX, UK (T.Lim@rl.ac.uk). ²Astronomical Institute Anton Pannekoek, University of Amsterdam, Kruislaan 403, 1098 SJ Amsterdam, The Netherlands (frankm@astro.uva.nl), ³Department of Physics and Astronomy, University College London, Gower Street, London WC1E 6BT.

Introduction: Spectra in the 2.5–97- μm region obtained by the Infrared Space Observatory (ISO) SWS and LWS spectrometers have provided evidence for the presence of crystalline silicates in a number of different objects. The first evidence was provided by the ISO SWS instrument and was reported soon after the ISO launch by Waters et al. [1]. The reason that laboratory studies had concentrated on glassy/amorphous silicates prior to ISO was because the broad 10- μm silicate features observed from the ground and with the IRAS LRS were broad and smooth and could not be fitted with crystalline silicates. Since ISO's discovery of large concentrations of astronomical crystalline silicates, efforts have been made to characterize their optical properties at infrared wavelengths, most recently by the group at the University Observatory in Jena [2], where new optical constants for the astronomically important minerals, e.g., enstatite, have recently become available.

We report on the study of a range of broad features exhibited in the spectrum of the planetary nebula NGC 6302. Full-range grating spectra were taken by both ISO spectrometers (SWS and LWS) with a combined wavelength coverage 2.5–197 μm . The spectrum, one of the richest observed by ISO, exhibits prominent broad features between 3.3 and 117 μm that are attributed to various silicate minerals, water ice, and PAH modes. A spline fit was made to a set of points assumed to be indicative of the continuum level and the spectrum was divided by the fit. The species present were then identified from the continuum divided spectrum and these were characterized by multiple gaussian fitting. An attempt has also been made to fit the whole spectrum with a combination of silicate species and water ice. The overall fit has two problems: The peak wavelengths of the emission bands of some species given by the model, which are based on laboratory spectra of minerals, do not match those observed with ISO, also not all the features are fitted. The mismatch of wavelengths can be attributed to probable differences between the composition and/or particle size of the samples used to obtain the optical constants and those present in the environment of NGC 6302. The origin of the observed features that lack laboratory matches is unknown and until optical constants from pure minerals are available in the ISO wavelength region, it is not possible to determine whether these unidentified features are due to impure samples of the minerals used for our fits, or to minerals whose optical constants are not yet available.

References: [1] Waters L. B. F. M. et al. (1996) *Astron. Astrophys.*, 315, L361. [2] Jäger C. et al. (1998) *Astron. Astrophys.*, 339, 904.

ADVENTURES IN MODELING THERMAL EMISSION SPECTRA OF COMETS. D. K. Lynch and S. Mazuk, The Aerospace Corporation, M2/266, P.O. Box 92957, Los Angeles CA 90009, USA.

We review some of the current problems in the interpretation of 8–13- μm thermal emission spectra and discuss a number of

aspects of small particles that are seldom included in modern work. Topics include relating observed color temperature to kinetic temperature, the effects of size and optical constants on temperature, the nearly ubiquitous existence of molecular disorder, estimating the optical constants of disordered material, the effects of nonspherical particles, and the wavelength shift of lattice resonances with particle size. We develop the analyses around the silicate emission feature observed in many comets and discuss why comets are ideal subjects for advancing our knowledge of thermal emission from small particles. The results are broadly applicable to all cosmic dust.

321-90
INFRARED SPACE OBSERVATORY SPECTROSCOPY OF CIRCUMSTELLAR DUST DISKS SURROUNDING "ISO"LATED HERBIG Ae/Be STARS, THEIR EVOLUTION, AND THE RELATION WITH OUR OWN SOLAR SYSTEM. K. Malfait¹ and C. Waelkens¹, ¹Instituut voor Sterrenkunde, Celestijnenlaan 200B, B-3001 Heverlee, Belgium (Koen.Malfait@ster.kuleuven.ac.be; Christoffel.Waelkens@ster.kuleuven.ac.be).

Introduction: During the last decade, there has been a growing interest in circumstellar dust disks surrounding young stellar objects. Herbig Ae/Be stars are assumed to be the evolutionary precursors of Beta Pictoris like stars. Today, the most studied Herbig Ae/Be stars are still embedded in the dust envelope from which they are formed. The isolated Herbig Ae/Be stars we study are not obscured by filaments of a star formation region; all the infrared excess they possess comes from their circumstellar dust disk. Therefore, these stars are very good targets for infrared spectroscopy.

We will present the ISO spectra of several isolated Herbig Ae/Be stars and we will demonstrate that the spectra evolve during the pre-main-sequence phase. Remarkable similarities with solar system dust occurs. The ISO spectrum of Beta Pictoris will be mentioned as well.

Observations and Reduction: In the guaranteed time proposal of Waelkens, a sample of more than 20 isolated Herbig Ae/Be stars with reasonable infrared fluxes has been studied using the Short Wavelength Spectrometer onboard the Infrared Space Observatory (ISO). In five cases, this 2.3–45- μm spectrum is combined with a spectrum obtained with the Long Wavelength Spectrometer. The resulting resolution of the spectra varies from 250 to 1500, depending on the target dedicated time.

Results: While the youngest, most embedded Herbig Ae/Be stars [1] exhibit ice absorption bands and amorphous silicates, the spectra of the isolated Herbig Ae/Be stars seem to be dominated by optically thin solid state emission features. A wide variety of solid state features is visible, such as the PAH bands, silicates (both amorphous and crystalline), oxides, and cold water ice.

The spectra of some isolated, and therefore assumed to be the most evolved, Herbig Ae/Be stars present astonishing similarities with solar system objects. The ISO spectrum of HD 100546 reveals a forest of solid-state features attributed to crystalline silicates, mainly forsterite, the Mg-rich end member of the olivine family. Next to this crystalline dust component, also amorphous silicates, FeO, PAHs, and crystalline water ice are present [2]. The similarity between the spectrum of HD 100546 and that of Comet Hale-Bopp [2–4] is astonishing. The crystalline material in the

520-90

environment of HD 100546 and in the comet has a temperature of less than 250 K. However, laboratory studies suggest that silicates can only crystallize at temperatures of more than 1000 K [e.g., 5].

The hot passages close to the Sun are too short to be able to crystallize the Hale-Bopp material. Therefore, we argue that the dust must have crystallized closer to the hot stellar photosphere. This implies that the radiation we see in the environment of HD 100546 emerges from a forming Kuiper Belt or an Oort Cloud. Indirectly, the presence of a giant planet in the environment of HD 100546 is likely, since the Oort Cloud and a Kuiper Belt in our solar system originate from ejection of inner solar system material by Neptune and Uranus [6].

HD 142527, a star much younger than HD 100546, does not exhibit the cold crystalline silicates, although some evidence for hot crystalline silicates is present. The cold dust radiation is composed of three components: Next to the omnipresent amorphous silicates and very cold crystalline water ice, hydrous silicates are a major constituent of the circumstellar dust [7]. A large fraction of the interplanetary dust particles that are gathered during atmospheric flights in our own atmosphere also have this lattice layer structure [8]. The temperature of the crystalline ice and the hydrous silicates again does not correspond to what can be expected from laboratory experiments. The location of the hydrous silicates further outside the stellar disk than the crystalline silicates is consistent with their temperature.

We will also present the spectra of HD 45677 and HD 179218, which are remarkably alike, although the nature and evolutionary status of HD 45677 is not clear. The age of HD 179218 and HD 142527 is comparable, though their ISO spectra differ strongly [9].

Conclusions: The similar nature of the solar system dust and the circumstellar dust surrounding young stars confirms that solar system formation occurs at this stage of stellar evolution. Although the resemblance between some spectra is very strong, a wide variety of spectra occurs. The estimated ages for HD 142527 and HD 179218 are of the same order, but their spectra do not resemble each other.

Although there is no evident correlation between stellar parameters, stellar age and the observed spectra, a general trend can be distinguished, going from optically thick radiation, characterized by ice absorption features and amorphous silicates, toward optically thin radiation that partially originates from crystalline dust. The 10- μ m silicate band of Beta Pictoris is dominated by crystalline silicates as well [10,11]. This confirms that the isolated Herbig Ae/Be stars are in an evolutionary passage from their embedded analogs toward Beta Pictoris objects, as can be seen from the evolution of the spectral energy distributions as well [12].

References: [1] Waelkens C. et al. (1998) to be published in the proceedings of the "First International Conference on Comet Hale-Bopp," held in Tenerife, March 1998. [2] Malfait K. et al. (1998) *Astron. Astrophys.*, 331, L25–L28. [3] Crovisier J. et al. (1997) *Science*, 1997, 1904–1907. [4] Lellouch E. et al. (1998) *Astron. Astrophys.*, 339, L9–L12. [5] Hallenbeck S. et al. (1998) *Icarus*, 131, 198–209. [6] Fernandez J. A. (1978) *Icarus*, 34, 173–181. [7] Malfait K. et al. (1999) *Astron. Astrophys.*, submitted. [8] Sandford S. A. and Walker R. M. (1985) *Astrophys. J.*, 291, 838–851. [9] Waelkens C. et al. (1998) to be published in the proceedings of "The Universe as seen by ISO," a conference held in Paris, France, October 1998. [10] Knacke R. F. et al. (1993) *Astrophys. J.*, 418, 440–450. [11] Pantin C. K. (1998) to be pub-

lished in the proceedings of "The Universe as seen by ISO," a conference held in Paris, October 1998. [12] Malfait K. et al. (1998) *Astron. Astrophys.*, 311, 211–223.

53-89

A COMPARATIVE STUDY OF INFRARED SPECTRAL FEATURES IN HERBIG Ae/Be STARS. G. Meeus¹ and C. Waelkens¹, ¹Astronomical Institute, Celestijnenlaan 200B, B-3001 Heverlee (gwendolyn@ster.kuleuven.ac.be).

Introduction: The observations of the Infrared Space Observatory (ISO) satellite revealed an amazing variety of spectral features in young stars. Both O- and C-rich dust was found, and silicates were seen both in amorphous and crystalline form. An important conclusion from ISO observations is that these crystalline silicates are, apart from seen in young stars [1], also found in meteors, comets [2], evolved stars, and interplanetary dust particles. We studied ISO spectra for a sample of 30 young stars, of which most are Herbig Ae/Be stars. Correlation between dust features on the one hand and extinction, age, spectral type, and amount of IR excess on the other are looked for. We notice an evolution in composition and amount of the dust when the star gets closer to the Main Sequence.

Observations: We dispose over ISO Short Wavelength Spectrometer (SWS) observations of a large sample of isolated Herbig Ae/Be stars, covering a wide range in spectral type. These spectra are part of the guaranteed time proposals of Waelkens and Wesselius. Observations are done with ISO SWS in mode AOT1; the spectra cover an interval from 2.3 to 45 μ m. For five of the stars we also have LWS spectra. The resolution varies between 250 and 1500, depending on the integration time.

Results: *Classification scheme.* The most important star-to-star differences are the absence/presence of silicate features, cool dust and PAHs, and a rising/flat continuum. From these differences seen in the spectra, we can distinguish five main groups: (1) rising, featureless spectrum (embedded sources); (2) rising, relatively featureless, silicate in absorption or absent; (3) rising with a prominent cool dust component, silicate emission; (4) silicate emission without a prominent cool dust component; and (5) featureless without cool dust. Further subdivision can be made, depending on the presence of PAHs and on the structure of the silicates.

Comparison with optical observations. We have already studied most of our sources through optical spectra and photometry. This studies reveal some of the sample stars to be variable, have outflows, or show signs of metal underabundance.

These findings were confronted with properties of the CS dust. Correlation between strength, structure, and presence of dust features on the one hand and spectral type, E[B-V], presence of accretion/outflow, chemical composition and evolutionary stadium on the other were looked for.

The following results were found: (1) There is no relation between the strength of the silicate features and the extinction (E[B-V]). (2) There is no relation between the spectral type of the star and presence/absence, structure, or strength of spectral features. (3) All stars showing crystalline silicates have a prominent cool dust continuum, and also show PAHs. PAHs are only present in stars from group 1 to 3. (4) Disk inclination has no influence on the IR spectral features, suggesting the material to be optically

thin. (5) No activity (infall or outflow) is seen in group 5. (6) Stars that are underabundant in metal all belong to group 5, and therefore are featureless. The stars with a solar composition show silicates in emission.

Conclusions: Group 1 stars have featureless IR spectra and are embedded, thus they are the youngest of the whole sample. Group 5 stars are inactive and not embedded, thus they probably are the most evolved ones.

These results suggest that the order of the groups indicates an evolutionary sequence and that PAHs and silicates seem to disappear with age.

The absence of PAHs and silicates can be explained by a lower UV flux (in the case of the PAHs), and by the formation of larger bodies out of small particles (in the case of the silicates).

As a result, the oldest stars from our sample are suggested to be the closest progenitors of β Pic and Vega-type stars.

References: [1] Malfait K. et al. (1998) *Astron. Astrophys.*, 331, L25–L28. [2] Crovisier J. et al. (1998) *Science*, 1997, 1904–1907.

CRYSTALLINE SILICATES: FROM NOTHING TO MAIN THING. F. J. Molster¹ and L. B. F. M. Waters^{1,2}, ¹Astronomical Institute Anton Pannekoek, University of Amsterdam, Kruislaan 403, 1098 SJ Amsterdam, The Netherlands, ²SRON Space Research Laboratory, P.O. Box 800, 9700 AV Groningen, The Netherlands (frankm@astro.uva.nl).

Introduction: One of the biggest surprises of the Infrared Space Observatory (ISO) was the discovery of crystalline silicates in the outflows of O-rich evolved stars. Before the launch of ISO it was commonly accepted that the silicates, apart from a few exceptions in the remnants of some accretion disks of young stars and of our own solar system accretion disk in the form of comets and interplanetary dust particles (IDPs), were of amorphous structure. The spectra taken with the Short and Long Wavelength Spectrometer (SWS/LWS) onboard ISO showed clear evidence of the presence of a significant fraction (5–15%) of crystalline silicates in the circumstellar environment (CSE) of evolved stars [1]. The most common found crystalline silicates are the (almost) pure Mg end members of the olivine ($\text{Mg}_{2x}\text{Fe}_{(2-2x)}\text{SiO}_4$) and pyroxene ($\text{Mg}_x\text{Fe}_{(1-x)}\text{SiO}_3$) solid solution series, i.e., $x > 0.99$, and are called forsterite ($\text{Mg}_{2x}\text{SiO}_4$) and enstatite (Mg_xSiO_3) [1,2]. This is in contrast with the relatively Fe-rich amorphous silicates. Since the Mg-silicates condense at higher temperatures than the Fe-rich silicates (see, e.g., Gail and Sedlmayr, in press) it is expected that the crystalline silicates are formed in the very early stages of the dust formation. Differences in the appearance of the crystalline silicates are therefore probably related to the different conditions in the dust forming areas.

Discussion of the Observations: In order to understand more of the (crystalline) dust formation we have observed with ISO SWS and LWS several evolved stars with crystalline silicate features. Where most stars have modest crystalline silicate abundances (<15%), some stars show a significantly higher abundances, up to 75%, of crystalline silicates. It appeared that all stars with a high abundances of crystalline silicates have a disk. Apart from the fact that the abundance of crystalline silicates might be a new indicator for the presence of a disk, it is also very intriguing how these

disks become so highly crystalline. The relatively low abundance found in “normal” outflow sources suggests that extra processing must have taken place in the disk. This is not an obvious process, since not only should most of the dust particles become crystalline, the chemical structure of the particles also has to change from Fe-rich to Fe-free. We shall discuss different scenarios to produce such highly crystalline dust disks in the context of these and other ISO observations.

References: [1] Waters L. B. F. M. et al. (1996) *Astron. Astrophys.*, 315, L361. [2] Jäger C. et al. (1998) *Astron. Astrophys.*, 339, 904.

504-71
MARTIAN MINERALOGY WITH THE INFRARED SPACE OBSERVATORY SHORT WAVELENGTH SPECTROMETER. P. W. Morris^{1,7,10}, T. de Graauw², E. Lellouch³, B. Henderson⁴, T. Encrenaz³, S. Erard⁵, H. Feuchtgruber⁶, M. Burgdorf⁷, G. Davis⁸, and M. Griffin⁹, ¹SRON Laboratory for Space Research, Sorbonnelaan 2, NL-3584 CA Utrecht, The Netherlands, ²SRON Laboratory for Space Research, Landleven 12, NL-9747 AD Groningen, The Netherlands, ³DESPA, Observatoire de Paris, Meudon, France, ⁴Earth Watch Inc., 1900 Pike Road, Longmont CO 80501, USA, ⁵CNRS/Universite Paris-Sud bat. 121, F-91405 Orsay, France, ⁶MPE Garching, D-85748 Garching, Germany, ⁷ISO Science Operations Center, Vilspa, E-28080 Madrid, Spain, ⁸University of Saskatchewan, Saskatoon, Saskatchewan, Canada, ⁹Queen Mary and Westfield College, London E1 4NS, UK, ¹⁰Astronomical Institute, University of Amsterdam, NL-1098 SJ Amsterdam, The Netherlands.

Thermal infrared spectroscopic observations of Mars covering 2.4–45 μm were obtained in mid-1997 with the Short Wavelength Spectrometer (SWS) onboard ESA's Infrared Space Observatory. At very high signal-to-noise ratios and spectral resolutions of up to 3000 using the grating sections of SWS, these data provide composite views of the gas and solid-state chemistry in three different pointings with unprecedented detail. Three observations with complete wavelength coverage were obtained in July–August 1997, with subsolar points located close to Elysium-Isidis Plantia, Tharsis-Lunae Planum, and Syrtis Major. We present our progress in analyzing these observations, with special emphasis on the features attributed to minerals of the dust aerosol and surface. A synthetic spectrum consisting of the surface thermal emission and gas atmosphere has been synthesized for each observation, using climate information from the ESA Martian Climate Database and the observed CO_2 and H_2O vapor lines. Division of the observed spectra by the synthetic atmospheres reveals an array of features that have allowed us to make certain mineral identifications by comparison to available libraries of laboratory mineral reflectance measurements. In this study we address the particulate effects of near-surface thermal gradients and resulting influence on band positions with respect to isothermal conditions and bulk samples.

225-89
ASTEROID 4 VESTA AS SEEN WITH THE INFRARED SPACE OBSERVATORY SHORT WAVELENGTH SPECTROMETER. P. W. Morris^{1,2}, A. M. Heras³, B. Vandenbussche⁴, and R. Dijkstra¹, ¹Astronomical Institute, University of Amsterdam, The Netherlands (pmorris@astro.uva.nl), ²SRON

Laboratory for Space Research, Utrecht, The Netherlands, ³European Space Agency, ESTEC/SCI-SAF, Noordwijk, The Netherlands, ⁴Institute of Astronomy, Catholic University of Leuven, Belgium.

The geological uniqueness and diversity of asteroid 4 Vesta is known from rotationally resolved spectroscopic measurements in the visible and near-infrared, and from polarimetry measurements. These measurements have demonstrated longitudinal variations in surface composition and albedo that can account for its lightcurve, compared to normal asteroid lightcurves induced by shadowing. Olivine in at least one small region has been previously detected, and is thought to have been excavated from the ferromagnesian mantle by a major impact event. The impact region is obvious in 1994 HST images. On the basis of the hemispheric dichotomy of albedo apparent in the HST WFPC2 images, the impact would seem not to have resurfaced the entire asteroid.

We have obtained a series of high spectral resolution (1000–3000) scans of 4 Vesta over the 4–45- μm range with the ISO Short Wavelength Spectrometer. The scans are resolved in steps of one quarter of Vesta's rotation period, of ~ 24 -min duration (0.075 P). In this presentation, we report the detection and variability of strong Si-O-Si asymmetric stretch fundamental of olivine near 11 μm (emission), and tentative pyroxene near 10 μm (absorption).

526-90

EFFECTS OF GRAIN MORPHOLOGY AND IMPURITIES ON THE INFRARED SPECTRA OF SILICON CARBIDE PARTICLES. H. Mutschke, D. Clement, and Th. Henning, Astrophysical Institute and University Observatory, Schillergässchen 2-3, D-07745 Jena, Germany (mutschke@astro.uni-jena.de).

Introduction: Thermal emission of solid silicon carbide (SiC) particles has been observed in carbon star outflows [1–3]. The identification is based on a broad infrared feature in the 10–13- μm wavelength range, which is ascribed to the fundamental phonon transition of SiC. Attempts have been made to derive the crystal type of the circumstellar SiC grains from a comparison of the observed band profiles to those measured on laboratory analogs [3]. However, due to the strength of the phonon transition the absorption by small SiC grains is determined by surface modes, which make the band profile extremely sensitive to the grain morphology (size, shape, and grain aggregation [4]). Unfortunately, at the moment light scattering theory is not in the position to calculate band profiles for arbitrary grain morphologies. Therefore, intensive laboratory studies must help to clarify the influence of morphology on the appearance of the SiC phonon band.

Experimental: We present experimental infrared absorption spectra, measured on SiC particulate samples of different grain sizes and shapes as well as in different agglomeration states. For this purpose, a number of preparational methods have been applied, including isolation in noble gas matrices, the KBr pellet technique and IR microscopy of grains supported by Si substrates. For the matrix-isolation spectroscopy, SiC particles have been produced in a gas-pyrolysis source.

Results and Discussion: With SiC particulate samples of different (partly commercial) origin we observe a wide variety of

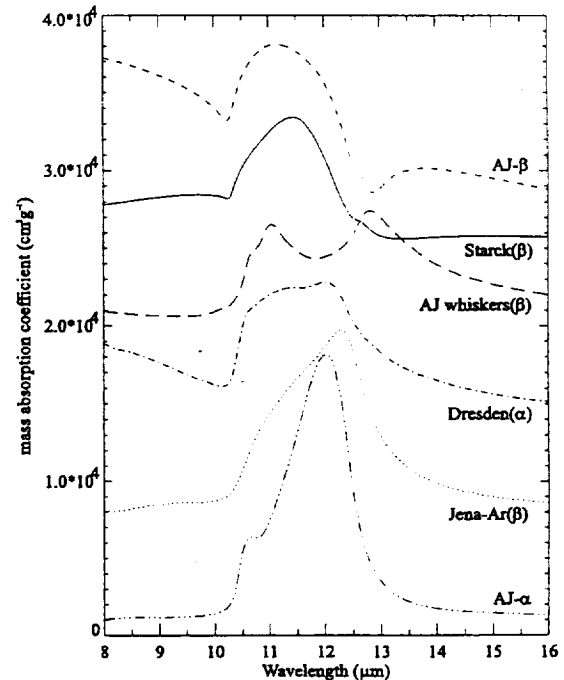


Fig. 1. Phonon band profiles of some SiC laboratory samples. The spectra have been shifted vertically for clarity. α and β indicate the hexagonal/rhombohedral and the cubic crystal types respectively.

SiC phonon band profiles, which is not primarily related to the crystal type (see Fig. 1). We show that both peak wavelength(s) and band shape depend on grain size, shape, and agglomeration state, as well as on the medium surrounding the grains. For a more detailed analysis of these effects it is necessary to separate the agglomeration effect from the one produced by the primary grain morphology. Matrix isolation can provide a means to solve this problem in the future.

Additionally, we find that surface plasmon absorption caused by impurities influences the phonon band via plasmon-phonon coupling. Moreover, it produces a very strong quasicontinuous absorption in the near- and mid-infrared, which could be important to take into account in models of the thermal dust emission of carbon star envelopes.

References: [1] Little-Marenin I. R. (1986) *Astrophys. J.*, 307, L15. [2] Goebel J. H. et al. (1995) *Astrophys. J.*, 449, 246. [3] Speck A. K. et al. (1997) *MNRAS*, 288, 431. [4] Papoular R. (1998) *Astron. Astrophys.*, 329, 1035.

527-90
DUSTY: A PUBLICLY AVAILABLE CODE FOR CONTINUUM RADIATIVE TRANSFER IN ASTROPHYSICAL ENVIRONMENTS. M. Nenkova¹, Z. Ivezić², and M. Elitzur¹, ¹Department of Physics and Astronomy, University of Kentucky, Lexington KY 40506-0055, USA (maia@pa.uky.edu; moshe@pa.uky.edu), ²Astrophysical Sciences Department, Payton Hall, Princeton University, Princeton, NJ 08544-1001, USA (ivezic@astro.princeton.edu).

External radiation. Thanks to scale invariance [2], the radiation illuminating the dusty shell needs to be specified only by its spectral shape. DUSTY provides options for entry in analytical or numerical form, as user-supplied files.

Dust optical properties. These are described by the absorption and scattering cross sections, which depend on the grain size and material. DUSTY contains data for the optical properties of six common grain types: Ossenkopf “warm” and “cold” silicates [4], silicates and graphite grains from Draine and Lee [5], amorphous carbon from Hanner [6], and SiC from Pegourie [7]. Additional optical properties for other grains can be supplied if needed. In this case, the user can either specify directly the absorption and scattering coefficients or have DUSTY calculate them from provided optical constants by using the Mie theory. Two types of size distribution functions are implemented in the code: MRN [8] and its modification KMH [9]. The user is free to adjust the parameters of size distribution as desired.

Density distribution. DUSTY accepts three methods for entering the density distribution: prescribed analytical forms, hydrodynamic calculation of winds driven by radiation pressure on dust particles, and numerical tabulation in a file.

Optical depth. For a given set of the parameters specified above, DUSTY can generate up to 99 models covering a range of optical depths τ_0 , specified at some fiducial wavelength λ_0 .

Output. A typical DUSTY run generates an enormous amount of information, and the user is in control of the volume of output, which may include spectra, imaging profiles, and radial distributions for each of the optical depths included in the run.

Details and instructions about the many options can be found in DUSTY’s manual [1]. The code is publicly available for various modeling purposes and the authors would appreciate any comments and suggestions leading toward improvement of the code and its capabilities.

References: [1] Ivezić Z. et al. (1999) User Manual for DUSTY, *Internal Report, Univ. of Kentucky* (accessible at <http://www.pa.uky.edu/~moshe/dusty>). [2] Ivezić Z. and Elitzur M. (1997) *MNRAS*, 287, 799. [3] Schmidt-Burgk J. (1975) *Astron. Astrophys.*, 40, 249. [4] Ossenkopf V. et al. (1992) *Astron. Astrophys.*, 261, 567. [5] Draine B. and Lee H. (1984) *Astrophys. J.*, 285, 89. [6] Hanner M. (1988) *NASA Conf. Pub. 3004*, 22. [7] Pegourie B. (1988) *Astron. Astrophys.*, 194, 335. [8] Mathis J. et al. (1977) *Astrophys. J.*, 217, 425. [9] Kim S. et al. (1994) *Astrophys. J.*, 422, 164.

5-18-90

NUCLEATION, GROWTH, ANNEALING, AND COAGULATION OF REFRACTORY OXIDES AND METALS: RECENT EXPERIMENTAL PROGRESS AND APPLICATIONS TO ASTROPHYSICAL SYSTEMS. J. A. Nuth¹, F. J. M. Rietmeijer², S. L. Hallenbeck³, and P. A. Withey⁴,
¹Astrochemistry Branch, Mail Code 691, NASA Goddard Space Flight Center, Greenbelt MD 20771, USA, ²Geology Department, University of New Mexico, Albuquerque NM 85131, USA, ³Mail Code SR, NASA Headquarters, Washington DC 20546, USA, ⁴Department of Physics and Engineering, West Virginia Wesleyan College, Buckhannon WV 26201, USA.

Introduction: Starting with cooling, refractory vapors diluted in significant quantities of H and He there are four processes that

most natural systems will undergo: nucleation, growth, annealing, and coagulation. Nucleation is the processes by which the first stable refractory nuclei form in the vapor. These are the seeds onto which the remaining vapors will condense during the growth stage. Solids of any composition will try to arrange themselves into the least energetic configuration, provided that there is sufficient energy available to support such processes as diffusion and the breaking of chemical bonds. There is a significant activation energy associated with the annealing process in refractory solids due to the relatively high energy of the chemical bonds in solids. The grains formed in most cosmochemical systems are extremely small and often tightly coupled to the gas. Because of their small physical cross sections coagulation may be a very slow process unless there is another driving force involved in addition to normal Brownian motion. In what follows we will briefly cover each of these four stages for refractory oxide and metal grains, although in inverse order.

Coagulation: Appropriate studies of the coagulation of refractory grains are just beginning to be carried out. In general, such studies are inherently difficult since, just as the grain size begins to become interesting, the aggregate settles out of the gas. To overcome this problem, experimenters are beginning to take advantage of the short-lived periods of microgravity available in drop towers and aircraft in preparation for work to be carried out on the International Space Station. We have recently demonstrated that the nucleation of very small Fe grains can lead to the formation of single-magnetic domain particles, e.g., fully magnetized iron dipoles [1] that might greatly enhance the coagulation efficiency of small particles [2]. This could lead to the formation of very low fractal dimension particles that might greatly increase the emission efficiency of these aggregates at submillimeter wavelengths [3].

Annealing: Over the last several years we have made significant progress in understanding spectra of circumstellar and interstellar oxide grains. In particular, based on experimental studies in our lab [4] we can now predict the mid-IR spectral evolution of silicate grains as they anneal in stellar outflows and in forming protostellar nebulae. This not only allows us to predict the emergent spectrum one might expect from obscured sources, but also allows us to set limits on the time-temperature history of dust grains based on their spectral properties. As an example, we have been able to show that the spectral properties of grains in Hale-Bopp, Halley, and other comets are the result of moderate temperature (1000 K) thermal processes in the solar nebula that require recirculation from the inner nebula to well beyond Jupiter’s orbit [5]. These large-scale circulation patterns are not currently part of any model of protostellar evolution, but, if they exist for any significant timescale, would have a large effect on the nebular production efficiency of prebiotic organic compounds and on the composition of volatile compounds sequestered in comets.

Growth: Another area where we have made significant progress in the last two years is in understanding the chemical speciation of grains as they grow in stellar outflows. Data acquired by careful analysis of the chemical compositions of individual grains condensed from mixed refractory vapors in our lab has demonstrated that these compositions are predictable based on the compositions of metastable eutectics in the appropriate phase diagrams [6–8] such as that shown in Fig. 1. Based on these experiments, we now hypothesize that the chemical compositions of the individual grains formed in such outflows are controlled by ther-

Introduction: Many astronomical objects are surrounded by dust and often can be entirely obscured. The dust scatters, absorbs, and reemits the radiation originating from the source, which results in an overall shift of the spectral energy distribution toward longer IR wavelengths. In many cases the emerging processed spectrum provides the only available information about the dust-embedded object. Thanks to the recent developments in IR techniques and facilities, the IR signature of many objects is now available, and the amount and quality of data is steadily increasing. Interpretation of these data can offer insight to the nature of optically obscured objects, making their IR signature a powerful tool of analysis. However, because of the complexity of the radiative transfer problem, proper computational modeling tools must aid such analysis. We have developed a publicly available code DUSTY, which solves the radiative transfer problem for a source embedded in a spherically symmetric dusty envelope. The code offers also an optional calculation for a dusty plane-parallel slab, illuminated from one or both sides at an arbitrary angle. The user specifies the properties of the radiation source and dusty medium, and the code calculates the dust temperature distribution, radiation field, and other quantities of interest [1].

Solution Method: The code fully utilizes the scaling properties of the radiative transfer problem, which are thoroughly discussed in [2]. DUSTY solves the integral equation for the energy density in a dusty shell obtained by analytically integrating the radiative transfer equation. This equation, coupled with the condition of radiative balance at any point of the envelope, is solved by a direct method, i.e., the numerical integration over angles and optical depth is transformed into multiplication with a matrix of weight factors [3]. The matrix is determined purely by the geom-

etry and is calculated only once for given space grids. The energy density and the next radiative moment — the flux at every point are then determined by direct matrix inversion, which solves the scattering problem and eliminates the need of iterations over the energy density itself. That gives our method an edge in speed over other schemes (e.g., iterations over variable Eddington factor). The employed direct method of solution provides fast and stable convergence even for optical depths as large as $\tau_V \sim 1000$. The radiative transfer problem in spherical symmetry is solved on grids for dimensionless radius and impact parameter, whereas for the plane-parallel case the calculation is performed in optical depth space. The wavelength grid is predetermined in the code and contains 98 points from 0.01 μm to 3.6 mm. The spatial grids are automatically generated and adjusted to ensure flux conservation.

Code Capabilities: One of the goals while developing DUSTY was to design a flexible, user-friendly input/output interface. Another advantage of the code is that the number of independent input model parameters is minimal since it fully utilizes the scaling properties of the radiative transfer. The input contains three types of data: physical parameters, numerical accuracy parameters, and flags for optional output files. The physical parameters include characteristics of the external radiation, properties of the dust grains, and the envelope density distribution. An example of a code application is shown in Fig. 1., a set of models for an envelope with silicate dust and $1/r^2$ density distribution around a 2500 K central star.

Plane-parallel slab. This option offers calculation of the radiative transfer through a dusty homogeneous slab of material illuminated from one or both sides at user-specified angles of incidence (Fig. 2).

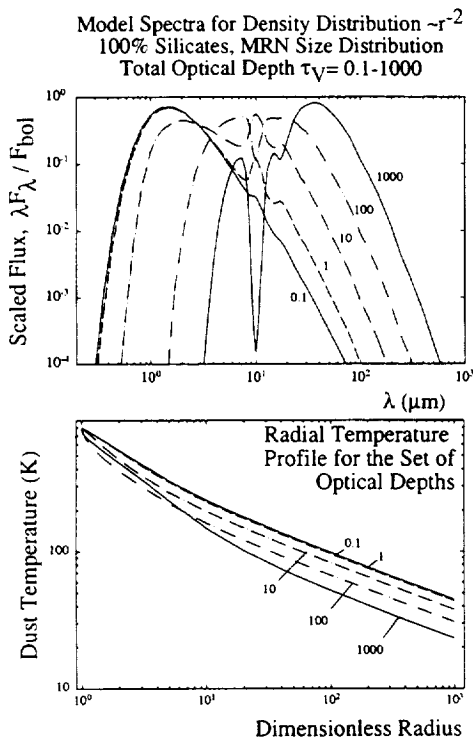


Fig. 1.

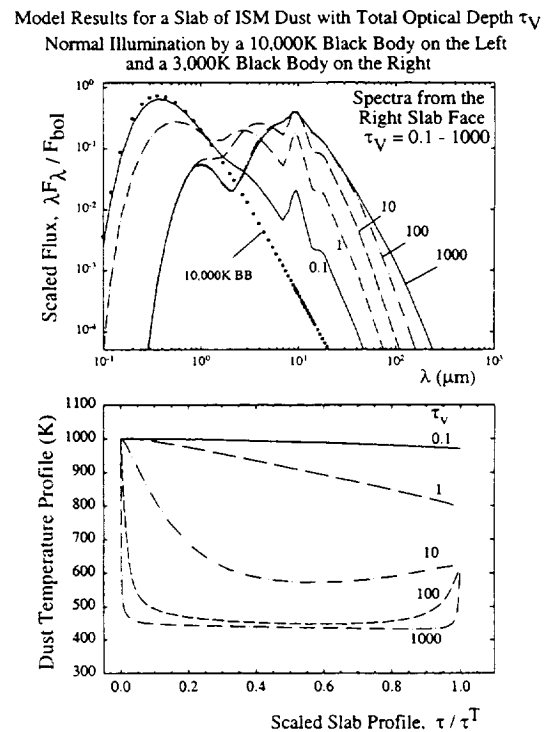


Fig. 2.

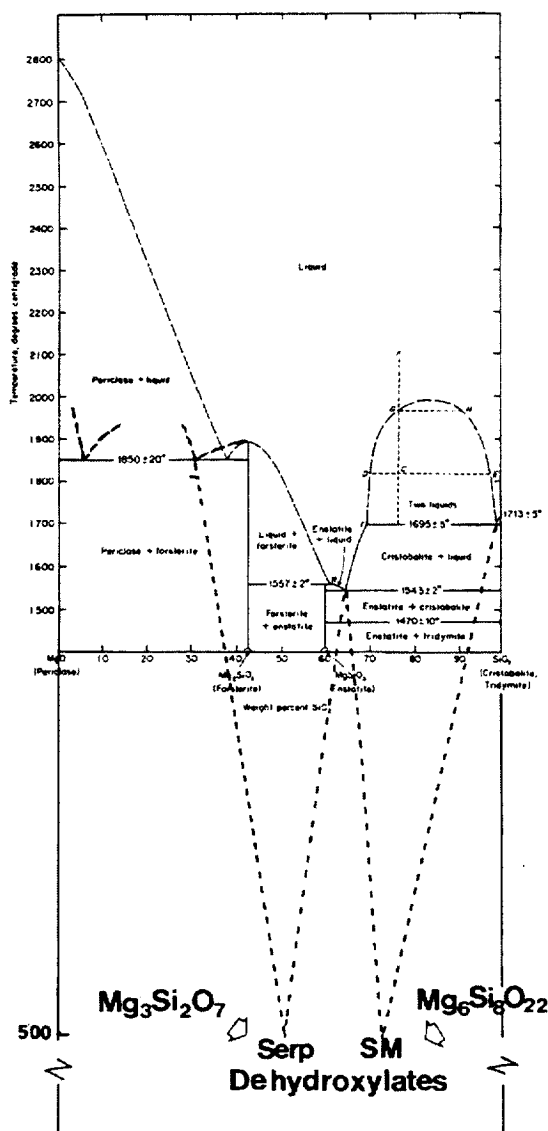


Fig. 1. Phase diagram for the MgO-SiO₂ system showing the compositions of the observed metastable eutectics that also correspond to observed abundance peaks in the composition of the grains condensed from mixed Mg-Si-O-H vapors.

modynamic factors and can be predicted by appropriate chemical phase diagrams. Although the relative proportions of the individual grain compositions will vary from star to star based on the overall chemical composition of the outflow; the compositions of the individual grains themselves will remain unchanged. This observation explains the remarkable similarity of the spectra of grains produced in a very wide range of environments, from circumstellar outflows to protostellar nebulae.

Nucleation: The only area of grain research where we have not made significant progress over the past several years is in our ability to predict when refractory grains will condense from the vapor. Theoretical treatments of the nucleation process [9,10] are almost exclusively based on experimental studies of volatile com-

pounds, such as water-vapor or low-molecular-weight hydrocarbons, and are marginally applicable — at best — to formation of refractory materials in astrophysical environments [11]. Our recent efforts have been devoted to expanding the experimental database on the nucleation of simple, refractory materials using a single, experimental technique and testing various theoretical treatments against our results. It is obvious that grains forming in expanding, cooling vapors will anneal to significantly different degrees depending on the temperature where they nucleate. In all cases, grains formed at higher temperatures will look much more crystalline than will grains formed in cooler environs [12]. ISO observations of crystalline magnesium silicate grains in high mass loss rate AGB outflows have provided support for our models of both the growth and annealing stage of refractory evolution [13,14].

References: [1] Withey P. A. and Nuth J. A. (1999) *Icarus*, in press. [2] Nuth J. A. and Wilkinson G. M. (1995) *Icarus*, 117, 431–434. [3] Nuth J. A. et al. (1994) *Icarus*, 107, 155–163. [4] Hallenbeck S. L. et al. (1998) *Icarus*, 131, 198–209. [5] Nuth J. A. (1999) *LPS XXX*. [6] Rietmeijer F. J. M. and Karner J. M. (1999) *JCP*, 110, in press. [7] Rietmeijer F. J. M. et al. (1999) *European J. Miner.*, in press. [8] Rietmeijer F. J. M. et al. (1999) *Phys. Chem. Phys.*, 1, in press. [9] Becker R. and Doring W. (1935) *Ann. Physik*, A125, 719. [10] Hale B. N. (1986) *Phys. Rev. A*, 33, 4156. [11] Donn B. and Nuth J. A. (1985) *Astrophys. J.*, 288, 187. [12] Sogawa H. and Kozasa T. (1999) *Astrophys. J. Lett.*, in press. [13] Waelkens C. et al. (1996) *Astron. Astrophys.*, 315, L245–L248. [14] Waters L. B. F. M. et al. (1996) *Astron. Astrophys.*, 315, L361–L364.

509-91

THERMAL EMISSION SPECTRA OF MERCURY. A. E. Potter¹, B. L. Cooper², R. M. Killen³, and T. H. Morgan⁴, ¹Lunar and Planetary Institute, 3600 Bay Area Boulevard, Houston TX 77058, USA, ²B. Cooper and Associates, Houston TX 77058, USA, ³Southwest Research Institute, 6220 Culebra Road, San Antonio TX 78228, ⁴Mail Code SR, NASA Headquarters, Washington DC 20546, USA.

Introduction: The emission spectrum of Mercury may hold clues as to the mineral composition of the surface from reststrahlen bands. Unfortunately, these bands are very weak in finely powdered materials, such as are expected on the mercurian surface, and they lie in a region of the spectrum where there are substantial atmospheric absorptions. We have been measuring the 8–14- μ m spectra of Mercury and the Sun at a resolution of about 0.03 wavenumbers, using the Fourier Transform Spectrometer (FTS) located at the National Solar Observatory, Kitt Peak, Arizona. The objective of using such a high resolution for the measurement is to be able to look between atmospheric absorption lines as much as possible. The atmospheric effects are largely canceled by ratioing Mercury spectra to Sun spectra taken at nearly the same airmass, although small differences in airmass produce some residual atmospheric absorptions in the ratio spectra. We expect that spectral features of Mercury, if any, should appear in the ratio spectra, since the 8–14 μ m spectrum of the Sun approximates a black body.

Measurements: We have measured Fourier transform spectra of the Mercury and the Sun at intervals when we could gain use of the FTS at the McMath Solar Telescope at Kitt Peak. Dates

include January 18, 1995, April 1, 1997, November 12, 1997, and November 10, 1998, with a spectral range of ~750–1250 wavenumbers. The whole planet was observed for these measurements. Fourier transform spectra have some unique features that must be taken into account when interpreting the spectra. The sampling frequency of the interferogram introduces a low-amplitude, high-frequency signal into the spectra. Slight differences in the sampling frequency can occur from run to run as a result of gain changes or slow drift in the circuits. When we divide one spectrum by another, these oscillations can come into exact phase with one another at a particular wavenumber region, resulting in a spurious spectral feature. We identified this effect by ratioing spectra of the Sun taken under different gains. Another problem has to do with the atmospheric absorption lines in the spectra. Where the lines are extremely dense, as in the ozone absorption region, and in the water absorption region near 8 μm , the resolution is not sufficient to see between the lines. Then, small differences in air mass between the Mercury and Sun spectra can produce sufficiently different absorptions in these regions to distort the ratio spectra. We plan to implement atmospheric corrections to these regions to minimize this effect. The ratio spectra are still at a resolution of 0.03 wavenumbers, but the reststrahlen features of interest have widths of tens of wavenumbers. It is sensible to reduce the resolution to a value corresponding to the features of interest. Initially, we used Fourier and wavelet transforms to accomplish this filtering, with some success. But recently we have employed a median filter, which is more robust, in that it ignores wild spikes in the data, which the other filters tend to include.

Results: A preliminary result from our most recent analysis is shown in Fig. 1. This is a measurement taken on April 1, 1997, when the Mercury phase was 0.562. The ratio spectrum has been filtered with a 5-wavenumber wide median filter. There are several features of interest in the spectrum. The feature near 1050 wavenumbers results from incomplete cancellation of the ozone band. The feature near 940 wavenumbers is apparently an instrumental effect, resulting from slight differences in sampling fre-

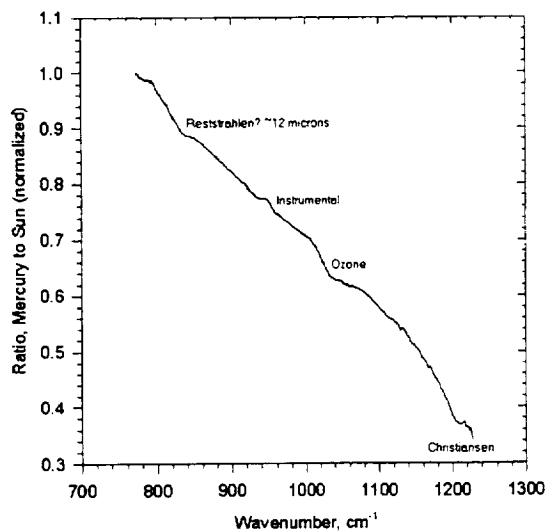


Fig. 1.

quency between Mercury and the Sun interferograms. There is a suggestion of the Christiansen peak beginning at about 1220 wavenumbers. The wavenumber range is insufficient to determine the peak location. Finally, there appears to be a weak feature that might be a reststrahlen band at about 830 wavenumbers. The Christiansen peak and a 830-wavenumber feature have been observed by Sprague et al. [1], who suggested that a basaltic composition could account for the latter feature.

Conclusions: Mercury-Sun ratio spectra give promise for study of reststrahlen bands from Mercury's surface in the spectral range 750–1250 wavenumbers. However, for unambiguous interpretation of these spectra, very high signal-to-noise ratios are required to define spectral bands, with the exception of the Christiansen peak near 8 μm . Salisbury et al. [2] suggested that S/N values of the order of 1000 are required to detect reststrahlen bands in lunar soils. Further improvements in our data analysis procedures can improve our S/N past 100, but probably not to 1000. The Christiansen peak remains the most clearly identifiable mineralogical feature.

References: [1] Sprague A. L. et al. (1994) *Icarus*, 109, 156. [2] Salisbury J. W. et al. (1997) *Icarus*, 130, 125.

033-89
EXES: AN ECHELON-CROSS-ECHELLE SPECTROGRAPH FOR SOFIA. M. J. Richter, J. H. Lacy, D. T. Jaffe, and M. K. Hemenway, Astronomy Department, University of Texas at Austin, Austin TX, USA.

Introduction: We are building a mid-infrared spectrograph as a PI-class instrument for the Stratospheric Observatory for Infrared Astronomy (SOFIA) that will give a new perspective on how molecular gas turns into stars and planets. Our instrument, EXES, uses an echelon grating cross-dispersed by an echelle grating. EXES will operate at wavelengths from 5.5 to 28.5 μm and have a resolving power of $R \geq 10^5$ at 10 μm . At altitudes reached by SOFIA, the reduced water burden and atmospheric pressure will allow observations of H_2 , H_2O , and CH_4 transitions that are totally blocked or heavily attenuated from the ground.

Although our goals focus on high-resolution observations, we have designed EXES to be a versatile instrument. There will be three spectral modes: high spectral resolution in a cross-dispersed format, and medium and low spectral resolution in a long-slit format. There will also be a camera mode suitable for target acquisition. The low- and mid-resolution capability of EXES will find a broad range of applications in studies of planets, late-type stars, ionized nebulae, and external galaxies.

Science Goals: We can use high spectral and spatial resolution observations of H_2 , H_2O , and CH_4 to study the temperature, density, dynamics, and chemistry of star-forming gas. H_2 rotation lines provide a direct tracer of warm ($100 \text{ K} \leq T \leq 500 \text{ K}$), molecular gas such as may be found in disks, the edges of molecular clouds, and behind shocks. H_2O and CH_4 will be seen in absorption against bright continuum sources located behind or embedded within molecular clouds. Doppler shifts of 30 km s^{-1} are sufficient to separate the astronomical H_2O from telluric absorption at SOFIA altitudes. While millimeter and submillimeter emission line studies of molecular clouds are biased toward the regions within the beam producing the strongest emission in a given transition, absorption line studies provide clear advantages: The line of sight is well-defined by the diameter of the continuum

TABLE 1. Typical EXES operating modes and estimated sensitivities.

λ (μm)	R ($\lambda/\Delta\lambda$)	Slit Width ("/pixels)	Slit Length (")	Bandwidth ($\mu\text{m}/\text{km s}^{-1}$)	NEFD (Jy)	NELB ($\text{W m}^{-2} \text{sr}^{-1}$)
6	120,000	1.4/3.4	7	0.023/1200	1.7	3.1×10^{-7}
	14,000	2.0/4.8	90	0.023/1200	0.6	4.6×10^{-7}
	1800	2.0/4.8	90	0.17/9000	0.2	1.1×10^{-6}
13.5	120,000	1.4/3.4	14	0.053/1200	4.1	3.2×10^{-7}
	14,000	2.0/4.8	90	0.053/1200	1.6	5.3×10^{-7}
	1400	2.0/4.8	90	0.53/12,000	0.6	2.1×10^{-6}
18	80,000	2.0/4.8	20	0.13/2100	4.6	2.2×10^{-7}
	10,000	2.8/6.8	180	0.13/2100	1.4	3.6×10^{-7}
	1300	2.8/6.8	180	0.95/16,000	0.5	9.6×10^{-7}
27	60,000	2.8/6.8	28	0.19/2100	7.6	1.7×10^{-7}
	6800	4.0/9.6	180	0.19/2100	3.3	2.8×10^{-7}
	700	4.0/9.6	180	1.9/21,000	1.1	9.3×10^{-7}

source, so all measurements refer to the same volume of gas, and it is possible to observe spectral lines arising from many different energy levels, often at the same time. By matching our resolution to the width of the lines, we maximize our sensitivity to weak features and simplify subsequent quantitative analysis of the physical conditions and the kinematics in star-forming gas.

Although our own interest in the properties of molecular gas in star forming and protostellar regions relies almost entirely on EXES's high-resolution capability, the instrument design does not compromise the capabilities of the low- and moderate-resolution long-slit mode. EXES's resolving power ranges of ~ 1500 , 10^4 , and 10^5 , its high sensitivity, and its ability to observe at many wavelengths inaccessible from the ground make EXES on SOFIA a valuable tool for many types of studies including planetary atmospheres, recombination lines, fine-structure lines, extragalactic PDRs, circumstellar envelopes, novae, and supernovae.

Optical Design: The EXES optics consist of three sections: focal reducing fore-optics, an echelon chamber, and a grating chamber with the cross-dispersion/long-slit gratings. The fore-optics image the telescope secondary onto a cold pupil and reimage the telescope focal plane with 2:1 demagnification through a filter wheel onto a slit wheel. The echelon chamber contains the high-resolution echelon grating and its collimator/camera mirror. (An echelon is a coarsely-ruled grating used at very high incidence angle.) The grating chamber contains an echelle and a low-order grating, their collimator/camera mirror, focal reduction lenses, and the detector array.

EXES can be used in four different modes. In high-resolution cross-dispersed mode ($R \approx 10^5$), all three chambers are used, with the echelle grating serving as the cross-disperser for the echelon. In medium-resolution long-slit mode ($R \approx 10^4$), the echelon chamber is not used and the echelle serves as the primary disperser. In low-resolution long-slit mode ($R \approx 1500$), the low-order grating mounted back-to-back with the echelle is used. In acquisition camera mode, the low-order grating is turned face-on to act as a low-efficiency ($\eta \sim 10\%$) mirror.

Capabilities: The calculated sensitivity of EXES in the three spectroscopic modes, and at four representative wavelengths, is given in Table 1. The wavelengths selected are at typical grating

angles. The slit widths were selected to give particular resolving powers. In calculating the resolving power, we included diffraction and aberrations as well as the slit width. Of course, the echelle and low-order grating resolutions vary with grating angle. High-resolution slit lengths are chosen to avoid echelon order overlap. Long slit lengths are matched to the unvignetted field. Our estimate for Noise Equivalent Flux Density (NEFD, appropriated for observations of a pointlike continuum source) is for $10\sigma:100\text{s}$ including nodding along slit. The estimate for Noise Equivalent Line Brightness (NELB, appropriate for observations of an angularly extended emission line source) is for $10\sigma:100\text{s}$ including nodding off slit.

At those wavelengths where our groundbased instrument can observe on Gemini, the NEFD will be $\sim 5\times$ better on Gemini and the NELB $\sim 2\times$ worse. Although the NELB is more often the parameter of interest for observations made by a high-resolution spectrometer, the gain in sensitivity that results from the lower telescope temperature of SOFIA is too small to justify observations at wavelengths with acceptable atmospheric transmission from Mauna Kea. Rather, we conclude that the sensitivity achievable on SOFIA is comparable to that achievable on the largest ground-based telescopes, allowing us to observe the same sources as would be observed by Gemini at wavelengths inaccessible from Mauna Kea.

Acknowledgments: This work is sponsored by grant USRA 8500-98-008.

531-91
INVESTIGATING THE MARTIAN ENVIRONMENT WITH THE MARS GLOBAL SURVEYOR THERMAL EMISSION SPECTROMETER. T. L. Roush, Mail Stop 245-3, NASA Ames Research Center, Moffett Field CA 94035-1000, USA (troush@mail.arc.nasa.gov).

The Thermal Emission Spectrometer (TES) onboard Mars Global Surveyor (MGS) is being used to investigate the surface and atmosphere of Mars and the martian moons Phobos and Deimos. As such, it builds upon infrared observations obtained by previous spacecraft, e.g., Mariner 9 and Viking Orbiters [1-4].

The objectives of the TES experiment are: (1) determine and map surface minerals, rocks, and ices; (2) study the atmospheric dust composition, particle size, and spatial and temporal distribution; (3) investigate condensate clouds, CO₂ and H₂O, location, temperature, and height; (4) investigate polar cap deposits, e.g., growth, retreat, and energy balance; (5) measure the thermo-physical properties of surface materials; and (6) characterize the atmospheric structure and dynamics [5].

The TES instrument is based upon a Michelson interferometer and collects data in the 1700–200 cm⁻¹ region (~6–50 μm) at 5 or 10 cm⁻¹ resolution. There are also broad-band bolometric (4.5–100 μm) and solar reflectance (0.3–2.7 μm) channels. The TES was designed to have a noise equivalent spectral radiance of 1.2×10^{-8} W⁻¹ cm⁻² sr⁻¹ cm⁻¹, corresponding to a signal-to-noise ratio of 490 at 1000 cm⁻¹ (10 mm) for a 270 K scene [5] and preflight data suggest a radiometric accuracy of about 1.2×10^{-8} W⁻¹ cm⁻² sr⁻¹ cm⁻¹ [6]. In-flight observations indicate a small systematic calibration offset of about 1.2×10^{-7} W⁻¹ cm⁻² sr⁻¹ cm⁻¹ is present in the TES data [6].

MGS achieved Mars orbital insertion September 11, 1997, and entered the initial aerobraking phase [7]. MGS should have reached a circular orbit by early 1998. However, structural damage to one solar panel occurred during its deployment in the cruise phase and ultimately required an assessment of the extent of the damage and a much slower aerobraking period. This has delayed reaching the final circular orbit until March 1999 [7].

TES and the other MGS science instruments began operating just after orbital insertion and continued to obtain data until November 1998 when the TES was turned off to reduce power consumption on the spacecraft. TES data obtained during orbits 2 to 53 have previously been published [6] and clearly illustrate the variety of scientific questions that can be addressed with them. There are clear spectral distinctions due to atmospheric dust, atmospheric condensates, and surface materials [6]; an example is provided in Fig. 1.

The Mariner 9 spacecraft carried an infrared interferometer spectrometer (IRIS) that clearly defined a broad atmospheric dust absorption band between about 1300 and 200 cm⁻¹ [2]. The depth of this feature increases with increasing emission angle, indicating

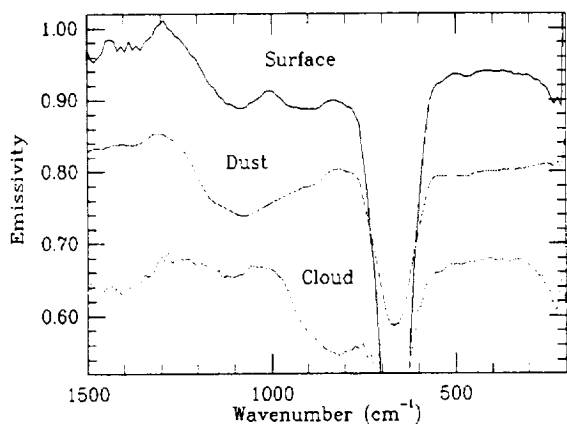


Fig. 1. Emissivity spectra of atmospheric components and surface region of Mars.

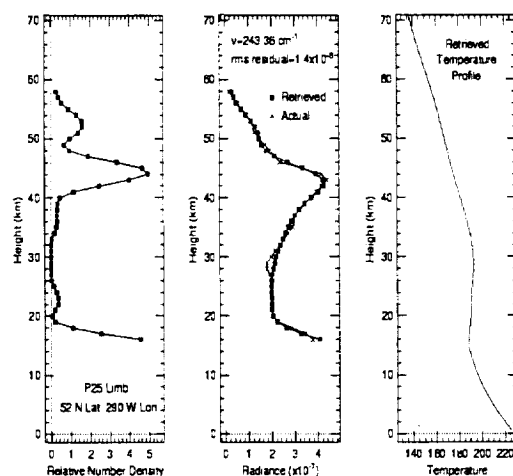


Fig. 2. Number density of the ice cloud (left), radiance (center), and temperature profile retrieved from limb observation (right), all as a function of height.

it is due to materials suspended in the martian atmosphere. The IRIS data have been interpreted to suggest that either a clay component or palagonite, a weathering product of basaltic glass, was responsible for the atmospheric dust signature [8,9]. This absorption is also readily observed by the TES. To date, there has been no mineralogical interpretation of the dust spectral signature based upon the TES data. However, the appearance of the emissivity maximum, commonly referred to as the Christiansen frequency, at wavelengths <8 μm, suggest that ultramafic materials cannot be responsible for the atmospheric dust signature [e.g., 10,11].

Atmospheric temperature profiles were obtained using the 15-μm CO₂ absorption band from nadir observations. Using these profiles, an estimate of the surface temperature from a nearly transparent spectral region (~7.7 μm), a unit surface emissivity, and uniform vertical mixing, the dust optical depth can be determined. Dust optical depths, scaled to a 6.1-mbar surface, range from ~0.15–0.25 during the early orbits [6]. During the onset of a dust storm (~orbit 51), centered near Nochiya Terra, these optical depths increase by a factor of 2 to 4 and the spread and decay of the dust storm was readily monitored [6]. This clearly illustrates the capability of the TES data to monitor the spatial and temporal variability of dust loading in the martian atmosphere.

These same vertical temperature profiles can be used to monitor large-scale zonal atmospheric motion [6]. Based upon thousands of retrieved profiles, evidence for a strong polar vortex centered near 50°N latitude is clearly indicated [6].

Vertical temperature profiles to higher altitudes can be derived from observations of the martian limbs with the TES and provide better vertical resolution than the nadir observations [6]. Using this technique, discrete water ice clouds were detected and characterized [6]. An example of the indication of discrete clouds at altitudes of 45 and 53 km is provided in Fig. 2 [6].

The TES data have also been used to monitor the recession of the seasonal south polar cap [6]. The asymmetric nature of the polar cap recession monitored by TES is consistent with historical observations [e.g., 12]. The radius of the seasonal cap is about

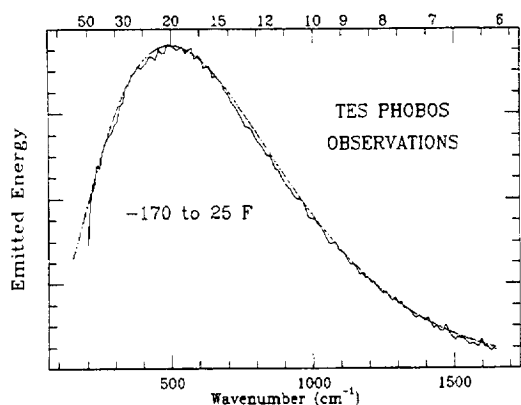


Fig. 3. Phobos spectrum (dashed line) compared to a mixture of Planck blackbody spectra (solid line). Approximate wavelengths (in micrometers) are given at the top.

6° smaller, based upon the TES observations, when compared to previous estimates [6]. This difference may be due to the effects of subpixel mixing of bare ground and frost near the cap edge when comparing thermal and visual estimates of the cap edge [6].

Early interpretations of surface signatures [6] are currently under reevaluation due to the recognition of the significant distribution and occurrence of atmospheric condensates. Nonetheless, there are clear indications of spatially restricted occurrences of hematite on the martian surface. A region of ~500 km diameter is centered near 1°S latitude and 3°W longitude.

In addition to the martian surface, the TES has also observed the martian moon Phobos. These observations clearly indicate that Phobos' surface is composed of a fine particulate powder. Initial interpretations suggest that the surface particulates have a very low thermal inertia and are likely ~1 m thick. Compositional interpretation of the Phobos data is currently underway. An example spectrum is shown in Fig. 3.

References: [1] Hanel R. et al. (1972) *Science*, 175, 305. [2] Conrath B. et al. (1973) *JGR*, 78, 4267. [3] Kieffer H. et al. (1970) *Science*, 193, 790. [4] Kieffer H. et al. (1977) *JGR*, 82, 4249. [5] Christensen P. et al. (1992) *JGR*, 97, 7719. [6] Christensen P. et al. (1998) *Science*, 279, 1692. [7] Albee A. et al. (1998) *Science*, 279, 1671. [8] Toon O. et al. (1977) *Icarus*, 30, 663. [9] Clancy R. et al. (1995) *JGR*, 100, 5251. [10] Logan L. et al. (1973) *JGR*, 78, 4983. [11] Salisbury J. and Walter L. (1989) *JGR*, 94, 9292. [12] James P. et al. (1994) in *Mars* (H. Kieffer et al., eds.), Univ. of Arizona, Tucson.

522-116
DEVELOPMENT OF THERMAL INFRARED EMISSION SPECTROSCOPY FOR GEOLOGICAL INVESTIGATIONS OF EARTH AND MARS. S. W. Ruff, Department of Geology, Arizona State University, Tempe AZ 85287-1404, USA (ruff@tes.la.asu.edu).

Introduction: The Thermal Emission Spectrometer laboratory at Arizona State University was established to support the observations of the Thermal Emission Spectrometer instrument onboard the ill-fated Mars Observer spacecraft. The opportunity to refly this

instrument was made available with the advent of the Mars Global Surveyor spacecraft, currently in orbit around Mars. Over the 15 years since the laboratory was established, the thermal-IR emission technique has matured to the point that it can serve as an effective and reliable tool to address a wide range of geological questions. An overview emphasizing laboratory-based problems, solutions, and applications of the technique will be presented.

Rationale for Developing Emission Technique: Infrared transmission, reflection, emission, and Raman techniques are available for measuring the vibrational spectra of geologic materials in the laboratory. However, only the emission technique is well suited for performing such measurements remotely or in a field setting. Reflection techniques can be used to produce comparable spectra, but only the hemispherical reflection version strictly obeys Kirchhoff's law relating reflectivity and emissivity [1]. Current detector technology limits hemispherical reflection measurements to a narrower spectral range compared with emission measurements. The desire to match the spectral range offered by the TES instrument and to simulate the type of measurement it would make motivated the development of the emission technique.

Experimental Challenges and Solutions: It has long been recognized that emissivity spectra are more challenging to measure than reflectivity or transmissivity spectra. Factors unique to the emission measurement include instrument self-emission, reflected environmental energy, temperature stability of the sample and instrument, and sample temperature determination. A detailed analysis of each of these factors has been performed and the means of dealing with them have been described in [2]. The result is a method for generating emissivity spectra of minerals and rocks that is efficient, accurate, and reproducible. The apparatus developed for this purpose is relatively simple in its design and could be incorporated into most commercial FTIR spectrometers.

Spectral Library Development: Having overcome the challenges of the emission measurement, it has been possible to develop a library of emissivity spectra. The emphasis of this activity has been to gather examples of common rock-forming minerals that are well characterized and of great purity [3]. Most of the samples in this collection are of a single particle size range (710–1000 μm) to ensure uniform spectral behavior, i.e., to avoid particle size effects. Future additions to the library will include a greater range of particle sizes and the inclusion of rock spectra. The full library will be made available in digital form to all researchers.

Spectral Deconvolution Capability: It has been well established that thermal-IR spectral mixtures can be deconvolved linearly [e.g., 4]. This allows for the development of linear deconvolution strategies to interpret mineral mixtures. The ASU group has developed [4] and is actively using a linear least-squares algorithm that incorporates subsets of the spectral library to deconvolve rock and soil spectra into endmember components [e.g., 5–7]. This same algorithm will be employed for the deconvolution of Mars surface spectra.

Application to Mars: The Mars Global Surveyor Thermal Emission Spectrometer can be described simply as a FTIR spectrometer with a telescope placed in orbit around Mars. It covers a spectral range of ~1670–200 cm⁻¹ with 143 spectral channels and a 3 × 2 detector array. The field of view of the detector array combined with the motion of the spacecraft in its polar orbit will produce an image cube of the entire planet at 3-km spatial

resolution over the 2-yr lifetime of the mission [8]. The spectral features of the martian atmosphere dominate the TES spectra of Mars, requiring atmospheric correction of the data before surface mineralogy can be addressed. To date, significant progress has been made in this effort, allowing for geologic observations of the planet. Some of these results will be presented during the workshop.

References: [1] Salisbury J. W. et al. (1994) *JGR*, 99, 11897–11911. [2] Ruff S. W. et al. (1997) *JGR*, 102, 14899–14913. [3] Christensen P. R. et al. (1999) *JGR*, submitted. [4] Ramsey M. S. and Christensen P. R. (1998) *JGR*, 103, 577–596. [5] Thomson J. L. and Salisbury J. W. (1993) *Rem. Sens. Environ.*, 45, 1–13. [6] Feely K. C. (1997) M. S. thesis, Arizona State University. [7] Ruff S. W. (1998) Ph.D. dissertation, Arizona State University. [8] Christensen P. R. et al. (1992) *JGR*, 97, 7719–7734.

533-90

MRS 2007

EXTRAZODIACAL LIGHT DETECTION PROSPECTS WITH THE KECK INTERFEROMETER. E. Serabyn, Mail Stop 171-113, Jet Propulsion Laboratory, 4800 Oak Grove Drive, Pasadena CA 91109, USA (Gene.Serabyn@jpl.nasa.gov).

Introduction: The Keck interferometer currently under development will include a midinfrared nulling experiment that is designed to search for extrazodiacal dust around nearby stars. The potential of this technique, as well as the basic experimental approach, will be discussed. The initial goal is to search for extrazodiacal emission around nearby stars at the 10 solar-zodi-equivalent level, with a long-term goal of 1 solar zodi.

534-13

SILICON CARBIDE: THE PROBLEM WITH LABORATORY SPECTRA. A. K. Speck¹, A. M. Hofmeister², and M. J. Barlow¹, ¹Department of Physics and Astronomy, University College London, Gower Street, London WC1E 6BT, UK (aks@star.ucl.ac.uk), ²Department of Earth and Planetary Science, Washington University, St. Louis MO 63130, USA.

Introduction: Most of the solid material in the solar system is believed to have originated as small particles that condensed in outflows from evolved stars. However, most solar system solids (predominantly silicates) have been reprocessed and/or homogenized so extensively that even the most primitive meteorite silicate samples have lost the isotopic indicators of their presolar origins. But some types of dust particles in the solar system have not been reprocessed and can potentially be associated with their stellar origins. One such dust type, silicon carbide (SiC), has been found in primitive meteorites [1] and is believed to be a significant constituent of the dust around C-rich asymptotic giant branch (AGB) stars [23]. Silicon carbide grains can be divided into two basic groups: α -SiC if the structure is one of the many hexagonal or rhombohedral polytypes, and β -SiC if the structure is cubic [4]. Silicon carbide grains exhibit a strong midinfrared feature between 10 and 12 μm with the peak of the β -SiC feature occurring about 0.4 μm shortward of that for α -SiC. Until now the observed peak wavelengths of the SiC feature in astronomical spectra have been interpreted as indicating α -SiC to be the dominant type of SiC around C stars [e.g., 5–9]. In fact, [8,9] found no evidence of β -SiC in these circumstellar environments. Silicon

carbide grains found in meteorites have isotopic compositions that imply that most of these grains were formed around C stars with small amounts forming around novae and supernovae [see 10–12 and references therein]. With the exception of a few grains found in and among the meteoritic diamonds (and of unknown origin [13]) studies of meteoritic SiC grains to date have found them to be exclusively of the β -type [14]. β -SiC will transform into α -SiC above 2100°C, but the reverse process is thermodynamically unlikely. There is therefore an apparent discrepancy between the meteoritic and astronomical SiC-types, which has been discussed in detail by [8,9].

This discrepancy is addressed by discussing the problems associated with previous interpretations of astronomical spectra that made use of laboratory infrared studies of terrestrial SiC. We have found that the problem in reconciling astronomical observations with meteoritic laboratory work has arisen from a misunderstanding and misinterpretation of laboratory spectra of SiC (and potentially other dust species). The results of fitting techniques used previously [5–9] are shown to be invalid due to the application of inappropriate matrix corrections to measured SiC optical properties. Furthermore, we show that IR spectra taken using the diamond anvil cell (DAC) thin film method provides data applicable to astronomical situations without further manipulation.

Laboratory Techniques and Results: New infrared (IR) absorption measurements of thin films of α - and β -SiC created by compression in a diamond anvil cell will be presented. Unlike some other methods, a dispersive medium (such as potassium bromide, KBr) is not used. This relatively new approach is quantitative if sufficient care is taken to produce an appropriately thin and uniform film as shown by comparison of thin film spectra of various minerals to reflectivity data from the same samples [15,16 and references therein]. Moreover, thin film spectra of garnets are nearly identical to single-crystal absorption data acquired in a vacuum [15], hence thin film spectra can be applied to astronomical data without further manipulation. Our measurements strongly suggest through comparison of the new thin film data with previous IR spectra collected for fine-grained KBr dispersions (in which the dust particles are dispersed in a KBr pellet) that the “matrix correction” wavelength shift invoked by [17] and adopted by other authors [e.g., 18,19] should not be applied to laboratory spectra of submicrometer grain size dispersions of SiC (see Fig. 1).

Results of Fitting Technique: Having established that previous fits of laboratory spectra for SiC to astronomical spectra

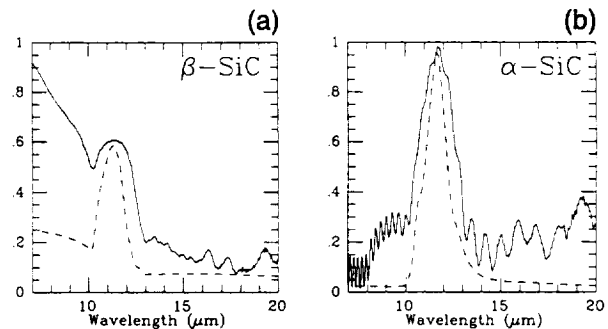


Fig. 1. Thin film spectra (solid lines) and the uncorrected KBr dispersion data [19] (dashed lines).

TABLE 1. Results of the χ^2 -fitting of C star spectra.

Source	T_{col}	SiC Type	T_{BB}	T_{SiC}	τ_{SiC}	$\tau_{9.7}$	χ^2_{R}
IRAS 21489 + 5301 [†]	455	β -SiC	449	293	—	—	0.515
IRC + 10216 [†]	520	β -SiC	511	230	—	—	1.260
AFGL 5076*	525	β -SiC	557	298	0.137	—	0.369
AFGL 2494*	525	β -SiC	516	383	0.167	—	0.306
AFGL 3099*	600	β -SiC	726	329	0.242	—	1.370
AFGL 5102*	600	β -SiC	650	355	0.161	—	0.345
AFGL 2155*	615	β -SiC	734	288	0.235	—	0.418
IRAS 02152 + 2822*	675	β -SiC	548	519	0.223	—	0.504
IRC + 40540*	680	β -SiC	859	313	0.173	—	0.508
AFGL 2368*	800	β -SiC	727	321	—	—	1.772
V Hya*	865	β -SiC	1129	393	0.211	—	0.761
IRC + 00365*	975	β -SiC	1788	215	0.114	—	2.316
CIT 6*	1100	β -SiC	960	363	0.217	—	1.294
IRC + 50096 [†]	1200	β -SiC	940	455	—	—	2.166
R For [†]	1400	β -SiC	906	800	—	—	1.237
R Lep [†]	1500	β -SiC	1284	573	—	—	5.267
UU Aur*	1500	β -SiC	2505	446	0.165	—	1.105
V Cyg*	1500	β -SiC	2556	568	0.139	—	1.014
CS 776 [†]	1600	β -SiC	993	576	—	—	1.879
V414 Per*	1600	β -SiC	1102	920	0.177	—	0.579
AFGL 3068 [†]	377	β -SiC	394	62	0.030	—	0.092
IARS 02408 + 5458 [‡]	320	β -SiC	388	96	0.152	—	1.686
AFGL 2477 [‡]	340	β -SiC	377	114	0.073	0.104	0.419
AFGL 5625 [¶]	333	β -SiC	358	185	0.097	0.113	0.306

$\tau_{9.7}$ is the optical depth at 9.7 μm .

* Fits with self-absorbed emission.

[†] Fits with pure emission only.

[‡] Fits with self-absorbed absorption.

[§] Fit with Trapezium interstellar silicate.

[¶] Fit with μ Cep interstellar silicate.

have been erroneous due to the unnecessary application of a KBr correction factor, we have refitted our own UKIRT CGS3 spectra of carbon stars [8,9] without such a correction. We have used the same χ^2 minimization routine [8], but the data to which the KBr correction had previously been applied [8,9] were used uncorrected this time. The results in Table 1 show that there is an obvious predominance of the β -SiC phase and that there is now no evidence for the α -SiC phase at all.

Conclusions: There is now no astronomical evidence for the presence of α -SiC in the circumstellar regions around C stars. While α -SiC might exist in small quantities, all observations to date are consistent with the exclusive presence of β -SiC grains. This resolves the past discrepancy reconciling astronomical observations and meteoritic samples of SiC grains. Furthermore, we have shown that laboratory IR spectra applicable to astronomical environments can be produced using the DAC thin film method.

References: [1] Bernatowicz T. et al. (1987) *Nature*, 330, 728. [2] Gilman R. C. (1969) *Astrophys. J. Lett.*, 155, L185. [3] Treffers R. and Cohen M. (1974) *Astrophys. J.*, 188, 545. [4] Bechstedt F. et al. (1997) *Phys. Stat. Sol. B*, 202, 35. [5] Baron Y. et al. (1987) *Astrophys. Astron.*, 186, 271. [6] Pégourié B. (1988) *Astrophys. Astron.*, 194, 335. [7] Groenewege M. A. T. (1995) *Astrophys. Astron.*, 293, 463. [8] Speck A. K. et al. (1997) *MNRAS*, 288, 431. [9] Speck A. K. et al. (1997) *Meteoritics & Planet. Sci.*, 32, 431. [10] Anders E. and Zinner E. (1993) *Meteoritics*, 28, 470. [11] Hoppe P. and Ott U. (1997) in *Astrophys.*

cal Implications of the Laboratory Study of Presolar Materials (T. Bernatowicz and E. Zinner, eds.), p. 27. AIP Conference Proceedings. [12] Ott U. (1993) *Nature*, 364, 25. [13] Daulton T. L. et al. (1996) *GCA*, 60, 4853. [14] Bernatowicz T. (1997) in *From Stardust to Planetesimals* (Y. Pendleton and A. G. G. M. Tielens, eds.), p. 227, ASP Conference Series 122. [15] Hofmeister A. M. (1995) in *Practical Guide to Infrared Microspectroscopy* (H. Humicki, ed.), Marcel Dekker Inc., New York, 377 pp. [16] Hofmeister A. M. (1997) *Phys. Chem. Mineral.*, 24, 535–546. [17] Dorschner J. et al. (1978) *Astron. Nachr.*, 299, 269. [18] Friedemann C. et al. (1981) *Astrophys. Space Sci.*, 79, 405. [19] Borghesi A. et al. (1985) *Astrophys. Astron.*, 153, 1.

535-90

THERMAL EMISSION SPECTROSCOPY OF SOLAR SYSTEM REGOLITHS. A. L. Sprague, Lunar and Planetary Laboratory, University of Arizona, 1629 East University Boulevard, Tucson AZ 85721-0092, USA.

Many years of difficult Earth-based observations analysis laboratory work and modeling have laid a firm foundation for what can be learned from thermal emission spectroscopy of regoliths in the solar system. At first, most observations were of rather low resolving power and most groundbased successes lie in measuring absolute fluxes of the Moon, Mercury, the Galilean satellites, and asteroids through terrestrial atmospheric windows. Measurements

in the 1960s determined that these remote bodies have thermal flux characteristics indicative of silicate surfaced bodies. Systematic thermal spectral photometry of the Moon and many diverse asteroids allowed the study of the emissivity relation with phase and local illumination angle. More recently, spectrometers utilize technically advanced gratings electronics and detectors, permitting high signal-to-noise ratio thermal emission spectroscopy using resolving powers suitable for examining spectral features that are diagnostic of the actual chemical makeup of rocks and minerals comprising the regolith.

To date, actual detailed compositional measurements of distant regoliths by thermal emission spectroscopic techniques are few because astronomers are inhibited by (1) the Earth's atmosphere — it restricts the use of spectral regions to those where atmospheric absorptions and emissions are slight and can be removed; (2) the lack of availability of reference laboratory emission spectra of rocks and minerals (ideally obtained in simulated conditions of insolation, low or no atmospheric pressure, and a variety of grain sizes); and (3) the scarcity of facility instruments designed for remotely sensing regoliths at infrared telescopes, e.g., appropriate apertures and long-slit (near the diffraction limit and with array detectors for good spatial resolution), large dynamic range (to accommodate both standard stars and warm planets), suitable resolving power (idealized for spectral activity seen in particulate mineral and rock mixtures).

Actual identification of rock types on solar system bodies have been made by measuring the wavelength of the emissivity maximum that is associated with the Christiansen frequency (for silicates, normally between 7.5 and 9.5 μm). Such identifications have been made for several locations on the Moon and a few locations on Mercury. Emission spectra from asteroids, the Galilean satellites, the Moon, and Mercury exhibit spectral features that are not yet fully understood. Actual mineral identifications resulting from thermal emission spectroscopy of regoliths are (1) Moon: a spectral minimum at 10.5 μm identifying olivine, and (2) Mercury: spectra between 7.7 and 13 μm identifying plagioclase feldspar with the presence of Na-rich albite at about 20–40%.

In the future the deficiencies listed above may be overcome, and groundbased observing and modeling may add more successes to the list. In addition, the Stratospheric Observatory for Infrared Astronomy (SOFIA) and the Space Infrared Telescope Facility (SIRTF) will offer spectroscopic platforms above most (SOFIA) and all (SIRTF) the molecular absorptions of the Earth's atmosphere. Both DLR (Institute for Planetary Exploration, Berlin) and NASA (Arizona State University) have funded measurements of emission spectra of rock mineral and particulate samples in one atmosphere environments.

SHADOW-HIDING EFFECT IN REGOLITHLIKE MEDIA.

D. G. Stankevich and Yu. G. Shkuratov, Astronomical Observatory of Kharkov State University, Kharkov 310022, Ukraine.

To estimate emissivity/reflectivity properties of the planetary regoliths it is necessary to calculate the shadow-hiding effect for this class of media. Usually analytical models of the shadow-hiding effect are very cumbersome and direct computer simulations are more preferable. Our computer model of the effect supposes that (1) a regolithlike surface consists of a great number of ran-

domly packed spherical particles; (2) surface elements of these particles emits as the absolutely black body (or scatters radiation according to the Lambert law); (3) the geometrical optics approach is valid; (4) the first order of scatter/emitting dominates. Modifications of our computer model are possible, e.g., these can be (1) a monolayer of particles on an even substrate; (2) polydisperse media; (3) layered media with different statistical characteristics of layers. Our calculations show (1) for statistically homogeneous media the only significant characteristics of angular emissivity/reflectivity distributions is the volume packing density (the smaller density the more anisotropic emission/scatter indicatrix of regolithlike media); and (2) maximal energy flux is observed at the zero phase angle for scatter and at the surface normal for emittance: for layered surfaces, even a thin upper layer changes the angular distribution significantly.

537-89
THERMAL EMISSION SPECTROSCOPY WITH THE SPACE INFRARED TELESCOPE FACILITY. J. Van Cleve, Space Infrared Telescope Facility, Infrared Spectrograph Boulder Field Office, FA-3, Room 16321W, Ball Aerospace, 1600 Commerce Street, Boulder CO 80306, USA.

The Space Infrared Telescope Facility (SIRTF) will have an Infrared Spectrograph (IRS) as one of its three focal plane instruments. The IRS is composed of four modules, two of which are relevant to the study of dust, the solid component of disks, and regoliths. The Short Lo/Peak Up (SL/PU) module performs spectroscopy between 5.5 and 14 μm and imaging in broad bands centered at 15 (blue) and 22 (red) μm . Both blue and red peak-up fields are $1' \times 1.3'$. The Long Lo module performs spectroscopy between 14 and 40 μm .

The instrument performance requirements for the IRS were derived in part from the science goal of establishing the mineralogy, particle size distribution, and thermal profile of dusty circumstellar disks. For example, the spectral resolution of both low-resolution modules is between 60 and 120, which is well-matched to the structure of solid-state emission features in micrometer-sized olivine grains. The wavelength coverage is well suited to dust at temperatures between 600 K and 60 K, corresponding roughly to the region of our solar system between Venus and Uranus.

The same instrument capabilities can be used to study absorption and emission features in interstellar dust in our own galaxy and identify the composition and temperature of dust in other galaxies. The redshift of distant galaxies can be determined from these features as well. Solar system science enabled by the instrument includes mineralogy of cometary grains, identification of solid hydrocarbons such as PAHs or tholins, and measurement of the thermophysical properties of main belt asteroids, satellites of the outer planets, and loose icy bodies between the orbits of Jupiter and Uranus. For objects colder than 60 K, SIRTF observations with the spectral energy distribution (SED) of the Multiband Imaging Photometer (MIPS) would be useful for thermal studies.

538-90
DUST EMISSION FROM HERBIG Ae/Be STARS: EVIDENCE FOR DISKS AND ENVELOPES. D. Vinkovic¹, A. Miroshnichenko², Z. Ivezić³, and M. Elitzur¹, ¹Department of Physics and Astronomy, University of Kentucky, Lexington KY

40506, USA (dejan@pa.uky.edu; moshe@pa.uky.edu), ²Pulkovo Observatory, St. Petersburg 196140, Russia (amiroshn@infopro.spb.su), ³Department of Astrophysical Sciences, Princeton University, Princeton NJ 08544, USA (ivezic@astro.princeton.edu).

Introduction: To date several attempts have been made to determine the geometry of dust around Herbig Ae/Be (Haebe) stars from IR and millimeter-wave data. The analysis was based on one of two possibilities: an optically thick disk, or an optically thin spherical envelope. From the shape of the spectral energy distribution (SED), Hillenbrand et al. [1] suggested that IR emission from 30 Haebes is dominated by optically thick accretion disks, while Hartmann et al. [2] proposed envelopes. Both models reproduce the observed $\lambda F_{\lambda} \propto \lambda^{-4/3}$ shape.

Miroshnichenko et al. [3] were able to successfully fit the detailed SED of eight Haebe stars with optically thin envelopes in spherical free fall. The motivation was that the free fall model, like a Keplerian disk, gives $\lambda F_{\lambda} \propto \lambda^{-4/3}$. With this model we can explain the strong silicate 10- μm feature in emission, which indicates optically thin dust. However, imaging at millimeter-wavelengths by Mannings and Sargent [4] (MS hereafter) clearly shows disks around their sample of seven Haebe stars. They also find that thin envelopes cannot explain the observed image sizes.

Furthermore, Henning et al. [5] were able to fit the SED of AB Aur by spherical envelope, while its observed small size rules out such dust configuration. They use this contradiction to rule out spherical models even though AB Aur shows the silicate 10- μm feature in emission. Additional controversy is introduced with imaging at far IR wavelengths by Di Francesco et al. [6]. They have observed objects with image size at 100 μm smaller than the one at 50 μm . This contradicts the fact that the temperature decreases with distance from the central star and therefore the image size at longer wavelengths must be larger.

We propose a simple solution that resolves the apparent inconsistencies of observations at different wavelengths, namely, the dust distribution in these sources has both spherical and disk components. The former can be large and dominates the SED at IR wavelengths; the latter is smaller and dominates at longer wavelengths. Because of its very low surface intensity, the envelope is not visible at millimeter-wavelengths but becomes detectable and bright at shorter wavelengths.

The Model: The fact that there are indications of optically thin and thick dust in the same object leads us to a model where a thick disk is surrounded and heated by a thin envelope. Such heating is possible because the envelope has higher temperature than the disk at the same distance from the star. The reason for

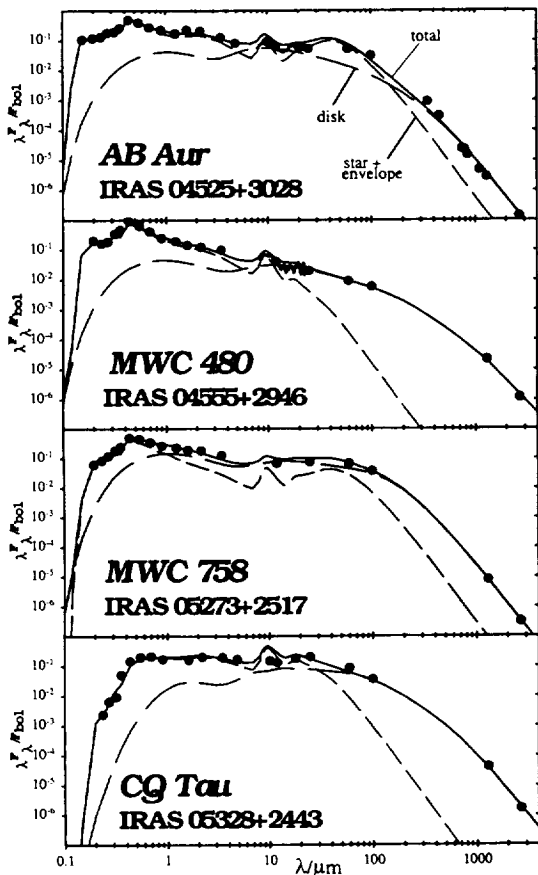


Fig. 1. Modeling of the Haebe stars in MS sample. Short-dashed line is the SED of star and envelope, long-dashed line is the disk's SED, and solid line is the total theoretical SED.

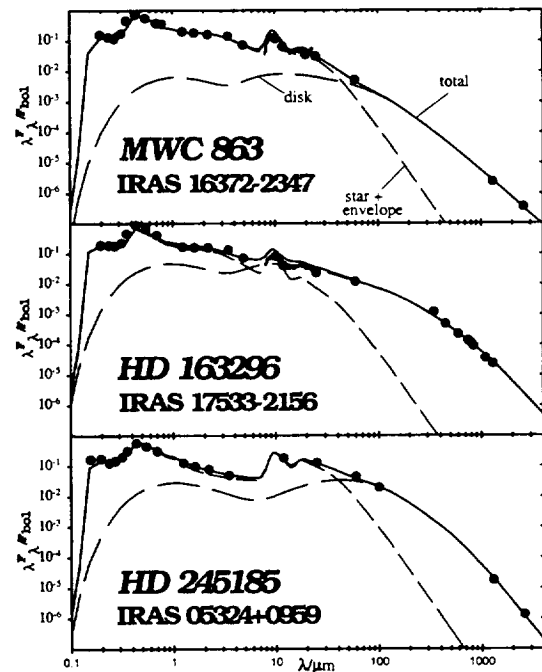


Fig. 2. Modeling of the Haebe stars in MS sample (see Fig. 1 for details).

having a cooler disk is twofold: It is heated by the central star at a grazing angle, and it is optically thick.

We model the radial density profile of the envelope with a broken power law. It extends from an inner radius corresponding to dust evaporation (we use an evaporation temperature of 1500 K) to an outer radius R_{out} .

We consider also some transitional radius R_p where the power p of the density power law $\rho(r) \sim r^{-p}$ changes from p_{in} to p_{out} . The dust in our models consists of the standard ISM mixture of silicate and graphite grains from Draine and Lee [7]. The disk is geometrically thin and has an inner radius at the stellar surface with temperature $2^{-1/4}T_*$, where T_* is the stellar temperature. It extends to a radius R_{out} specified by the disk's outer temperature T_d . The transition of the disk from optically thick to thin is defined by τ_{350} , the optical depth at 350 μm . When $\tau_{350} = 1$, the disk will be thin at $\lambda \geq 350 \mu\text{m}$. Modeling with a thick disk is plausible when the optical depth at the wavelength corresponding to T_d is larger than 1.

We have analyzed this model with the aid of the scaling theory by Ivezić and Elitzur [8], where the radius is dimensionless $Y = R/R_1$ (R_1 is the inner envelope radius). The SED was calculated by the code DUSTY [9]. The stellar spectral shape was taken from Kurucz [10].

Results and Conclusions: We applied the described model to the MS objects. In our search for the fitting parameters we used $0.5 \leq p_{\text{in}} \leq 2$, $50 \leq Y_p \leq 500$, $0 \leq p_{\text{out}} \leq 2$, $150 \leq Y_{\text{out}} \leq 10000$, $\tau_{350} \geq 0.2$, and $T_d \leq 50 \text{ K}$. The optical depth of the envelope was described by the visual optical depth τ_v . The correction for interstellar extinction A_v was considered a free-fitting parameter. It is mainly constrained by the short-wavelength data and results are consistent with the published estimates. The fitting yields a range of possible parameters for each object, and in all of them we are able to satisfy the observed size constraints and fit the SED from UV to millimeter-wavelengths (see Figs. 1 and 2). We can also rule out the flared disk model described by Chiang and Goldreich [11] because their optically thin layer surface corresponds to our envelope with a much smaller $\tau_v \sim 0.01$ than we get from the fit (τ_v is always larger than 0.1 and smaller than 1 except in CQ Tau, where it is ~ 2.5). The near IR is dominated in almost all objects by the envelope with $1.5 \leq p_{\text{in}} \leq 2$. We also give an upper limit on T_d for each object. The inclination angle is not a free parameter and can be derived from the fitting results. Usually it has a large uncertainty. The only noticeable difference between the models and observations is in the 10- μm region, and may be due to somewhat incorrect chemical composition and/or grain size distribution. Details of our results and theory will be published in a separate publication.

We conclude that the dust around MS objects includes both an optically thick and compact disklike component, and an optically thin, more extended component. The disk extends to several $10^4 R_*$ (R_* is the stellar radius). The envelope starts at $\sim 100 R_*$ and extends to $\sim 10^5 R_*$. Dust density in the inner envelope (up to several $10^4 R_*$, similar to the disk extent) resembles a steep power-law $1/r^2$ and flattens out to roughly $1/r$ at larger radii.

References: [1] Hillenbrand L. A. et al. (1992) *Astrophys. J.*, 397, 613. [2] Hartmann L. (1993) *Astrophys. J.*, 407, 219. [3] Miroshnichenko A. et al. (1997) *Astrophys. J. Lett.*, 475, L41. [4] Mannings V. and Sargent A. I. (1997) *Astrophys. J.*, 490, 792. [5] Henning Th. et al. (1998) *Astron. Astrophys.*, 336, 565.

[6] Di Francesco J. et al. (1994) *Astrophys. J.*, 432, 710. [7] Draine B. and Lee H. (1984) *Astrophys. J.*, 285, 89. [8] Ivezić Z. and Elitzur M. (1997) *MNRAS*, 287, 799. [9] Ivezić Z. et al. (1999) *User Manual for DUSTY*, Internal Report University of Kentucky (accessible at <http://www.pa.uky.edu/~moshe/dusty>). [10] Kurucz R. L. (1979) *Astrophys. J. Suppl.*, 40, 1. [11] Chiang E. I. and Goldreich P. (1997) *Astrophys. J.*, 490, 368.

539-90

THERMAL EMISSION SPECTROSCOPY OF LABORATORY REGOLITHS. C. Wagner, Institute of Planetary Exploration, German Aerospace Center (DLR), Rudower Chaussee 5, Berlin, Germany.

Introduction: Thermal emission spectra of samples of known mineralogic composition and well-defined grain size and porosity are valuable for interpreting remote sensing emissivity data obtained for the various planetary objects in the solar system. Because spectral reflectance of a material is more convenient to measure in the laboratory than spectral emissivity, it is common practice to interpret emissivity spectra of planetary objects by use of reflectance spectra of terrestrial minerals or rocks. The then required conversion of spectral reflectance (R) at any given wavelength into spectral emissivity (E) at this wavelength is carried out by a complementary relationship between emissivity and reflectance $E = 1 - R$ according to Kirchhoff's law. But Kirchhoff's law holds only under conditions of thermodynamic equilibrium, and is violated when the emitting material is nonisothermal. Planetary objects with little or no atmosphere, however, can evolve significant thermal gradients in the uppermost surface layer due to near-surface radiative cooling [1,2]. The effect of thermal gradients on the emissivity spectra of particulate minerals is complicated, and unfortunately "the spectral emissive properties of particulate materials in nonterrestrial conditions are understood neither theoretically nor experimentally" [3]. At any rate, use of reflectance data can provide only a more or less justified approximation for the actual emissivity spectrum. The (unknown!) degree of approximation depends on the thermal gradient within the radiating surface layer and is difficult to estimate for a remote target. This gives reasons for measurements of spectral emissivity of minerals and rocks in a simulated space environment (i.e., at low atmospheric pressure). But up to now such measurements are very scarce and comprise (as far as I know) only six published studies [1,3-7].

An important point is that even if emissivity measurements carried out at atmospheric pressure cannot provide a true analog for emissivity spectra of airless planetary objects, they still prove to be a valuable and interesting link and intermediate result between (1) emissivity measurements *in vacuo* and (2) reflectance measurements at atmospheric pressure. This is due to the following: For a material with a (vertical) temperature gradient the emission spectrum is controlled not only by the material's emissivity, but also by the interplay of (1) the wavelength-dependent opacity of the material, and (2) the varying brightness temperature [cf. 8-11].

Experimental Procedure: The apparatus and experimental procedure are similar to that used by Christensen and Harrison [12] and are described in more detail in [13]. For emissivity measurements the sample is placed in an Al cup (3-cm diameter) and heated from below to a constant temperature of 90°C. The

samples' thermal radiation emitted normal to the sample surface within a circular area of 2.5-cm diameter is collected by a Au-coated parabolic off-axis mirror and reflected to the entrance port of a Fourier transform infrared spectrometer (Bruker IFS 88). The emissivity of the sample is obtained by ratioing the background-corrected signals obtained for the sample and for the reference blackbody [e.g., 3]. For a thick sample of particulate material, however, the vertical thermal gradient is larger than for the blackbody (a 6-mm-thick Cu disk with a Nextel Velvet coating). Therefore, a systematically too low emissivity would be obtained. According to common practice [3,5,10,12], this systematic error is corrected by a fit procedure. It is assumed that the sample approached a known maximum emissivity (usually 1.0) somewhere in the measured spectral range. At this wavelength a Planck curve is fitted to determine the actual sample temperature and then the emissivity of the sample is scaled to that of the blackbody [12]. Fortunately, for many minerals the assumption $E = 1$ is justified at the materials' Christiansen wavelength, i.e., where $n(\lambda) = 1$. Another approach to get the samples' true emissivity spectrum is keeping the temperature gradient low within the sample by using a very small sample thickness. Then no fit procedure is required. The results of the two methods practically agree as can be shown by experiment [14]. Using a thin sample may be advantageous if only a small quantity of material is available or when no fitting point for E is known. Though in the thin-layer approach erroneous spectra are possible due to an insufficient optical depth, but they result only if the sample thickness falls below a certain minimum value.

Results: Emission spectra in the wavelength range from 4 to 17 μm were measured for the well-characterized materials listed below for several (usually seven) grain-size fractions ranging from $<25 \mu\text{m}$ to 180–200 μm , and, where samples are available, spectra were also measured for the massive material.

1. Carbonates and sulphates. Calcite magnesite siderite dolomite/ankerite; anhydrite and kieserite.

2. Mars soil analogs and ingredients. Four palagonites and the JSC Mars-1 martian soil simulant (these spectra are not for several grain sizes!), two hematites, two maghemites, three magnetites.

3. Feldspars. Six plagioclase feldspars (albite, oligoclase, andesine, labradorite, bytownite, anorthite), five alkali feldspars (albite, anorthoclase, sanidine, orthoclase, microcline), and three feldspathoids (leucite, nepheline, sodalite), all for at least seven grain sizes.

4. Pyroxenes. Augite, bronzite, and hedenbergite, all for the full range of grain-sizes.

In the future we plan to measure emissivity from:

1. Lunar soils of different exposure age obtained from the Apollo 12, 14, and 16 missions, i.e., samples 12023.83, 12070.12, 14259.602, 60051.32, and 61241.65.

2. Feldspar-pyroxene-mixtures. (1) 25 and 50 wt% bytownite in hedenbergite (i.e., Ca-rich feldspar mixed with Fe-rich pyroxene as a model for the Moon); grain sizes $<63 \mu\text{m}$ and 125–180 μm . (2) 25 and 50 wt% albite in bronzite (i.e., Na-rich feldspar with Mg-rich pyroxene as a model for Mercury); grain sizes as in (1).

References: [1] Logan L. M. and Hunt G. R. (1970) *JGR*, 75, 6539–6548. [2] Henderson B. G. and Jakosky B. M. (1994) *JGR*, 99, 19063–19073. [3] Henderson B. G. et al. (1996) *JGR*,

101, 14969–14975. [4] Logan L. M. et al. (1972) *Proc. LSC 3rd*, 3069–3076. [5] Logan L. M. et al. (1973) *JGR*, 78, 4983–5003. [6] Salisbury J. W. et al. (1973) *Proc. LSC 4th*, 191–196. [7] Lucey P. G. et al. (1993) *LPS XXIV*, 911–912. [8] Salisbury J. W. and Walter L. S. (1989) *JGR*, 94, 9192–9202. [9] Henderson B. G. and Jakosky B. M. (1994) *JGR*, 99, 19063–19073. [10] Henderson B. G. and Jakosky B. M. (1997) *JGR*, 102, 6567–6586. [11] Sprague et al. (1995) *Icarus*, 109, 156–167. [12] Christensen P. R. and Harrison S. T. (1993) *JGR*, 98, 19819–19834. [13] Wagner C. and Schade U. (1996) *Icarus*, 123, 256–268. [14] Wagner C. (1997) *LPI Tech. Rpt. 97-03*, 33–35.

340-90
SOLID-STATE SPECTROSCOPY OF CIRCUMSTELLAR DUST: INFRARED SPACE OBSERVATORY RESULTS. R. Waters, University of Amsterdam, Kruislaan 403, Amsterdam NL 1098 SJ, The Netherlands.

The Short and Long Wavelength Spectrometers (SWS and LWS) onboard the Infrared Space Observatory (ISO) have yielded a wealth of new information concerning solid-state spectra of circumstellar dust. For the first time, a full inventory of solid-state bands over a wide wavelength range with moderate spectral resolution has been obtained. An overview will be given of highlights of the ISO results in this area for both the O-rich and the C-rich dust chemistry. A comparison between dust surrounding young and evolved stars is made with some surprising analogies.

321-90
THERMAL EMISSION SPECTROSCOPY OF 1 CERES: EVIDENCE FOR OLIVINE. F. C. Witteborn¹, T. L. Roush², and M. Cohen³. ¹SETI Institute, Mail Stop 245-6, NASA Ames Research Center, Moffett Field CA 94035-1000, USA, ²Mail Stop 245-3, NASA Ames Research Center, Moffett Field CA 94035-1000, USA, ³Radioastronomy Laboratory, University of California, 601 Campbell Hall, Berkeley CA 94720, USA.

Thermal emission spectra of the largest asteroid 1 Ceres obtained from the Kuiper Airborne Observatory [12] display features that may provide information on its surface mineralogy. The plot in Fig. 1 is the Ceres spectrum (calibrated using α Boo as a standard) divided by a standard thermal model (STM). Also shown is the emissivity spectrum deduced from reflectivity measurements by Mustard and Hays [3] for olivine grains $<5 \mu\text{m}$ in diameter. The general shape of the Ceres and the olivine curves agree in essential details, such as the maxima from 8 to 12 μm , the minimum between 12 and 14 μm , the broad peak near 17.5 μm , and the slope beyond 22 μm . (Use of the 10- to 15- μm grain reflectivities [3] provides a better match to the 12- to 14- μm dip. We used a value of unity for β , the beaming factor associated with small-scale surface roughness in our STM. Adjustment of β to a lower value raises the long-wavelength side of the Ceres spectrum, providing an even better match to the olivine curve.) The emissivity behavior roughly matches the emission coefficients calculated by Mukai and Koike [4] for olivine particles with a particle radius of 3 μm . Their calculations show not only the negative slope from 23 to 25 μm , but a continued decrease past 30 μm . The Ceres emissivity is thus similar to that of small olivine grains from 8 to 30 μm , but olivine's emissivity is lower from 5 to 8 μm .

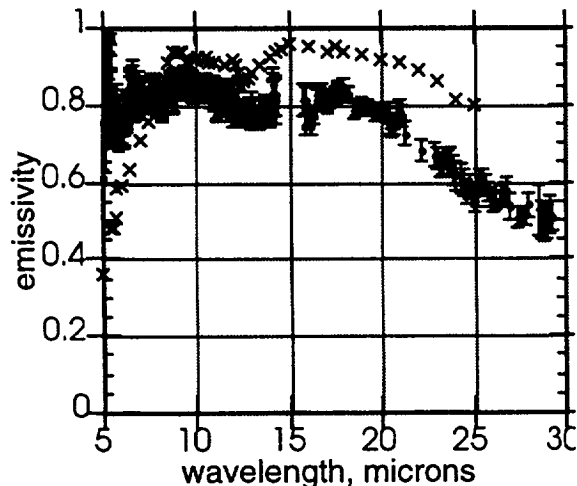


Fig. 1. Ceres emissivity vs. wavelength. Measured Ceres emissivity values (points with error bars) are compared with those measured for small olivine grains by Mustard and Hays [3] denoted by an x.

Although no olivine features have been identified for Ceres from reflectance spectra (0.4–2.5 μm), such features have been detected in several small asteroids [5]. The largest of the asteroids, Ceres is a prime candidate to have undergone differentiation. Olivine is expected to be a major product of differentiation and typically forms at depth due to its relatively high density. Subsequent impacts are expected to have emplaced the olivine-rich material at the surface of the differentiated asteroids and perhaps spread it to others as well [6,7]. The reflectance spectra of Ceres have been interpreted to indicate a surface consisting of hydrous silicate(s) with low ferric iron content and an opaque phase [8a].

Thus we are left with the question of why reflection spectroscopy provides no indication of olivine on Ceres, whereas the thermal observations reported here clearly suggests its presence.

Reflectance spectra probe the uppermost layers of a surface and spectral features are readily subdued or masked by trace amounts of opaque materials [e.g., 8b]. Surfaces emit energy from a variety of depths, and at these wavelengths the vibrational fundamentals are so strong that they are not as readily subdued or masked by overlying materials [8c]. One possibility that could account for the absence of olivine absorption features in the Ceres reflection spectrum is a thin layer (say a few micrometers or less) of dust enriched in opaque material. In fact, a mixture of olivine with some opaque material might explain the additional emissivity shortward of 8 μm seen in the emissivity spectrum of Ceres. While small asteroids are thought to be depleted in small dust grains [8], Ceres is large enough to retain fine-grained dust. For example, Le Bertre and Zellner [9] conclude that Vesta's surface has particles larger than 50 μm coated with particles smaller than 10 μm . Masking of olivine features in the Ceres reflectance spectrum could have broader implications because the apparent paucity of olivine-rich asteroids is regarded as a mystery [6,7]. This raises the question: Could a fine dust layer obscure the olivine component of large asteroids in the near infrared, thus accounting for the apparent deficit of olivine in the asteroid belt?

References: [1] Witteborn F. C. et al. (1999) *Astrophys. J.*, in press. [2] Cohen M. et al. (1998) *Astrophys. J.*, 115, 1671–1679. [3] Mustard J. F. and Hays J. E. (1997) *Icarus*, 125, 145–

163. [4] Mukai T. and Koike C. (1990) *Icarus*, 87, 180–187. [5] Cloutis E. A. (1993) *LPS XXIV*, 317–318. [6] Bell J. F. et al. (1989) in *Asteroids II* (R. P. Binzel et al., eds.), pp. 921–945, Univ. of Arizona, Tucson. [7] Burbine T. H. (1994) *Meteoritics*, 29, 453. [8] Dollfus A. et al. (1989) in *Asteroids II* (R. P. Binzel et al., eds.), pp. 594–616, Univ. of Arizona, Tucson. Ceres emission: Witteborn Roush and Cohen [8a] Gaffey M. J. and McCord T. B. (1979) in *Asteroids* (T. Gehrels, ed.), pp. 688–723, Univ. of Arizona, Tucson. [8b] Clark R. N. (1983) *JGR*, 88, 10635–10644. [8c] Christensen P. R. and Harrison S. T. (1993) *JGR*, 98, 19819–19834. [9] Le Bertre T. and Zellner B. (1980) *Icarus*, 43, 172–180.

542-90

CLOSE

ABUNDANT COOL MAGNESIUM-RICH PYROXENE CRYSTALS IN COMET HALE-BOPP. D. H. Wooden, Mail Stop 245-3, NASA Ames Research Center, Moffett Field CA 94035, USA.

Modeling of the observed dust emission from Comet Hale-Bopp over a large range of heliocentric distances (2.8 AU – 0.93 AU – 1.7 AU) led to the discovery of Mg-rich pyroxene crystals in the coma. These pyroxene crystals are apparent in the 10- μm spectrum only when the comet is close to perihelion ($r_p = 1.2$ AU) because they are cooler than the other silicate minerals. The pyroxene crystals are cooler than the other species because of their high Mg-content: They do not absorb as efficiently as the other silicate minerals. Given the same high Mg content of $\text{Mg}/(\text{Mg} + \text{Fe}) = 0.9$, radiative equilibrium computations show that pyroxene crystals are expected to be 150 K cooler than olivine crystals. The pyroxene crystals are also about 10 \times more abundant than the other silicate mineral species. Their high Mg content and relatively large abundance are in agreement with the preponderance of pyroxene interplanetary dust particles (IDPs) and the recent reanalysis of the PUMA-1 flyby of Comet Halley. Before Hale-Bopp, only olivine crystals were detected spectroscopically in comets, probably because the pyroxene crystals are less optically active, hence significantly cooler and harder to detect in contrast to the warmer silicate species. Determining the relative abundances of silicate minerals depends on their Mg contents.

If the pyroxene crystals in Comet Hale-Bopp are solar nebula condensates, then they probably had to form during the early FU Orionis epoch when the inner disk was hot enough and be transported out to the region of formation of icy planetesimals without being reheated. Reheating events appear to reincorporate Fe back into the crystals or form Fe-rich rims, which are not consistent with the high-Mg-content crystals. The condensation of Mg-rich pyroxene crystals is expected from solar nebula thermal equilibrium computations. However, their subsequent transport to the outer solar nebula unaltered has yet to be theoretically demonstrated.

The discovery of Mg-rich crystals in Comet Hale-Bopp and in AGB stars opens the possibility that these crystals are relic interstellar grains. One-third of IDPs have been shown to have significant deuterium enrichments, thus indicating that they contain presolar material. By spectroscopic analogy to IDPs the Mg-rich pyroxene crystals in Comet Hale-Bopp may be presolar grains. If so, then the comet contains largely ISM silicates. ISM grains may have been the dominant source of dust in the outer early solar nebula.